



Cite this: *Chem. Soc. Rev.*, 2022, **51**, 4786

Multicharged cyclodextrin supramolecular assemblies

Zhixue Liu^a and Yu Liu *^{ab}

Multicharged cyclodextrin (CD) supramolecular assemblies, including those based on positively/negatively charged modified mono-6-deoxy-CDs, per-6-deoxy-CDs, and random 2,3,6-deoxy-CDs, as well as parent CDs binding positively/negatively charged guests, have been extensively applied in chemistry, materials science, medicine, biological science, catalysis, and other fields. In this review, we primarily focus on summarizing the recent advances in positively/negatively charged CDs and parent CDs encapsulating positively/negatively charged guests, especially the construction process of supramolecular assemblies and their applications. Compared with uncharged CDs, multicharged CDs display remarkably high antiviral and antibacterial activity as well as efficient protein fibrosis inhibition. Meanwhile, charged CDs can interact with oppositely charged dyes, drugs, polymers, and biomacromolecules to achieve effective encapsulation and aggregation. Consequently, multicharged CD supramolecular assemblies show great advantages in improving drug-delivery efficiency, the luminescence properties of materials, molecular recognition and imaging, and the toughness of supramolecular hydrogels, in addition to enabling the construction of multistimuli-responsive assemblies. These features are anticipated to not only promote the development of CD-based supramolecular chemistry but also contribute to the rapid exploitation of these assemblies in diverse interdisciplinary applications.

Received 28th February 2022

DOI: 10.1039/d1cs00821h

rsc.li/chem-soc-rev

1. Introduction

Cyclodextrins (CDs), the well-known family of supramolecular macrocyclic host molecules, have been widely applied in analytical chemistry,^{1–5} catalysis,^{6–10} materials science,^{11–14} biological science,^{15–19} and other fields.^{20–23} Recently, these macrocyclic

systems have also emerged as promising building blocks for functional nanomaterials based on the host-guest chemistry of CDs.^{24–27} CDs are macrocyclic oligosaccharides connected by α -1,4-glycosidic bonds.²⁸ The most commonly used CDs are α -, β -, and γ -CDs, which consist of six, seven, and eight D-glucose units, respectively (Fig. 1a),^{29–34} although larger CDs containing more than 100 glucose units and smaller CDs containing as few as three glucose units have also been reported.^{35,36} The macrocyclic rings of D-glucose units endow CDs with a toroidal three-dimensional (3D) shape featuring a hydrophilic surface and a relatively hydrophobic cavity.^{37–40} The hydroxy groups are

^a State Key Laboratory of Elemento-Organic Chemistry, College of Chemistry, Nankai University, Tianjin 300071, P. R. China. E-mail: yuliu@nankai.edu.cn

^b Haihe Laboratory of Sustainable Chemical Transformations, Tianjin 300192, China



Zhixue Liu

Zhixue Liu received his PhD degree from Yanbian University in 2017 under the supervision of Prof. Xue Wu. After that, he worked as a lecturer at Jilin Normal University for one year. Since 2018, he has been working as a postdoctoral fellow at Nankai University under the supervision of Prof. Yu Liu. His current research focuses on the construction of supramolecular optical probes and functional supramolecular assemblies.



Yu Liu

Yu Liu graduated from the University of Science and Technology of China in 1977, and received his PhD degree from Himeji Institute of Technology, Japan, in 1991. Then he moved to Nankai University as a full professor in 1993. His research focuses on molecular recognition and assembly of macrocyclic receptors.

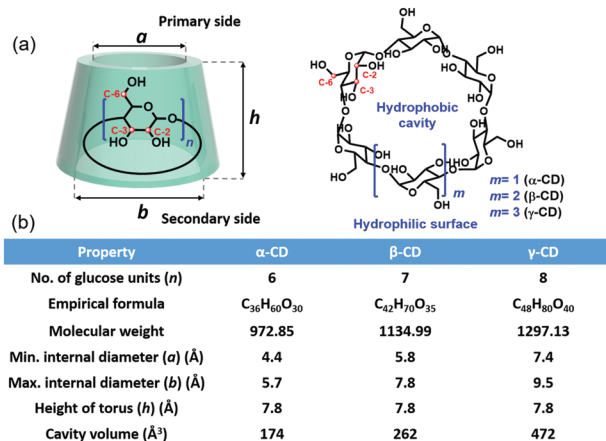


Fig. 1 (a) Schematic illustration of CDs and general molecular structures of α -, β -, and γ -CDs. (b) Selected structural parameters of α -, β -, and γ -CDs.^{5,89,90}

located on the outer surface of CDs, with the C-6 hydroxy groups on the narrow primary side and the C-2 and C-3 hydroxy groups on the wider secondary side. These groups not only give CDs excellent water solubility but also serve as convenient handles for derivatization.^{41–44} However, since the C-6 hydroxy groups on the primary face are more reactive than the C-2 and C-3 hydroxyl groups on the secondary face, most reports are on the modification of the C-6 hydroxy groups to obtain mono- and per-substituted CDs, as well as site-selective poly-heterofunctionalized CDs,^{45–49} although C-2 and C-3 hydroxy modifications are also used in the derivation of CDs.^{50–54} Therefore, the regioselective modification of CDs is a very challenging issue that can further enrich the CD supramolecular assemblies and their applications in various fields. The inner cavity is typically used to encapsulate size-matched guest molecules to form complexes through host–guest interactions.^{55–59} Because of the differences in the number of D-glucose units in α -, β -, and γ -CDs, the minimum internal diameter on the primary side, the maximum internal diameter on the secondary side, and the cavity volume are also different (Fig. 1b), meaning that guest molecules of different sizes can be encapsulated into the three hosts. For instance, α -CD tends to bind guests such as small derivatives of benzene,^{60,61} azobenzene (Azo),⁶² polyethylene glycol (PEG),^{63,64} etc.; β -CD tends to bind guests such as larger derivatives of Azo and naphthalene,^{65–68} polypropylene glycol,^{69,70} adamantane,^{71–73} ferrocene,^{74–76} cholesterol,^{77,78} cholic acid,⁷⁹ imidazole,⁸⁰ phenolphthalein,⁸¹ reduced methyl viologen,⁸² *N*-isopropylacrylamide,⁸³ etc.; and γ -CD tends to bind guests such as tetraaniline,⁸⁴ pyrene dimer,^{85–87} anthracene dimers,⁸⁸ etc.

In an effort to improve the molecular recognition and assembly characteristics of the parent CDs and broaden their applicability, the hydroxy groups have been modified with numerous functional groups, such as alkyl chains,⁹¹ PEG chains,⁹² luminophores,^{93,94} photosensitizers,⁹⁵ sulfhydryl moieties,⁹⁶ mannose and glycoclusters,^{97,98} carbenes,^{99,100} amino acids,¹⁰¹ pillararenes,^{102,103} polymers,^{104–107} co-polymers,^{108–110} and metal complexes.^{11,41,111} In particular, synthetic multicharged CDs have

attracted considerable attention in a variety of research fields, including medicine, biological science, and materials science. In general, positively charged CDs exhibit enhanced antibacterial activity,¹¹² whereas negatively charged CDs display antiviral activity¹¹³ and inhibit protein fibrosis¹¹⁴ through interactions between opposite charges. In addition, the electrostatic interaction as a kind of supramolecular interaction is widely used in molecular assembly.^{115–118} Interactions occur between oppositely charged groups, and the interaction energy is proportional to the number of charges carried by the groups.^{119–123} Therefore, most reported positively charged functional groups (imidazolium salts,¹²⁴ ammonium salts,^{125,126} guanidinium salts,¹²⁷ etc.) and negatively charged functional groups (carboxylates,^{128–131} phosphates,¹³² sulfonates,^{133–138} etc.) attached to the C-2, C-3, or C-6 hydroxy groups of CDs can interact with oppositely charged molecules through electrostatic interactions.¹³⁹ The presence of multiple charges can not only effectively induce the formation of charged supramolecular assemblies but also improve their stability. However, components of the guest molecules such as polymer chains, azobenzene, ferrocene, adamantane, and hydrophobic drugs can also be modified with charged groups to improve their host–guest interactions with CDs. The exposed charges can be exploited to induce co-assembly with oppositely charged molecules through electrostatic interactions, as well as multilevel assembly with other supramolecular macrocycles such as charged calixarenes,^{140,141} cucurbit[*n*]urils (CB[*n*]s),^{142–145} and charged pillar[*n*]arenes,^{146,147} which are conducive to constructing multifunctional supramolecular assemblies, such as rotaxanes^{148–150} and hydrogels,^{151–155} applied in the field of electrophoresis.^{156–160}

Although the literature contains numerous reviews covering the diverse applications of CDs and CD-based assemblies, including metal complexation,^{11,41,161,162} cyclodextrin metal–organic frameworks,¹⁶³ cyclodextrin covalent organic frameworks,^{164–167} supramolecular catalysis and synthesis,^{168–170} multistimuli-responsive materials,^{15,171–173} polymer materials,^{13,24,174–181} self-healing materials,¹⁸² amphiphilic materials,^{90,183} crystalline organic materials,¹⁸⁴ liquid crystal materials,¹⁴ rotaxanes/poly-pseudorotaxanes/catenanes/polyrotaxanes,^{185–190} drug/protein/gene delivery,^{16,19,23,191–194} molecular recognition and imaging,^{1,195–199} molecular machines,²⁰⁰ thiolated cyclodextrins,²⁰¹ cyclodextrin–porphyrinoid systems,²⁰² foods and antioxidants,^{203,204} electrochemical analysis,⁵ and chiral analysis,²⁰⁵ to the best of our knowledge, multicharged CDs as an important building block have not been comprehensively reviewed. Multilevel supramolecular assembly based on electrostatic interactions between opposite charges, including parent CDs modified with multiple charges or encapsulating charged guest molecules, has enabled the construction of a diverse variety of multifunctional materials, and these have been widely applied in drug delivery,^{206–214} bioimaging,^{215–218} molecular recognition,^{219–231} nanochannels,^{232,233} molecular switches,^{26,234} adsorbents and enrichment,^{235–237} surfactants,²³⁸ electrospinning supramolecular systems,^{239,240} supercapacitors,²⁴¹ CD–polyoxometalate complexes,^{242–245} liquid crystal materials,²⁴⁶ multistimuli-responsive materials,^{247–252} pseudorotaxanes,²⁵³ conductive polymers,²⁵⁴ photodynamic/chemotherapy,²⁵⁵ molecular

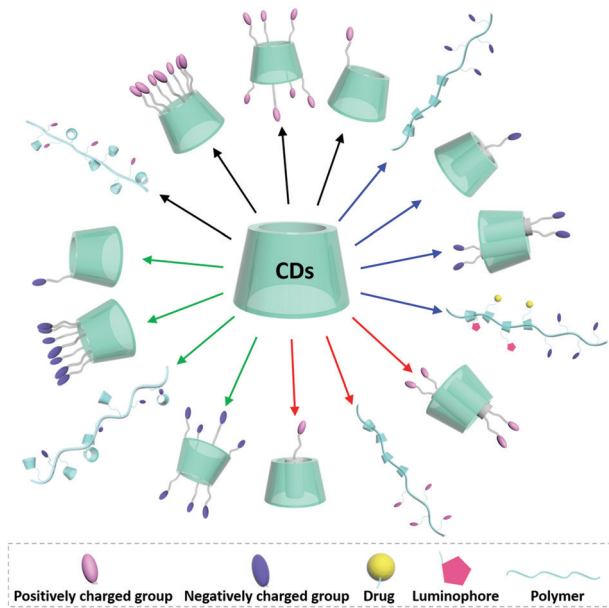


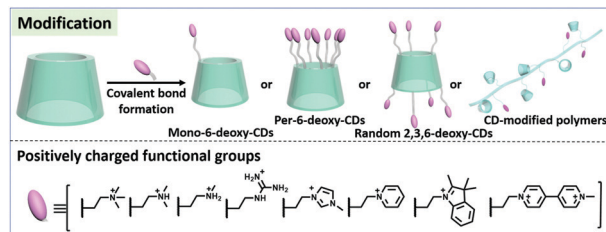
Fig. 2 Schematic illustration of multicharged CD supramolecular assemblies, including positively/negatively charged functional group modified mono-6-deoxy-, per-6-deoxy-, random 2,3,6-deoxy-CDs and CD-modified polymers, as well as supramolecular assemblies formed by CDs binding positively/negatively charged guests.

shuttles,^{256,257} *etc.* Therefore, CD-based multicharged supramolecular assemblies are anticipated to attract even more attention in the future. In this review, we mainly discuss the supramolecular assembly mechanisms of multicharged CDs (Fig. 2) and their emerging applications in the fields of biological science, medicine, environmental science, and materials science, providing a general overview and describing the crucial roles of electrostatic interactions in various multicharged supramolecular assemblies. We can see that combining the supramolecular chemistry of CDs and multicharged functional groups can inspire new developments and applications of CDs.

2. Assemblies of charged CDs and guests

2.1 Assemblies of positively charged CDs and guests

Positively charged CDs can be synthesized through covalent modification of one or more of the C-2, C-3, or C-6 hydroxy groups with cationic functional groups to afford mono-6-deoxy-, per-6-deoxy-, and random 2,3,6-deoxy-CDs or through the attachment of the parent CDs to positively charged polymers. As shown in Scheme 1, some representative positively charged functional groups include pyridinium salts, imidazolium salts, indolium salts, ammonium salts, and guanidinium salts. Depending on the degree of substitution, positively charged CDs can be divided into monosubstituted derivatives, multisubstituted derivatives, and CD-modified polymers, and these have been used to realize various topological morphologies and applied in numerous research fields.



Scheme 1 Schematic diagram of various types of positively charged CDs and structures of typical positively charged functional groups.

Antibacterial materials

Positively charged CDs are frequently used in biological research because of their antibacterial activity and drug-delivery capabilities. It is well known that cationic quaternary ammonium compounds with a large number of positively charged sites and cationic polymers such as polyethyleneimine derivatives, chitosan, and ϵ -poly-L-lysine exhibit broad-spectrum antibacterial activity.^{258–260} Therefore, numerous researchers have introduced cationic functional groups into macrocyclic compounds or constructed antibacterial supramolecular assemblies through host-guest interactions.^{261–265} For example, Wang and co-workers used a supramolecular approach to modulate the antibacterial activity of CD-attached cationic ammonium surfactants.²⁶⁶ In this report, two cationic ammonium-modified β -CDs featuring dodecyl chains (APDB) and hexadecyl chains (APCB) were synthesized (Fig. 3a). Four guest molecules (AD-NH₃⁺, DB, DTAB, and CTAB) were then used to enhance the antibacterial activities of APDB and APCB through host-guest interactions by modulating their electrostatic or hydrophobic interactions with

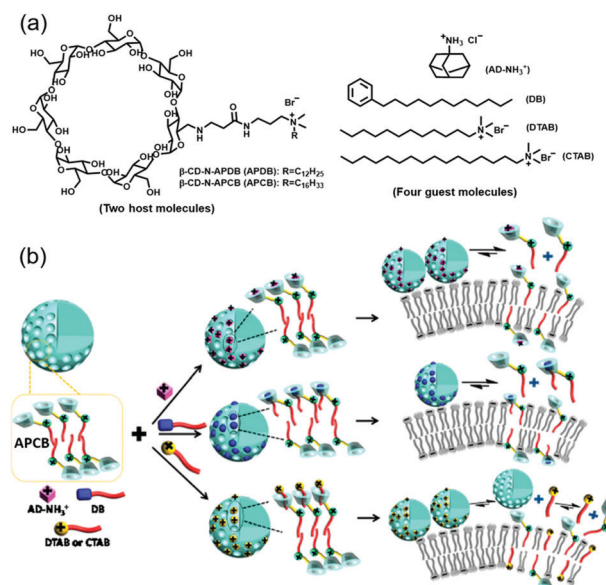


Fig. 3 (a) Chemical structures of cationic ammonium-modified β -CDs with dodecyl chains (APDB) and hexadecyl chains (APCB) and four guest molecules (AD-NH₃⁺, DB, DTAB, and CTAB). (b) Interaction modes of four guest molecules with APCB in spherical aggregates and their antibacterial mechanisms. Reproduced with permission from ref. 266. Copyright 2017, American Chemical Society.

bacteria. AD-NH₃⁺ and DB increased the killing efficacy of APCB against *Staphylococcus aureus* from 59% to 75%, while DTAB and CTAB increased the killing efficacy to over 90%. Notably, because of the formation of spherical aggregates between APCB and guest molecules (Fig. 3b), only a very small amount of CTAB could enhance the antibacterial activity of APCB to a very high level, which was accompanied by extremely low cytotoxicity. In contrast, the mixtures of the various guest molecules with APDB did not exhibit any activity against *S. aureus* because they were unable to form aggregates at lower concentrations. The guest molecules were trapped in the APCB spherical aggregates, resulting in different interaction patterns of the aggregates with *S. aureus* and distinct antibacterial activities. This supra-molecular assembly strategy provides a convenient approach to develop efficient antibacterial agents with low cytotoxicity.

Exogenous NO delivery systems also have potential therapeutic applications for bacterial infections.^{267–270} For example, Schoenfish and co-workers reported that *N*-diazoniumdiolate-modified β-CD derivatives exhibited highly tunable NO release.²⁷¹ β-CD derivatives fully modified with the *N*-diazoniumdiolate precursors (Fig. 4a) resulted in significant NO payloads and maximum bactericidal activity against *Pseudomonas aeruginosa*. The primary-amine-terminated β-CD derivatives exhibited greater antibacterial activity than analogues bearing other terminal functional groups with equivalent NO payload, which was ascribed to their positive charge and correspondingly superior ability to associate with the negatively charged bacterial cell wall. Meanwhile, the NO-donor-modified β-CD could also encapsulate and deliver promethazine (PM) through host-guest interactions, thus showing potential as a therapeutic agent for dual drug release (Fig. 4b). The combined action of NO and PM using PM/β-CD-DETA/NO demonstrates the potential application of co-delivering NO with another drug from the same complex.

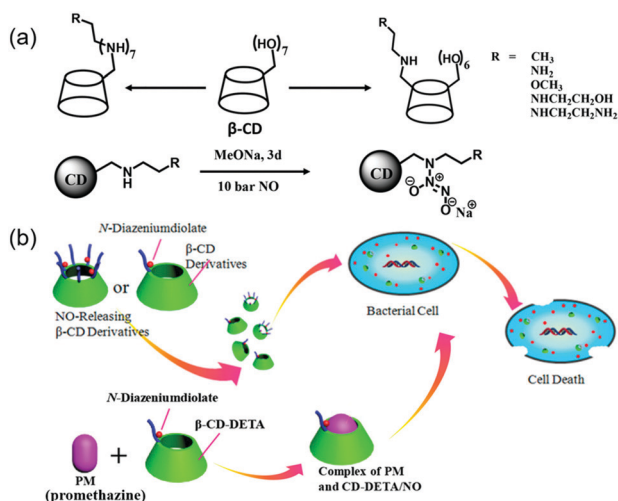


Fig. 4 Chemical structures of secondary-amine-modified β-CDs and *N*-diazoniumdiolate-modified β-CDs. (b) Illustration of NO delivery and promethazine/NO co-delivery for antibacterial activity. Reproduced with permission from ref. 271. Copyright 2018, American Chemical Society.

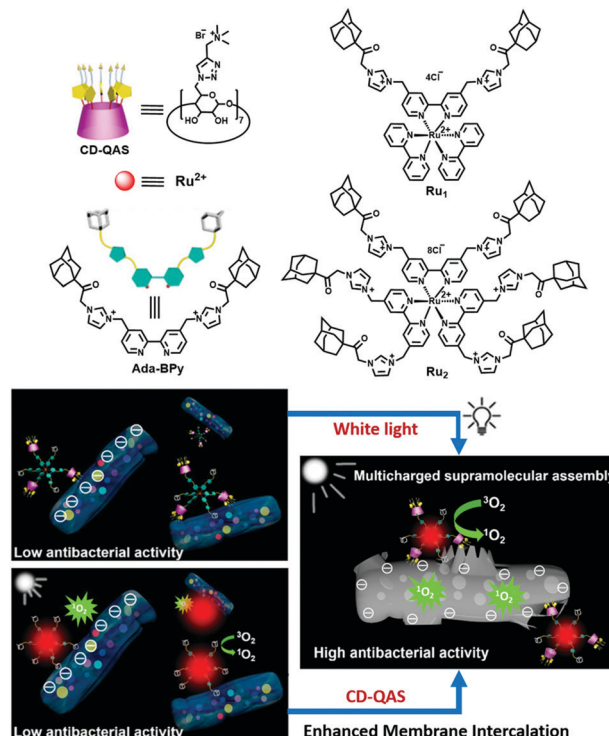


Fig. 5 (a) Chemical structures of two guest molecules Ru₁ and Ru₂. (b) Schematic illustration of the multicharged supramolecular assembly between polycationic β-CD (CD-QAS) and Ru₂ for highly efficient photodynamic antibacterial therapy. Reproduced with permission from ref. 112. Copyright 2021, American Chemical Society.

In an effort to realize potent antibacterial activity, a synergistic strategy involving the co-assembly of a positively charged macrocycle and a photosensitizer was recently explored by Liu and co-workers.¹¹² The authors prepared a multicharged supramolecular assembly based on polycationic cyclodextrin (CD-QAS) and hexa-adamantane-appended ruthenium polypyridyl for highly efficient photodynamic antibacterial therapy (Fig. 5). As a positively charged macrocyclic receptor, CD-QAS not only displayed excellent water solubility, good biocompatibility, and low toxicity but also tightly bound to and accumulated in the negatively charged membranes of bacteria. After combining with adamantane-modified Ru₁ and Ru₂ through host-guest interactions, the resulting complexes exhibited excellent water solubility and high-efficiency generation of reactive oxygen species (ROS) upon light irradiation. Antibacterial assays revealed that Ru₂/CD-QAS with high density of quaternary ammonium salt groups inhibited the growth of *Escherichia coli* by approximately 25% in the absence of light, but upon irradiation the killing efficiency reached 99%. This multicharged supramolecular assembly simultaneously achieved effective membrane accumulation and *in situ* ¹O₂ generation, thus providing a simple method for synergistic photodynamic antibacterial therapy.

Delivery systems

In drug delivery and controlled release, the conversion of hydrophobic chemotherapeutic drug molecules to a hydrophilic

formulation prior to administration is sometimes required. To address this issue, He and co-workers reported that CD-based nanoparticles could be used as a multifunctional carrier for the enhanced cellular delivery of the hydrophobic compound alliin. ²⁷² Positively charged polylysine (PL) was attached to NH₂-β-CD to synthesize the amphiphilic PL/NH₂-β-CD carrier, which facilitated cellular uptake by using the high affinity of PL for negatively charged cell membranes. Compared with the parent β-CD (Fig. 6a), PL/NH₂-β-CD displayed enhanced alliin encapsulation efficiency *via* the host-guest and hydrophobic interactions (Fig. 6b). In addition, doxorubicin was encapsulated in the nanoparticles as a fluorescent model drug and evaluated for cellular uptake and cell cycling. The experimental results demonstrated that the combination of alliin and PL/NH₂-β-CD nanoparticles can induce cell apoptosis during the S and G2/M phases of the cell cycle, with important applications in killing cancer cells. The use of PL/NH₂-β-CD as a carrier to deliver alliin in this work effectively prevented it from being trapped by proteins and fatty acids in the plasma membrane, thus improving its therapeutic effect.

Wu and co-workers reported star polymers based on cell-penetrating poly(disulfide) (CPD) for the simultaneous intracellular delivery of miRNAs and hydrophobic drug camptothecin (CPT). ²⁷³ The star-like polymers consisted of a β-CD core modified with guanidinium disulfide and multiple poly(disulfide) arms (Fig. 7a), which could not only encapsulate the CPT in the β-CD core through host-guest interactions but also co-assembled with miRNAs to form CPT@βCD-CPD-miRNAs through charge interactions. This polymer co-delivery system enabled the rapid and simultaneous delivery of miRNAs and CPT in living cells, followed by subsequent release of this cargo in the presence of endogenous GSH, providing superior gene transfection efficiency (Fig. 7b). This platform could be exploited to minimize potential cytotoxicity concerns associated with many cationic branched polymer systems for miRNA delivery, thus representing an important method for designing personalized delivery platforms based on CPD-based polymers.

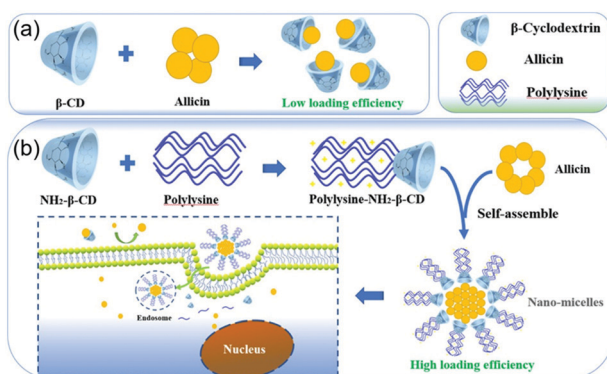


Fig. 6 (a) Schematic illustration of self-assembling β-CD-based nanoparticles for alliin encapsulation. (b) Schematic illustration of self-assembling polylysine–NH₂-β-CD-based nanoparticles for enhanced cellular delivery of alliin. Reproduced with permission from ref. 272. Copyright 2020, American Chemical Society.

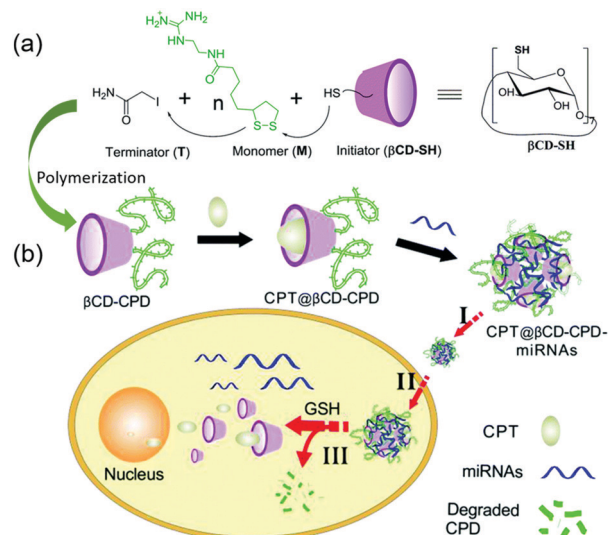


Fig. 7 (a) Polymerization of βCD-CPD based on βCD-SH. (b) Overall strategy for the simultaneous delivery and controlled release of miRNAs and camptothecin (CPT) by βCD-CPD-based systems. Reproduced with permission from ref. 273. Copyright 2017, Royal Society of Chemistry.

Liu and co-workers reported a synergistic coagulant formed by the co-assembly of amphiphilic positively charged cyclodextrin (AMCD) and vitamin K (VK) (Fig. 8). ²⁷⁴ AMCD contained positively charged imidazolium cations bearing alkyl chains at the lower rim of β-CD. Owing to its amphiphilic nature, AMCD could self-assemble and co-assemble with VK in aqueous media. The imidazolium cation moieties, in conjunction with the β-CD cavity at the surface of the AMCD assembly, were able to capture heparin through synergistic multivalent binding, resulting in an improved neutralizing effect toward both unfractionated heparin and low-molecular-weight heparin compared with protamine in plasma. After capturing heparin, the high binding affinity between heparin and the AMCD

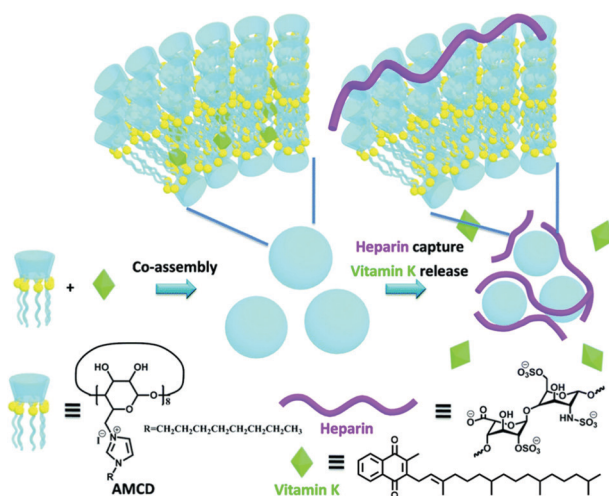


Fig. 8 Schematic illustration of the construction of the AMCD-VK co-assembly and the process of heparin capture and vitamin K release, as well as the molecular structures of AMCD and VK. Reproduced with permission from ref. 274. Copyright 2019, Royal Society of Chemistry.

assembly enables the release of VK. This AMCD-VK co-assembly for synergistic coagulation based on heparin neutralization and VK supplementation represents a promising candidate for clinical use as an anti-heparin coagulant.

It is well known that positively charged composite nanoparticles facilitate more efficient cellular uptake through electrostatic interactions with cell membranes during the *in vivo* drug-delivery process.²⁷⁵ However, they also attract serum components during circulation and interact with non-targeted tissues, resulting in reduced circulation time and toxic effects. Therefore, covering the nanoparticles with anionic polymers can effectively prevent serum inhibition and improve transfection efficiency *in vitro*.²⁷⁶ Recently, Li and co-workers reported extracellular pH (pHe)-responsive surface-charge-switchable polymer/DNA nanoparticles for tumor-triggered enhanced gene delivery (Fig. 9).²⁷⁷ First, the β -CD-oligoethylenimine star cationic polymer (CD-OEI) and plasmid DNA (pDNA) were co-assembled to form positively charged CD-OEI/pDNA polyplex nanoparticles. Subsequently, the CD-OEI/pDNA nanoparticles were coated with various ratios of pHe-responsive anionic block copolymers of PEG and poly(2-aminoethyl methacrylate) (pAEMA) modified with 2,3-dimethylmaleic anhydride (PPD) and pHe-insensitive PEG-pAEMA modified with succinic anhydride (PPS) through electrostatic interactions, thus forming CD-OEI/pDNA/PPD₉ + PPS₁ ternary complexes. At physiological pHe (7.4), the negatively charged CD-OEI/pDNA/PPD₉ + PPS₁

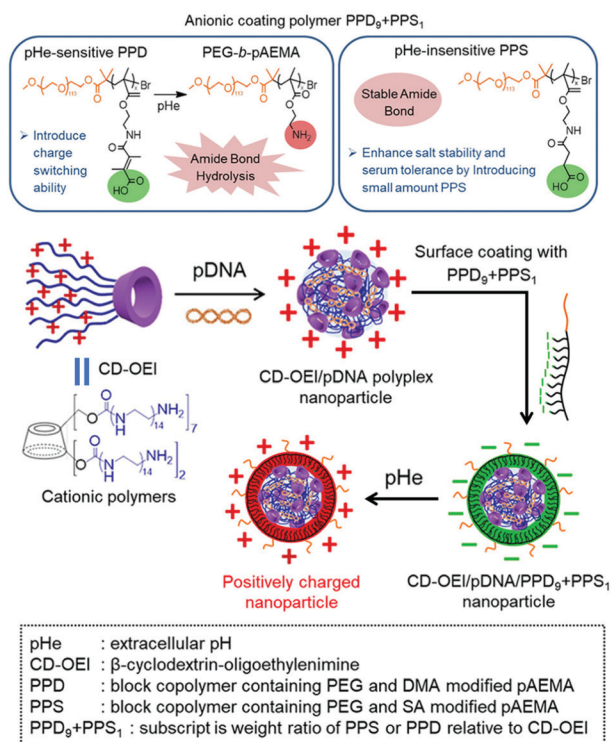


Fig. 9 Schematic illustration of the extracellular pH (pHe)-responsive surface-charge-switchable CD-OEI/pDNA/PPD₉ + PPS₁ gene delivery system (DMA: 2,3-dimethylmaleic anhydride, SA: succinic anhydride). Reproduced with permission from ref. 277. Copyright 2020, American Chemical Society.

ternary complexes could prevent adverse interactions with serum proteins and non-targeted components owing to charge shielding by the anionic surface coating and PEGylation effect. However, as a result of nucleophilic catalysis by the carboxylic acid groups, the amide bonds of PPD were easily hydrolyzed to form the primary amine groups under acidic pHe (<6.8), thus endowing the system with charge-switching ability. In other words, by means of the enhanced permeability and retention effect, the relatively acidic pHe will stimulate the conversion of negative to positive charges when nanoparticles reach the tumor site, thereby promoting cellular uptake.^{278,279} *In vitro* gene transfection experiments showed that the ternary complex enhanced cellular uptake and facilitated gene transfection.

Stimuli-responsive functional groups can also be directly modified on CDs to construct surface charge switchable CDs carriers.²⁸⁰ Liu and co-workers reported two positively charged β -CD-based switchable DNA condensers with seven cationic imidazolium groups and cleavable carboxylic ester linkages linked by different alkyl chains (Fig. 10).²⁸¹ Both of the two positively charged β -CDs can self-aggregate in water due to the presence of the cationic heads and hydrophobic tails, which can be used to condense DNA *via* electrostatic interactions between cationic imidazolium and negatively charged phosphate in DNA. In an alkaline environment, carboxylic esters are hydrolyzed to the carboxylate anions, which changed the electrostatic properties from a highly cationic state to a neutral state, resulting in the loss of DNA condensation ability. In the presence of acetylcholinesterase, hydrophobic moieties with five-carbon alkyl chains exhibit significant resistance to esterase compared to one-carbon alkyl chains because the ester bond is protected by a deeper self-inclusion conformation from hydrolysis. These enzyme- and base-responsive positively charged β -CDs are expected to serve as efficient gene delivery vehicles by controlling charge switching on the CD surface.

Sollogoub and co-workers reported an adamantane-modified bridged β -CD (AdCD) that resisted competing self-inclusion and promoted supramolecular polymerization and cooperative interaction with nucleic acids (Fig. 11).²⁸² In this system, the bridge moiety was attached to β -CD through ammonium groups, which

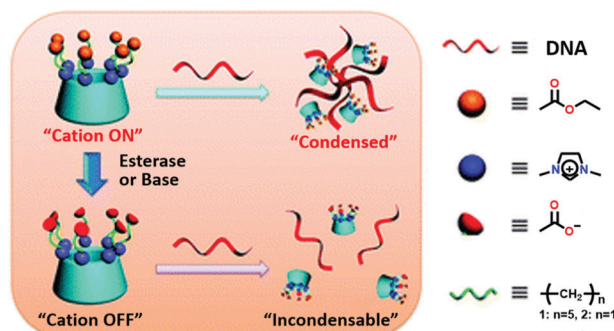


Fig. 10 Structure of the positively charged β -CD-based switchable DNA condenser, and the processes of esterase- and base-responsive systems. Reproduced with permission from ref. 281. Copyright 2015, Royal Society of Chemistry.

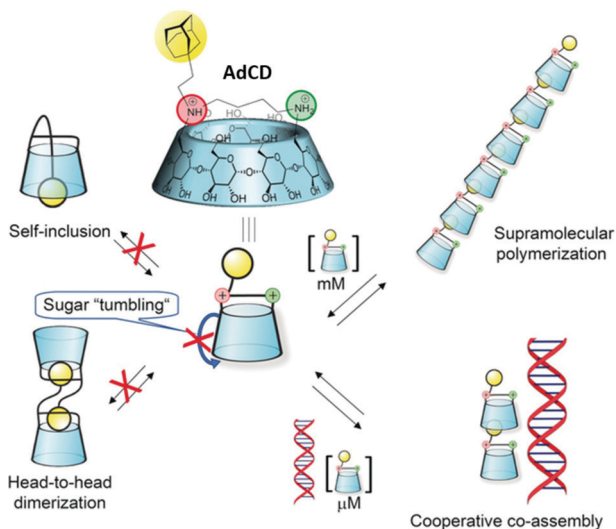


Fig. 11 Chemical structure of bridged functionalized β-CD (AdCD) and the process of supramolecular polymerization, as well as the induction of siRNA transfection based on the cooperative co-assembly strategy. Reproduced with permission from ref. 282. Copyright 2018, Wiley-VCH.

not only increased the solubility but also facilitated the interaction with nucleic acids. Consequently, AdCD could form supramolecular polymers at millimolar concentrations, whereas dimer formation was more favorable at micromolar concentrations. Notably, this assembly of AdCD also occurred in the presence of genomic DNA at micromolar concentrations, leading to efficient compaction of the DNA due to the highly cooperative interactions. In addition, the dimeric form of AdCD effectively prevented the migration of GL3 siRNA. Finally, at AdCD concentrations above 2 mM, the supramolecular polymers effectively induced siRNA transfection. These positively charged CD assemblies provide a novel approach for the application of siRNA transfection in gene silencing.

It is well known that interactions between cell membranes and biomaterials can be regulated by the binding of plasma membrane proteins to specific ligands on the surface of the material.²⁸³ Some studies have indicated the role of integrin–ligand interactions in directing cell fate, but the temporal aspects of this binding must also be considered. For example, Yui and co-workers reported that when a specific ligand (mannose) was introduced into a surface-immobilized receptor (concanavalin A) through a mobile α-CD, the ligand–receptor binding constant was greatly enhanced.^{284,285} The result indicates that the increased mobility of ligand molecules provided by the use of a polyrotaxane backbone can effectively increase the binding constant for the corresponding receptor protein. In 2013, the same group further reported a rapid response of integrin β₁ molecules to an Arg-Gly-Asp (RGD, a specific cell-binding motif) peptide on a dynamic polyrotaxane surface (Fig. 12).²⁸⁶ On account of the interactions between α-CD and PEG, the α-CD molecules could move freely along the PEG backbone due to the formation of a non-covalent inclusion complex. Therefore, in the early stage of material–cell interaction, the introduction of cyclodextrin molecules increases the

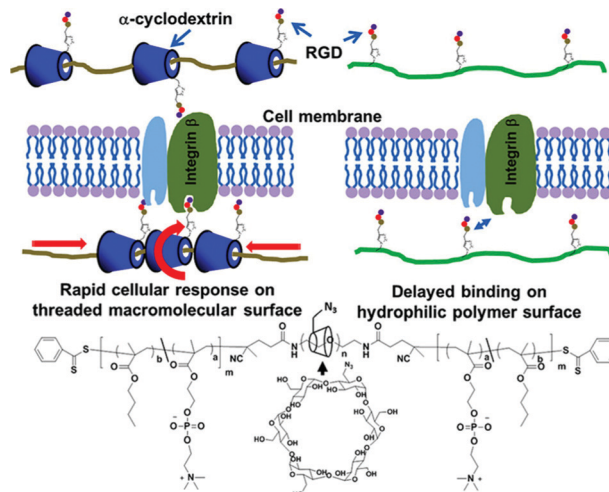


Fig. 12 Schematic illustration of the RGD-containing α-CD-based polyrotaxane (PRX) block copolymer and random copolymers, as well as the regulation of cell–material interactions. Reproduced with permission from ref. 286. Copyright 2013, American Chemical Society.

contact frequency of RGD peptides with specific integrin units on the cell membrane.

Capture of toxic agents

Aside from the targeted delivery of drugs and genes, CD derivatives can also be applied to effectively remove toxic substances and harmful waste products from living organisms and the external environment. Liu and co-workers reported the use of tyramine-modified β-CD derivatives for reversal of bile acid cytotoxicity by supramolecular encapsulation (Fig. 13a).²⁸⁷ The tyramine modification led to efficient inhibition and reversal of the inherent cytotoxicity of deoxycholic acid (DCA). Structurally, the decarboxylation from tyrosine (L-Tyr-β-CD and

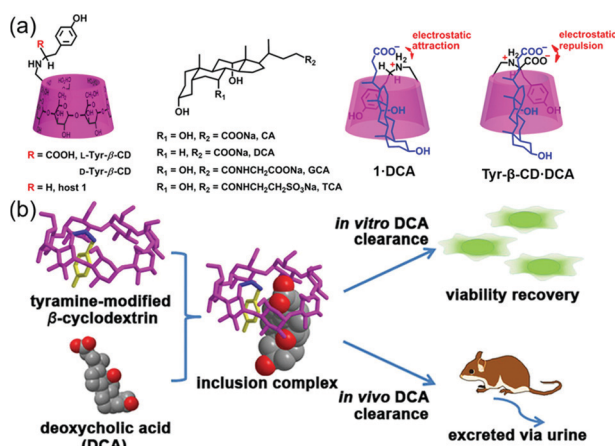


Fig. 13 (a) Chemical structures of tyramine-modified β-CD (1) and Tyr-β-CDs, and four selected bile acids (CA: cholic acid, DCA: deoxycholic acid, GCA: glycocholic acid, and TCA: taurocholic acid), as well as the molecular binding modes for 1-DCA and Tyr-β-CD-DCA complexes. (b) Schematic illustration of the *in vitro* and *in vivo* clearance of DCA from the inclusion complex. Reproduced with permission from ref. 287. Copyright 2017, American Chemical Society.

D-Tyr- β -CD) to tyramine in host **1** was crucial for the mutual electrostatic communication, resulting in greatly enhanced binding affinity and molecular selectivity for bile acids. Thus, the biocompatible host **1** can largely eliminate DCA-mediated cytotoxicity. At the same time, the excess DCA was rapidly excreted from host **1** *via* urinary clearance in rats, thereby facilitating the decrease of the concentration of DCA in the blood (Fig. 13b). This study indicates that the supramolecular encapsulation strategy mediated by functional CD derivatives efficiently modulates cell progression and removes cytotoxic DCA, representing a practical method for preventing or treating diseases involving bile acids.

Adjust optical performance

Positively charged CDs can not only serve as efficient antibacterial compounds but may also enhance the luminescence properties of materials, such as phosphorescence and fluorescence. In contrast to numerous research efforts based on the use of phosphors in crystal lattices or phosphors embedded in rigid matrices,^{288–290} CDs can suppress non-radiative relaxation and shield phosphors from quenchers in the solid state, which enables luminescent molecules to exhibit efficient room-temperature phosphorescence (RTP) emission. For example, Tian and co-workers developed a series of β -CD-modified RTP molecules with multicolor photoluminescence *via* the host-guest strategy.²⁹¹ In this study, four amorphous organic small-molecule compounds displaying efficient RTP emission were conveniently synthesized by attaching phosphor moieties to β -CD (Fig. 14a and c), and the positively charged CDs exhibited the longest lifetimes and the highest quantum yields. The hydrogen bonding between the CD derivatives immobilized the phosphors to suppress non-radiative relaxation and shielded them from quenchers, which enabled these molecules to display efficient RTP emission with reasonable quantum

yields (Fig. 14b). In addition, by using one such CD derivative to encapsulate the amantadine-modified coumarin guest, excellent RTP and fluorescence dual-emission properties were achieved, accompanied by multicolor emission from yellow to purple, as well as white-light emission. This CD-modified lumiphore strategy provides a new approach to construct amorphous metal-free small-molecule RTP materials and organic white-light-emitting materials.

Phosphorescent materials based on the host-guest strategy have been gradually receiving more attention, providing a new approach for constructing organic RTP materials with long-wavelength emission and an extended lifetime.^{292–298} In addition to the ordered packing of two different small molecules, encapsulating guest molecules with macrocyclic hosts to induce phosphorescence emission is very promising.^{299–303} Liu and co-workers reported a light-harvesting phosphorescence energy transfer (PhET) system based on β -CD pseudorotaxane.³⁰⁴ By using the complex of 4-(4-bromophenyl)-pyridine-modified β -CD (CD-PY) and cucurbit[8]uril (CB[8]) as the donor, rhodamine B (RhB) as the acceptor, as well as adamantane-modified hyaluronic acid (HA-ADA) for targeting cancer cells, the authors exploited this multiple supramolecular assembly to achieve efficient phosphorescence-based energy transfer for mitochondria-targeted imaging (Fig. 15a). In this system, the free CD-PY exhibited no efficient RTP emission in aqueous solution, whereas strong RTP emission at 510 nm was observed after complexation with CB[8] through host-guest interactions. The addition of RhB led to an effective light-harvesting PhET process between CB[8]-CD-PY and RhB, with efficient energy transfer and a high antenna effect, resulting in fluorescence emission at

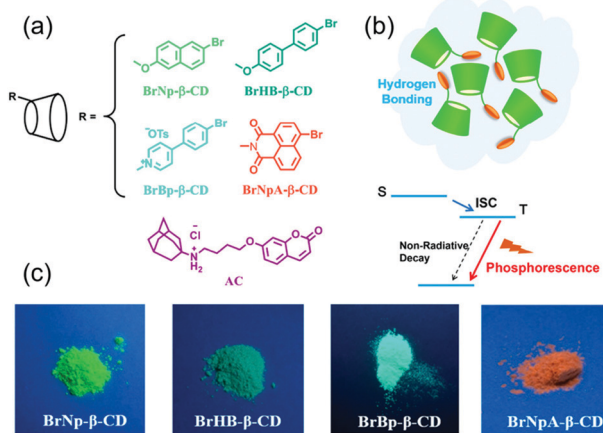


Fig. 14 (a) Chemical structures of four RTP-emissive β -CD derivatives (BrNp- β -CD, BrHB- β -CD, BrBp- β -CD, BrNpA- β -CD) and protonated amantadine-modified coumarin guest (AC). (b) Schematic illustration of the phosphorescence emission. (c) Photographs showing the RTP emission from solid BrNp- β -CD, BrHB- β -CD, and BrBp- β -CD under UV light at 254 nm and solid BrNpA- β -CD under UV light at 365 nm. Reproduced with permission from ref. 291. Copyright 2018, American Chemical Society.

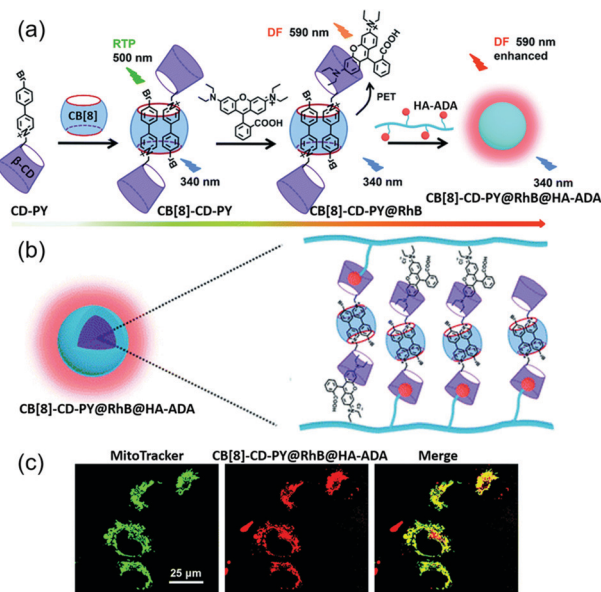


Fig. 15 (a) Schematic illustration of the purely organic light-harvesting phosphorescence energy transfer supramolecular assembly. (b) Possible assembly mode for CB[8]-CD-PY@RhB@HA-ADA. (c) Confocal images of A549 cells co-stained with MitoTracker Green and CB[8]-CD-PY@RhB@HA-ADA. Reproduced with permission from ref. 304. Copyright 2021, Royal Society of Chemistry.

590 nm accompanied by an increased RhB lifetime. Moreover, the addition of HA-ADA to the solution of CB[8]-CD-PY@RhB led to the formation of CB[8]-CD-PY@RhB@HA-ADA nanoparticles (Fig. 15b), further enhancing the fluorescence emission, which was successfully applied in cancer cell mitochondria-targeted imaging (Fig. 15c). This supramolecular assembly strategy based on the light-harvesting phosphorescence energy transfer system has potential applications in cellular imaging.

As a kind of smart rare-earth luminescent material, supramolecular assemblies based on positively charged CDs can also be achieved using photocontrolled redox reactions. Recently, Liu and co-workers reported a lanthanide luminescence supramolecular switch based on the positively charged β -CD and photoreactive ammonium molybdate.³⁰⁵ The lanthanide-containing supramolecular assemblies were constructed from mono-(6-ethylenediamine-6-deoxy)- β -cyclodextrin (ECD) and ammonium molybdate ($(\text{NH}_4)_6\text{Mo}_7\text{O}_{24}$, Mo_7) and further transformed into ternary assemblies with polyoxometalate $\text{Na}_9[\text{XW}_{10}\text{O}_{36}]\cdot 32\text{H}_2\text{O}$ (X-POM, X = Eu or Dy) (Fig. 16a). In this system, although ammonium molybdate tetrahydrate, as an oppositely charged polyanionic polyoxometalate, has reversible photochromic properties and high water solubility, it could not easily self-aggregate in the absence of other components. However, in the presence of the protonated ECD, the negatively charged Mo_7 effectively formed aggregates *via* electrostatic interactions, which brought the effect of shielding oxygen and led to a rapid and effective photoreduction process of $\text{Mo}_7(\text{VI})$. Upon the addition of X-POM to this secondary assembly, high Förster resonance energy transfer (FRET) efficiency between X-POM and $\text{Mo}_7(\text{VI})$ was observed, accompanied by fluorescence quenching during the photoreduction process. Meanwhile, the oxidation process of $\text{Mo}_7(\text{VI})$ rapidly occurred upon heating, allowing the recovery of X-POM fluorescence. Exploitation of these characteristics permitted the encryption and decryption of two-dimensionally encoded information under UV light and heating (Fig. 16b). These positively charged β -CD-mediated

supramolecular assemblies can not only tune the lanthanide luminescence, but can also greatly improve the luminescence performance.

Molecular recognition

In molecular recognition and imaging, the detection step can be accomplished by monitoring changes in luminescence, color, or an electronic signal,^{306–309} and activatable chemical sensors have emerged as an important research topic in organic supramolecular chemistry. Here, CDs modified with positively charged functional groups can serve as excellent supramolecular optical probes for the simple and sensitive detection of a wide variety of analytes that cannot be detected by traditional methods, especially when they occur in extremely complex environments such as biological systems.^{310–313} Introducing small-molecule fluorescent probes into CDs can not only provide highly efficient molecular recognition capability but also endow the fluorescent probes with excellent biocompatibility.^{314–317} Pu and co-workers reported the use of real-time near-infrared fluorescence (NIRF) imaging and urinalysis for the detection of bladder cancer.³¹⁸ The authors prepared a fluorescent macromolecular reporter (CyP1) composed of a specific biomarker-reactive group sensitive to aminopeptidase N (APN), a hemicyanine-based NIRF signaling moiety, and (2-hydroxypropyl)- β -cyclodextrin (HP- β -CD) (Fig. 17a).

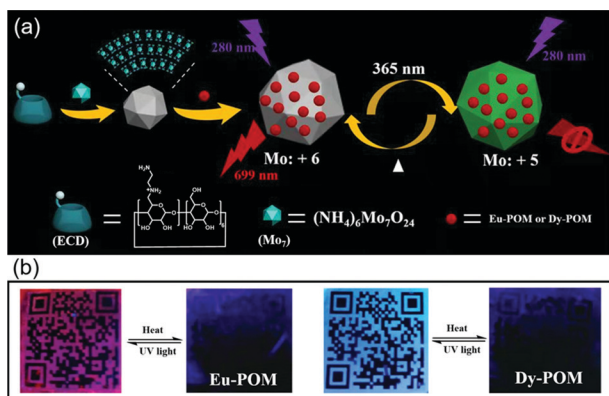


Fig. 16 (a) Lanthanide luminescence supramolecular switch construction based on protonated ethylenediamine β -CD and ammonium molybdate tetrahydrate (Mo_7). (b) Photographs of Eu-POM and Dy-POM with supramolecular hydrogels before and after UV irradiation at 365 nm and their reversibility after heating. Reproduced with permission from ref. 305. Copyright 2021, American Chemical Society.

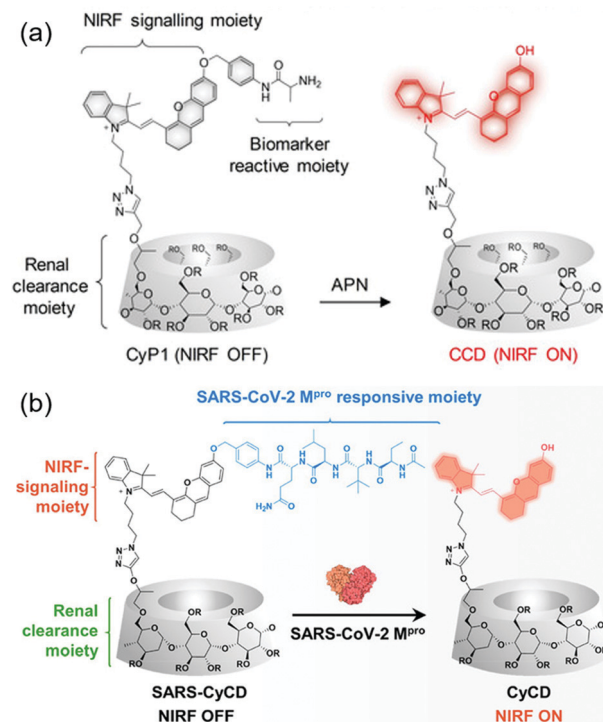


Fig. 17 (a) Schematic illustration of the renal-clearable macromolecular reporter (CyP1) in response to aminopeptidase N (APN) for NIRF imaging, and the chemical structures of CyP1 ($\text{R}=\text{H}$ or $\text{CH}_2\text{CHOHCH}_3$) and its activated form (CCD). Reproduced with permission from ref. 318. Copyright 2019, Wiley-VCH. (b) Scheme depicting the detection of SARS-CoV-2 *via* an M^{pro} -activatable NIRF probe (SARS-CyCD), and the chemical structures of SARS-CyCD ($\text{R}=\text{H}$ or $\text{CH}_2\text{CHOHCH}_3$) and its activated form (CyCD). Reproduced with permission from ref. 319. Copyright 2021, American Chemical Society.

Following the systemic administration of CyP1 to living mice, the reporter was specifically excreted by the kidneys and temporarily accumulated in the bladder, and the detection of bladder cancer was observed by NIRF signaling after reacting with APN. Meanwhile, on account of the presence of the common renal clearance moiety HP- β -CD, CyP1 displayed high renal clearance (approximately 94% of the injection dosage at 24 h post-injection). In addition, CyP1 can also be used in optical urinalysis, allowing *ex vivo* tracking of tumor progression for therapeutic evaluation. Therefore, CyP1 shows great potential for real-time monitoring of bladder cancer in preclinical settings and point-of-care diagnosis.

Recently, the same authors expanded this strategy by developing a renal-clearable molecular optical probe for protease-activatable NIRF imaging and urinalysis of SARS-CoV-2.³¹⁹ Because the SARS-CoV-2 main protease (M^{Pro}) is one of the key coronavirus proteases in viral polypeptide processing, a related M^{Pro} peptide substrate (*N*-acetyl-Abu-Tle-Leu-Gln(Trt)-OH) was selected as the biomarker for signal activation, and this was conjugated to an NIRF hemicyanine fluorophore-modified HP- β -CD to synthesize SARS-CyCD (Fig. 17b). *In vitro* experiments revealed that the “on” state of SARS-CyCD displayed 50-fold enhanced fluorescence at 710 nm toward SARS-CoV-2 M^{Pro} in addition to excellent enzyme specificity. Following intratracheal administration into the lungs of live mice, a strong NIRF signal was observed in the lungs of SARS-CoV-2 M^{Pro} -positive mice. In addition, because of its good renal clearance, activated CyCD was excreted into the urine for optical urinalysis of SARS-CoV-2, avoiding first-pass metabolism and displaying good bioavailability in the lungs. This work has great potential for preclinical high-throughput drug screening and clinical diagnosis of respiratory viral infections.

Supramolecular catalysis

Supramolecular assembly also provides a facile approach for developing catalytic systems, and has been widely applied in selective catalysis, modulation of catalytic rates, and photo-switchable catalytic activity.^{320–323} Positively charged CDs can play an important role in supramolecular catalysts. Liu and co-workers reported a supramolecular catalytic system comprising polycationic α -CD (6-*Iz*- α -CD) and citrate-stabilized gold nanoparticles (AuNPs) for selective catalysis and glucose recognition (Fig. 18).³²⁴ The positive charges of the imidazolium salts on the α -CD surface enabled effective assembly with the negatively charged citrate groups through electrostatic interactions. Meanwhile, the α -CD cavity was the main channel through which the substrate could make contact with the AuNP surface to undergo catalytic reactions. Taking advantage of the feature that AuNPs can catalyze the conversion of glucose into gluconic acid and hydrogen peroxide (H_2O_2), *L*-glucose can selectively enter the cavity of α -CD, contact with the catalytic center of AuNPs and undergo catalytic reactions to give rise to *L*-sodium gluconate. In contrast, the catalytic reaction of *D*-glucose is very inefficient. After that, upon the addition of azobenzene-modified diphenylalanine (Azo-FF) as a guest competitor, *trans*-Azo-FF could compete with the *L*-glucose for the cavity position, making

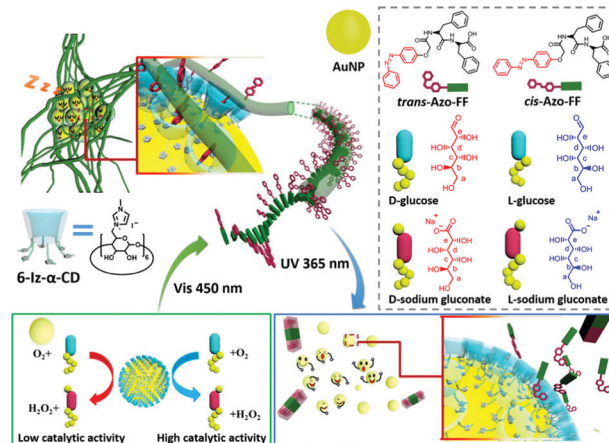


Fig. 18 Schematic illustration of AuNP@6-*Iz*- α -CD assemblies for photo-controlled glucose catalysis and chiral recognition. Reproduced with permission from ref. 324. Copyright 2021, Wiley-VCH.

the catalytic activity of the catalytic center dormant. Interestingly, the good photoisomerization performance of Azo-FF and the change of its photocontrolled morphology endowed the supramolecular assembly with precise optical adjustment of the catalytic activity. In addition, using the supramolecular catalytic system combined with the color reaction process of 3,3',5,5'-tetramethylbenzidine, various chiral monosaccharides could be colorimetrically distinguished in a short time.

Regulation of dimerization

The [4+4] photocyclodimerization of 2-anthracenecarboxylic acid (AC) is a widely studied supramolecular light-induced chiral reaction that typically yields [9,10:9',10']cyclodimers.^{325,326} As preferred chiral host compounds, γ -CD derivatives can form 1:2 host-guest complexes with AC, significantly accelerating the halodimerization and increasing the HT/HH ratio (Fig. 19a).^{327–331} Recently, Yang and co-workers reported pH-controlled chirality inversion in the enantiodifferentiating photocyclodimerization of AC mediated by different γ -CD derivatives.³³² Three γ -CD derivatives were synthesized by the introduction of amino (6), bis-quinoline (7), and *N*-methylated bis-quinoline (8) moieties (Fig. 19b). Compared with γ -CD (5) and (6), the bis-quinoline chromophore (7) greatly facilitated the initial binding of AC molecules because one of the bis-quinoline was encapsulated in the cavity (Fig. 19c). Under acidic conditions, AC became more soluble by complexation with the host through hydrophobic interactions and hydrogen-bonding interactions between bis-quinoline and the carboxylic acid moiety, providing the HH cyclodimer 3 with an enantiomeric excess (ee) of 25.2%. In contrast, at alkaline pH, the interaction between the carboxylate moiety of AC and 7 changed/reversed its interaction position and provided the enantiomeric HH cyclodimer (3) with an ee value of -64.4%. In the case of host 8, the positively charged nitrogen atom in the bis-quinoline chromophore complex exhibited stronger electrostatic interactions with the AC anion at basic pH than at acidic pH, therefore affording marked chirality reversal from

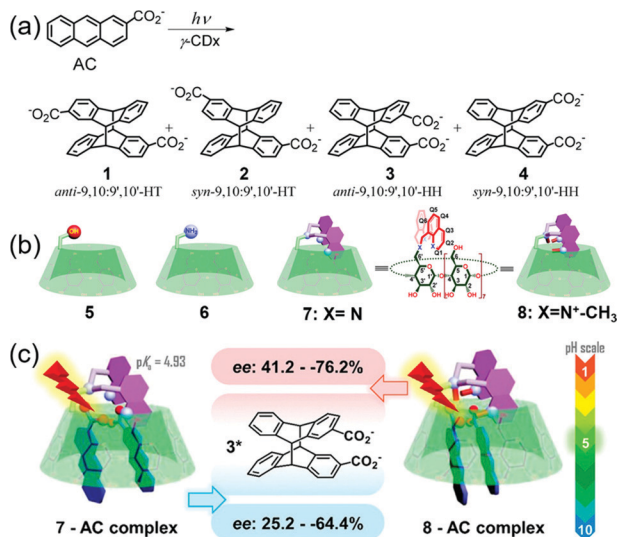


Fig. 19 (a) [9,10:9',10'] Cyclodimers (**1–4**) resulting from the photodimerization of 2-anthracenecarboxylic acid (AC) with γ -CD derivatives. (b) Structures of supramolecular hosts (**5–8**). (c) pH-controlled chirality inversion mediated by γ -CD derivatives in the enantiodifferentiating photocyclodimerization of AC. Reproduced with permission from ref. 332. Copyright 2020, American Chemical Society.

41.2% to -76.2% . These results open up a new approach for manipulating supramolecular chirality using CD derivatives.

Construction of hydrogels

Redox responsiveness can also be applied to the development of stimuli-responsive supramolecular hydrogels. The introduction of 1:1 host–guest inclusion complexes into hydrogels is a popular design strategy to achieve changes in crosslink density, such as the combination of α -CD and azobenzene or β -CD and ferrocene.^{333,334} In an effort to realize faster and more pronounced deformation characteristics, Yamaguchi and co-workers reported redox-responsive supramolecular polymeric networks based on double-threaded inclusion complexes.³³⁵ CDs and a viologen bearing an alkyl linker (VC11) were employed as the host and guest units, respectively (Fig. 20a). The obtained γ CD-VC11 hydrogel crosslinked by a γ -CD encapsulates two VC11 molecules, exhibiting faster and more pronounced deformation behavior than the α CD-VC11 and β CD-VC11 hydrogels crosslinked based on the 1:1 complex. According to the proposed hydrogel deformation mechanism, the γ -CD moiety and the two VC11 residues formed a 1:2 inclusion complex to afford a double-threaded structure in the oxidized state, and the reduction of the viologen units triggered the dimerization of their monocation radicals *via* cation– π electrostatic interactions, which increased the cross-linking density of the polymer network (Fig. 20b). In contrast, the small cavities of α - and β -CD were unable to stabilize the radical cation dimers, while the steric hindrance of α - and β -CD was not conducive to promoting their formation. In this work, the introduction of a 1:2 host–guest complex mechanism into the hydrogel provided the basis for the realization of novel stimuli-responsive materials.

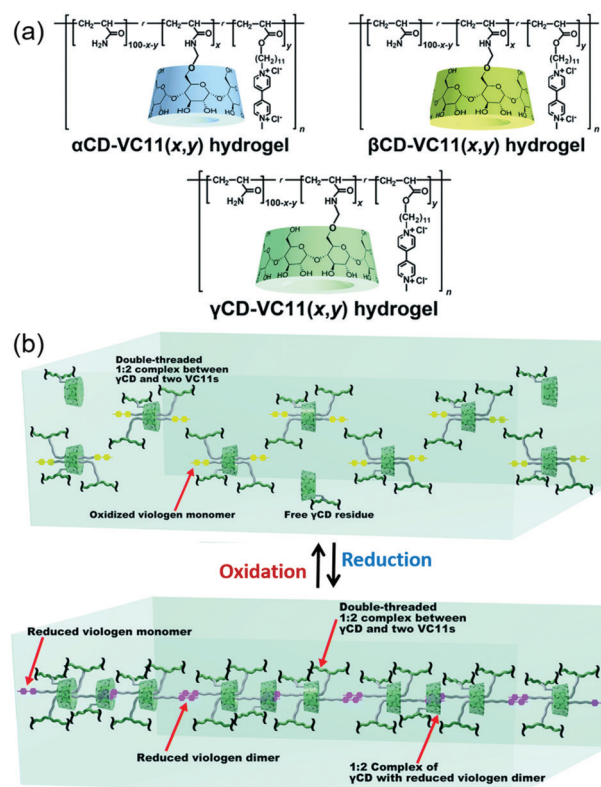


Fig. 20 (a) Chemical structures of the supramolecular α CD-VC11(x, y), β CD-VC11(x, y), and γ CD-VC11(x, y) host–guest hydrogels. (b) Schematic illustrations of the association/dissociation behavior of the γ CD-VC11(x, y) hydrogels leading to large volume changes. Green ribbons: polyacrylamide main chains; green truncated cones: γ -CD units; yellow circles: oxidized viologen moieties in VC11; purple circles: reduced viologen moieties in VC11; gray ribbons: undecyl linkers in VC11. Reproduced with permission from ref. 335. Copyright 2020, Royal Society of Chemistry.

Moreover, by exploiting the host–guest interactions between β -CD and PPG chains to form pseudopolyrotaxanes (PPRs), Liu and co-workers developed a self-supported supramolecular hydrogel based on the hierarchical organic–inorganic hybridization between a LAPONITE[®] matrix and β -CD-based PPRs.³³⁶ In terms of the structure, β -CD was modified with surface guanidinium cations and then assembled on the PPG chains through host–guest interactions, resulting in the distribution of guanidine groups along the axis of the PPG chain (Fig. 21a). This system was conducive to the realization of multivalent interactions between the β -CD-based pseudopolyrotaxanes and the LAPONITE[®] matrix (Fig. 21b). The mechanical properties of the resulting hydrogels could be adjusted by tuning the molecular weight of the polymer chains. This highly swollen supramolecular hydrogel system exhibited good mechanical strength, high water content, and self-healing properties, providing a feasible method for the preparation of organic–inorganic hybrids.

Construction of pseudorotaxanes

Sollogoub and co-workers reported the achievement of precise rate control over pseudorotaxane dethreading using pH-responsive amino-functionalized CDs (Fig. 22).³³⁷ This system consisted

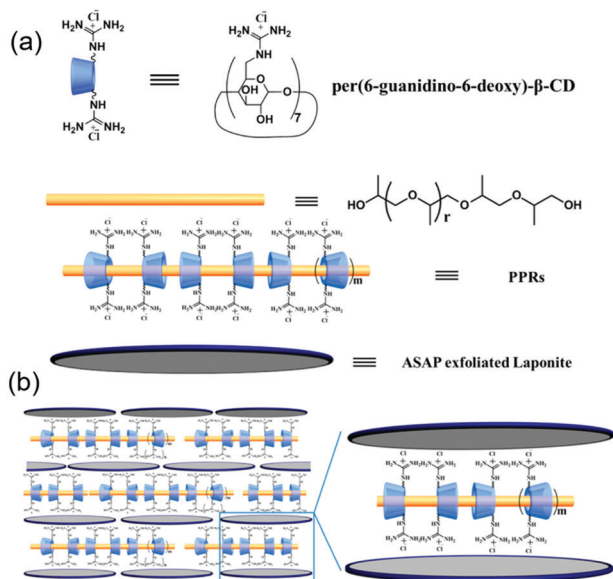


Fig. 21 (a) Schematic illustrations and molecular structures of per(6-guanidino-6-deoxy)- β -CD, PPG chains, ASAP-exfoliated LAPONITE[®], and pseudopolyrotaxanes (PPRs). (b) Assembly mode of ASAP-exfoliated LAPONITE[®] and PPRs. Reproduced with permission from ref. 336. Copyright 2017, American Chemical Society.

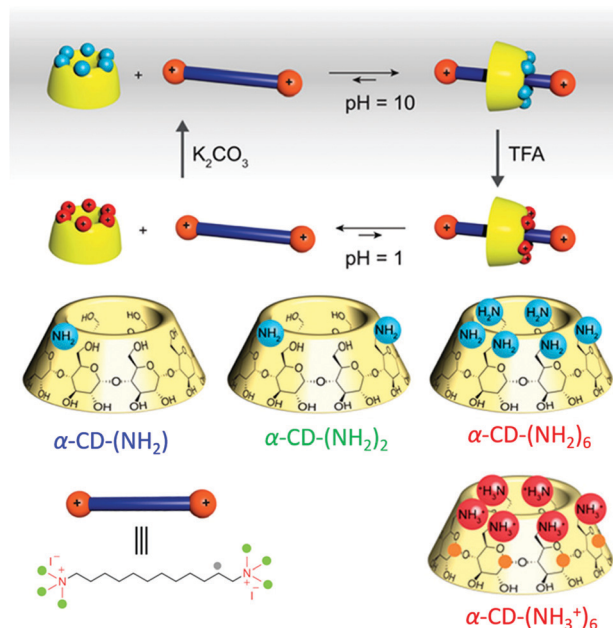


Fig. 22 Chemical structures of amine-functionalized CDs and the principle of pH-controlled threading of functionalized CDs. Reproduced with permission from ref. 337. Copyright 2021, American Chemical Society.

of a cationic molecular axle terminated at both ends by ammonium moieties acting as pseudostoppers and α -CD units functionalized with one α -CD-(NH₂), two α -CD-(NH₂)₂, or six α -CD-(NH₂)₆ amino groups as pH-responsive ring components. In this system, the trimethylammonium plugs were selected to ensure water solubility of the shaft and slow down the threading

process. At pH 10, α -CD-(NH₂), α -CD-(NH₂)₂, and α -CD-(NH₂)₆ threaded slightly faster than native α -CD, with α -CD-(NH₂)₆ exhibiting the highest threading speed. This may have been attributable to the functionalization of α -CD destabilizing the hydrogen-bonding network, making these α -CDs more flexible, lowering the threading energy barrier and increasing the threading rate. When trifluoroacetic acid (TFA) was added to solutions of the pseudorotaxanes based on amine-functionalized α -CDs to obtain pH 1 solutions, faster dethreading was observed for α -CD-(NH₂)₆, while α -CD-(NH₂) and α -CD-(NH₂)₂ displayed much lower dethreading speeds. The different dethreading rates were ascribed to differences in the number of protonated amino groups on α -CD-(NH₂), α -CD-(NH₂)₂, and α -CD-(NH₂)₆. Because the stimulus leading to dissociation is applied directly to the α -CD rather than the axle, this method of controlling the α -CD dethreading rate by changing the degree of substitution is remarkable. Furthermore, reversible α -CD-(NH₂)₆ threading/dethreading can be achieved by the sequential addition of potassium carbonate and TFA. Therefore, this system allowed manipulation of the stimulation directly on the macrocycle to control the rate of switching, providing a basis for active transport mechanisms in complex molecular machines.

Topological morphology regulation

Using the photoisomerization of Azo units, the morphology of supramolecular assemblies formed by positively charged CDs can be regulated in a photocontrolled manner. For example, Wu and co-workers reported the chiral self-assembly and reversible photomodulation of polyoxometalate complexes based on a pyridinium-containing β -CD (β -CD-Py) and an Azo-grafted POM (Azo-POM).³³⁸ Structurally, two Azo groups were chemically bonded on the two sides of the POM and two quaternized β -CD units served as the counterions, thus providing the opportunity to form self-crosslinking supramolecular structures (Fig. 23a). The *cis* isomer of CD-Azo-POM exhibited irregular nanofiber structures after UV light irradiation. In contrast, after aging in the dark to afford the *trans* isomer, micrometer-scale, right-handed twisted assemblies were formed with a well-defined layered structure (Fig. 23b). Interestingly, the inner chirality of the CD cavity was able to transfer to the

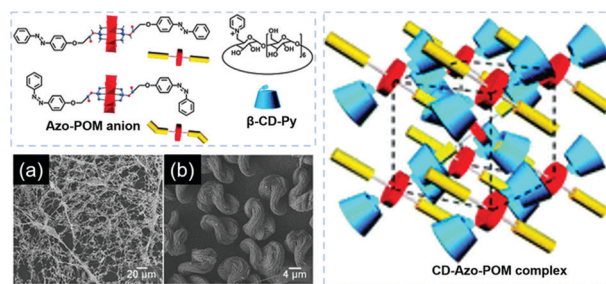


Fig. 23 Schematic illustrations and molecular structures of the Azo-POM anion in its *trans* and *cis* states and the β -CD-Py cation, as well as a possible packing model for the CD-Azo-POM complex. Morphological change of (I) CD-Azo-POM after initial UV light irradiation and (II) aging in the dark. Reproduced with permission from ref. 338. Copyright 2013, Royal Society of Chemistry.

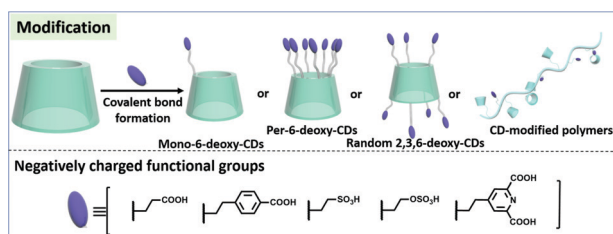
POM-linked Azo units through host-guest recognition and was then amplified to the entire assembly through orthogonal self-crosslinking, resulting in the right-handed twisted structure. Furthermore, the morphology of the assemblies could be regulated between the right-hand twisted and irregular nanofiber structures by isomerization of the Azo units. Thus, this supramolecular assembly strategy achieved chirality transfer and amplification from the host to the host-guest assembly.

2.2 Assemblies of negatively charged CDs and guests

In contrast to positively charged CDs, depending on the size of the functional groups, negatively charged CDs can not only wrap their negatively charged functional groups to afford self-inclusion complexes but also wrap the hydrophobic part to form intermolecular inclusion complexes. The most commonly encountered negatively charged functional groups are carboxylates and sulfonates, and CDs may also be attached to negatively charged polymers such as hyaluronic acid and carboxymethyl cellulose (Scheme 2). In terms of the degree of substitution, research into negatively charged CDs has primarily focused on multisubstituted derivatives, except for those studies involving the attachment of CDs to negatively charged polymers.

Antiviral materials

As early as 1990, sulfonated CDs were reported to exhibit antiviral activity against HIV,^{339–342} and this has been explored in more detail recently. Tapparel and co-workers modified CD scaffolds with various side chains containing sulfonic acid moieties to obtain highly efficient broad-spectrum virucidal compounds (Fig. 24a).¹¹³ CD1 strongly inhibited the growth of herpes simplex virus type 2 (HSV-2), whereas CD2 displayed no significant activity (Fig. 24b). To alter the properties of the linker, the sodium undec-10-enesulfonate moiety was replaced by an aromatic linker of similar overall length (CD3), which led to an enhanced antiviral effect but significantly reduced virucidal activity compared with CD1 (Fig. 24c), demonstrating the role of long flexible linkers in the mode of virucidal action. CD1 was found to exhibit an irreversible mechanism of action, which is associated with a high barrier to viral resistance, along with broad-spectrum *in vitro* virucidal effects at micromolar concentrations against multiple viral pathogens, including HSV, respiratory syncytial virus (RSV), dengue virus, and Zika virus. Furthermore, it was demonstrated to be effective *in vitro* against laboratory and clinical RSV and HSV-2 strains in respiratory and vaginal tissue culture models, respectively. In



Scheme 2 Schematic diagram of various types of negatively charged CDs and structures of typical negatively charged functional groups.

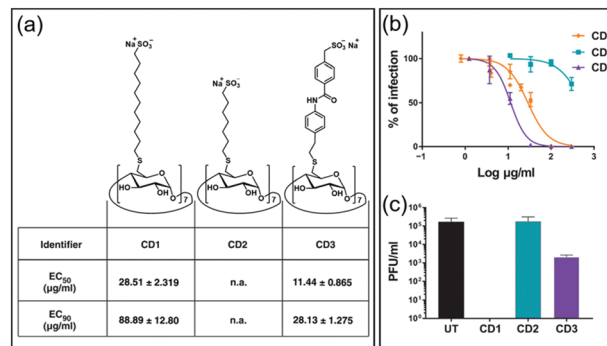


Fig. 24 (a) Chemical structures of CD1, CD2, and CD3 and relative effective concentrations for inhibition of HSV-2 growth. (b) Dose-response assay results for CD1, CD2, and CD3 in Vero cells. (c) Virucidal assay results. UT, untreated; n.a., not assessable. Reproduced with permission from ref. 113. Copyright 2020, AAAS.

addition, it was also effective when administered to mice prior to intravaginal HSV-2 vaccination and passed a mutational resistance test where the currently available anti-HSV drug (acyclovir) fails. Therefore, the reported sulfonated CDs may represent effective tools against a variety of viral infections.

Inhibit protein fibrosis

Sulfonated CDs may also have potential applications in inhibiting the fibrillation process and rupture of mature amyloid fibrils/plaques to combat neurodegenerative diseases. Mohanty and co-workers reported the use of commercial sulfobutylether- β -CD (SBE₇- β -CD) for the inhibition and destruction of amyloid fibrils (Fig. 25).¹¹⁴ The fibrotic process was monitored using the dye thioflavin T (ThT), which specifically interacts/binds with cavities in protein fibrils, thus causing the excited state to become more planar and rigid and leading to huge enhancements in its fluorescence emission and lifetime. The experimental results revealed that the SBE₇- β -CD macrocycle interacts with amino acid residues such as the aromatic amino acid tryptophan in proteins such as insulin and lysozyme *via* host-guest interactions, preventing the conversion of the native α -helix to the β -sheet conformer and effectively inhibiting its fibril formation, accompanied by a significant decrease in fluorescence intensity. A possible mechanism for this is interaction between

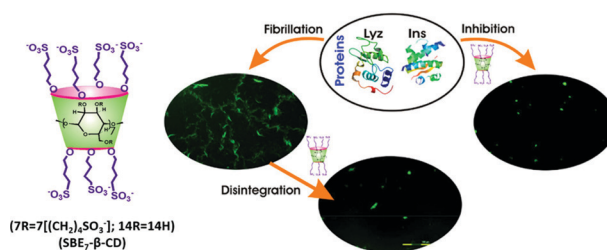


Fig. 25 Chemical structure of sulfobutylether- β -CD (SBE₇- β -CD) and schematic illustration of the fibril inhibition and disintegration pathways for lysozyme (Lyz) and insulin (Ins) proteins in the presence of SBE₇- β -CD. Reproduced with permission from ref. 114. Copyright 2017, American Chemical Society.

the positive surface charge of the fibrils and the negatively charged SO_3^- groups of SBE $_7$ - β -CD destabilizing the extended fibril structure to form soluble or fine particles. In addition, SBE $_7$ - β -CD does not introduce any additional toxicity in the system, thus making it a promising therapeutic agent for amyloidosis.

Delivery system

Aside from their antiviral activity and ability to inhibit protein fibrosis, sulfonated CDs can also assemble with positively charged prodrugs *via* electrostatic interactions to achieve effective drug delivery and controllable release. For example, Liu and co-workers reported an enzyme-responsive sulfato- β -CD (SCD)/prodrug supramolecular assembly for controlled release of chlorambucil (Cbl) (Fig. 26).³⁴³ In this work, the water-insoluble Cbl was modified with an quaternary ammonium group through the enzymatically removable ester bond to obtain the prodrug QA-Cbl. As a negatively charged macrocyclic receptor, SCD greatly reduced the critical aggregation concentration of QA-Cbl. Upon addition of butyrylcholinesterase (BChE), QA-Cbl underwent cleavage to afford Cbl and choline, resulting in the dissipation of the SCD/QA-Cbl supramolecular assembly. Compared with traditional drug-encapsulation methods, this supramolecular drug-delivery system directly uses the prodrug as the building block of supramolecular assembly to realize high drug loading efficiency, thus providing a feasible and practical approach for achieving controlled drug release.

Sulfonated CDs can also assemble with positively charged polymers to form stable supramolecular assemblies,¹³⁷ especially for loading oral drugs. Liu and co-workers reported a supramolecular assembly based on an SCD and chitosan for realizing stability in the stomach alongside controlled release in the intestine (Fig. 27).³⁴⁴ The SCD/chitosan assembly exhibited good stability under acidic conditions (pH 5.3) but disassembled under alkaline conditions (pH 10.4), demonstrating its pH responsiveness. This property originates from the influence of pH changes on the degree of protonation of the SCD and/or chitosan. Moreover, the assembly could encapsulate the

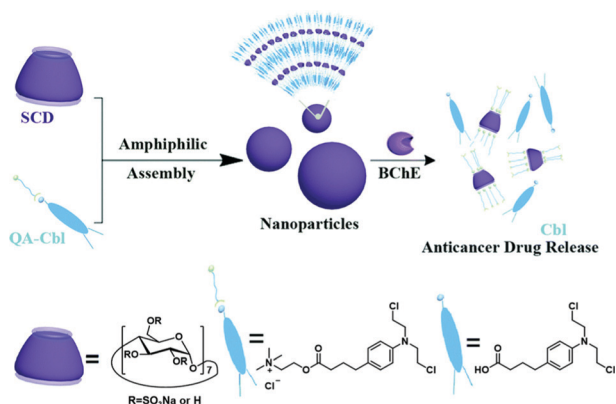


Fig. 26 Schematic illustration of the cholinesterase (BChE)-responsive drug-delivery system (SCD/QA-Cbl) based on SCD and chlorambucil prodrug (QA-Cbl). Reproduced with permission from ref. 343. Copyright 2019, Royal Society of Chemistry.

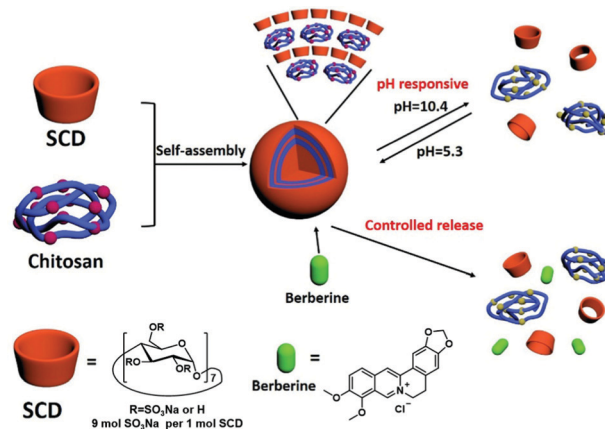


Fig. 27 Construction of an SCD/chitosan supramolecular assembly for pH-responsive encapsulation and release of berberine. Reproduced with permission from ref. 344. Copyright 2018, American Chemical Society.

bacteriostatic drug berberine chloride, and the formed nanoparticles displayed high stability in low-pH environments such as the stomach but released the berberine guest upon moving to high-pH environments such as the intestine, therefore enabling pH-controlled release. This provides these supramolecular nanoparticles with potential applications in the precise release of oral drugs.

In addition to pH-responsive supramolecular assemblies, magnetic-responsive ones have also attracted widespread attention. For instance, Liu and co-workers reported the preparation of supramolecular nanofibers that were sensitive to both magnetism and light for the inhibition of tumor invasion and metastasis.³⁴⁵ These supramolecular nanofibers were composed of β -CD-containing polysaccharides (HACD) multivalently bound to iron oxide magnetic nanoparticles (MNPs) coated with mitochondrion-targeting peptide (MitP), and they could undergo directional aggregation controlled by the magnetic field even in a relatively weak geomagnetic field (Fig. 28a). Furthermore, the formation of nanofibers could be modulated by light irradiation in the presence of arylazopyrazole carboxylate as a competing guest molecule (Fig. 28b). In the presence of a geomagnetic field and photoirradiation, the nanofibers can induce mitochondrial dysfunction and intercellular aggregation, resulting in the specific inhibition of tumor-cell invasion and metastasis *in vivo* (Fig. 28c). Therefore, the geomagnetic- and light-controlled nanofibers may promote the rapid development of effective anticancer therapies.

A synergistic strategy has also been employed to realize efficient anticancer therapy by the co-assembly of hyaluronic acid-grafted CDs and a photosensitizer. Liu and co-workers reported the preparation of β -CD prodrug-based supramolecular nanoparticles (NPs) for highly efficient synergistic cancer therapy.³⁴⁶ The nanoparticles consisted of a disulfide-linked permethyl- β -CD-camptothecin prodrug (PMCD-SS-CPT), an adamantane-modified porphyrin (aPs), as well as triphenylphosphine and β -CD grafted hyaluronic acid (PPh $_3$ -HACD). The aPs first assembled with PMCD-SS-CPT to afford PMCD-SS-CPT/aPs, and the exposed adamantane further co-assembled with PPh $_3$ -HACD to form the NPs (Fig. 29). Compared with 293T normal

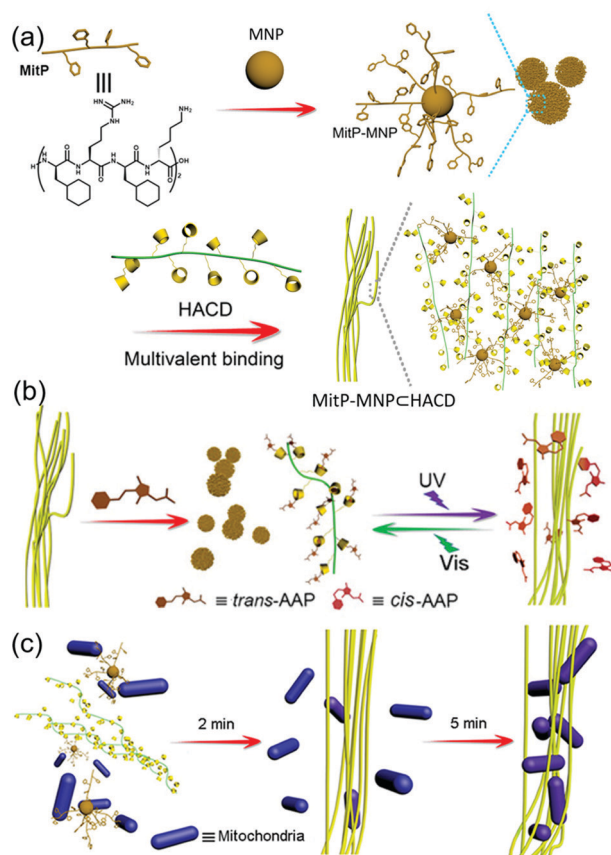


Fig. 28 (a) Schematic illustration of the formation of MitP-MNP=HACD nanofibers based on the multivalent binding between HACD and MitP-MNP. (b) Schematic illustration of the assembly and disassembly of MitP-MNP=HACD nanofibers under UV and visible light in the presence of arylazopyrazole (AAP) carboxylate. (c) Schematic illustration of the mitochondrial aggregation along the direction of the geomagnetic field around MitP-MNP=HACD nanofibers. Reproduced with permission from ref. 345. Copyright 2018, AAAS.

cells, the NPs were more readily taken up by the mitochondria of A549 cancer cells, thereby releasing the active drug CPT *in situ* through the cleavage of the disulfide bonds by overexpressed glutathione. Meanwhile, the porphyrin moieties generated $^1\text{O}_2$ under light irradiation, which seriously impaired the normal mitochondrial function and enhanced the cell death rate in a dose-dependent manner. Thus, this multicomponent supramolecular assembly strategy demonstrates the synergistic effect of chemo-photodynamic therapy in cancer therapy.

Ji and co-workers reported surface-charge-switchable supramolecular nanocarriers for the synergistic photodynamic eradication of biofilms by nitric oxide (NO).³⁴⁷ The supramolecular nanocarrier (α -CD-Ce6-NO-DA) was co-assembled from an α -CD-based NO prodrug (α -CD-NO), a chlorin e6 prodrug (α -CD-Ce6), and the pH-sensitive copolymer PEG-(KLAKLAK)₂-DA *via* host-guest interactions (Fig. 30a). The α -CD-Ce6-NO-DA nanocarriers possessed a negatively charged surface, which is beneficial for long-term circulation in the blood. However, the α -CD-Ce6-NO-DA nanocarriers exhibited a complete charge reversal from negative to positive in an acidic biofilm (pH 5.5), which

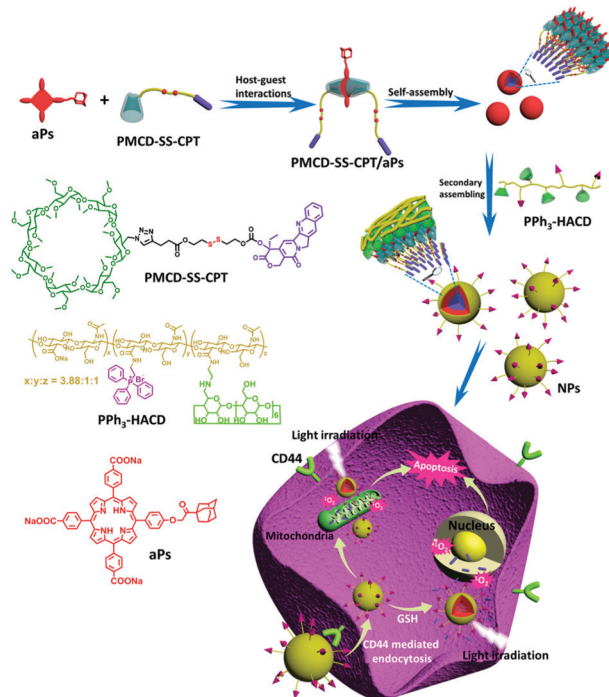


Fig. 29 Schematic illustration of the formation of nanoparticles (NPs) for synergistic chemo-photodynamic cancer therapy based on adamantane-modified porphyrin (aPs), β -CD-modified camptothecin (PMCD-SS-CPT), and hyaluronic acid grafted with triphenylphosphine and β -CD (PPh₃-HACD). Reproduced with permission from ref. 346. Copyright 2020, American Chemical Society.

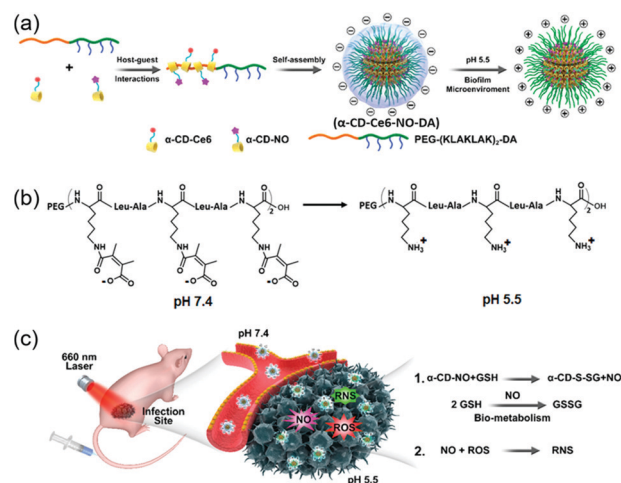


Fig. 30 (a) Schematic illustration of the construction of nanocarriers (α -CD-Ce6-NO-DA). (b) Reaction scheme showing the acid-activated charge reversal of pH-sensitive copolymer PEG-(KLAKLAK)₂-DA at pH 5.5. (c) Mechanism of eradication of methicillin-resistant *S. aureus* biofilm-associated infection *via* synergistic effects between ROS and NO generated by α -CD-Ce6-NO-DA. Reproduced with permission from ref. 347. Copyright 2020, American Chemical Society.

facilitated the efficient penetration of the nanocarriers into the biofilm and their adherence to negatively charged bacterial surfaces. The mechanism of surface-charge reversal originated from the strong electron-withdrawing effect of the carboxyl

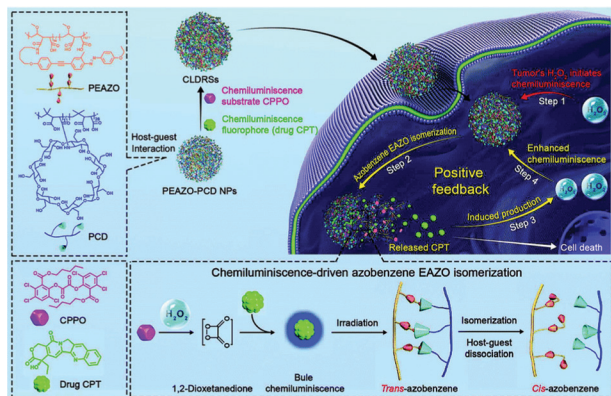


Fig. 31 Chemiluminescence-induced enhanced photoisomerization for a light-controlled drug release system based on *trans*-Azo/ β -CD complexes and its application to light-controlled CPT release for tumor chemotherapy. Reproduced with permission from ref. 348. Copyright 2019, Royal Society of Chemistry.

groups, which led to the facile hydrolysis of the amide bond in an acidic environment (Fig. 30b). After the α -CD-Ce6-NO-DA nanocarriers had penetrated into the biofilm, the GSH-triggered NO release significantly reduced the GSH concentration in the biofilm, which is a good strategy for inhibiting the consumption of ROS by GSH in the photodynamic therapy (PDT) process of Ce6, and this greatly improved the PDT efficiency (Fig. 30c). In addition, the released NO molecules could react with PDT-induced ROS to generate reactive nitrogen species (RNS) with stronger bactericidal ability, further enhancing the PDT efficiency. The surface-charge-switching strategy exploited in this work may offer great possibilities for combating biofilm infections.

Photoisomerization also shows great potential for the controlled release of chemotherapeutic drugs. Recently, Fan and co-workers reported a light-controlled drug release system for tumor chemotherapy based on chemiluminescence-initiated and *in situ* enhanced photoisomerization (Fig. 31).³⁴⁸ The chemiluminescence (CL) substrate peroxyoxalate (CPPO) and a CL fluorophore (CPT) were used as the building blocks for the construction of the CL source. The azobenzene-pendant polymer (PEAZO) and β -CD-pendant polymer (PCD) could self-assemble into nanoparticles (PEAZO-PCD NPs) *via* host-guest interactions, serving as the carrier to encapsulate CPPO and CPT. In tumors, the EAZO group underwent isomerization by the H_2O_2 -activated CL from CPT, thereby triggering the partial dissociation of the carrier and the release of the drug CPT. After that, the released CPT could again act as a H_2O_2 inducer to increase the H_2O_2 levels in the tumor, thus generating a positive-feedback mechanism for sustained drug release and *in situ* enhanced CL. This CL-driven photoisomerization process exhibited good efficiency and target specificity with a high tumor inhibition rate (73%) and no apparent therapeutic side effects *in vivo*, providing key insights for the design of various target-specific tissue-depth-independent photoisomerization-based drug-release systems.

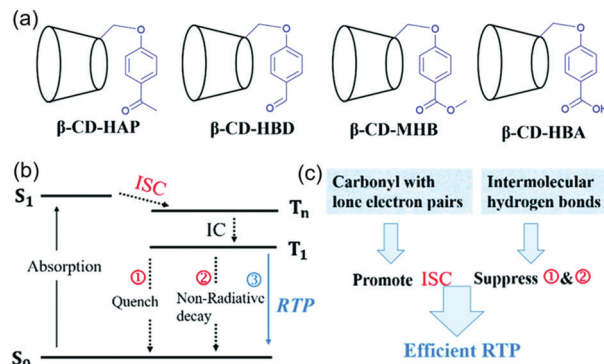


Fig. 32 (a) Chemical structures of four RTP-emissive β -CD derivatives (β -CD-HAP, β -CD-HBD, β -CD-MHB, β -CD-HBA). (b) Radiative and non-radiative processes in the Jablonski diagram. (c) Proposed mechanism for the carboxyl group and hydrogen bond enhanced RTP materials. Reproduced with permission from ref. 349. Copyright 2019, Royal Society of Chemistry.

Adjust optical performance

In the construction of RTP materials, Ma and co-workers reported heavy-atom-free amorphous materials based on β -CD derivatives featuring simple preparation and highly efficient RTP emission.³⁴⁹ Four β -CD derivatives were synthesized by attaching methyl 4-hydroxybenzoate (MHB), 4-hydroxyacetophenone (HAP), 4-hydroxybenzaldehyde (HBD), or 4-hydroxybenzoic acid (HBA) to the primary side of β -CD (Fig. 32a). The hydrogen-bonding network resulting from the presence of β -CD effectively inhibited the non-radiative decay of the excited triplet state, suppressed the vibration and rotation of the phosphor, and shielded the phosphorescence moiety from the quencher (Fig. 32b). These four carbonyl-containing compounds were selected as the unique electronic arrangement of the carbonyl moiety can promote intersystem crossing, and this is necessary for RTP emission that leads to improved phosphorescence quantum yield (Fig. 32c). Among the four compounds, β -CD-HBA exhibited the highest phosphorescence quantum yield and the longest lifetime, which was presumably attributable to the presence of the carboxyl group. These RTP materials are easy to prepare and process, and this makes them more favorable than the conventional crystalline state for application in areas such as bioimaging, organic light-emitting diodes, and anti-counterfeiting.

Recently, artificial light-harvesting systems with strong antenna effects have been widely applied in various fields, including bioimaging, photocatalysis, and molecular recognition.^{350–355} Among them, the construction of light-harvesting systems by means of electrostatic interactions is a simple and fast method that can realize strong antenna effects and efficient energy transfer.^{356,357} Liu and co-workers reported a highly efficient artificial light-harvesting energy-transfer system with an ultrahigh antenna effect based on SCD.³⁵⁸ In this system, SCD induced the oligo(phenylenevinylene) derivative (OPV-I) to assemble into nanoparticles, accompanied by an obvious fluorescence enhancement (Fig. 33). Furthermore, simply mixing the acceptor Nile red (NiR) into a solution of the OPV-I/SCD assembly resulted in a highly efficient FRET process between the two components, with a strong

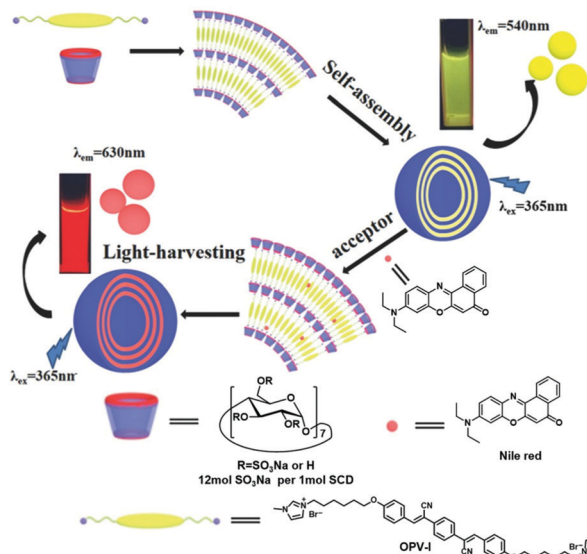


Fig. 33 Construction of an artificial light-harvesting system based on the oligo(phenylenevinylene) derivative (OPV-I), sulfato- β -cyclodextrin (SCD), and Nile red. Reproduced with permission from ref. 358. Copyright 2017, Wiley-VCH.

antenna effect (up to 32.5) and a high donor/acceptor ratio (up to 125 : 1). This study represents a good example of the combination of aggregation-induced emission and assembly-induced luminescence strategies.

Subsequently, the same authors reported an aggregation-induced excimer emission light-harvesting supramolecular assembly in aqueous solution based on polyanionic γ -cyclodextrin (COONa- γ -CD), a pyrene derivative (PYC12), and NiR (Fig. 34).³⁵⁹ Benefiting from the aggregation of PYC12 induced by COONa- γ -CD, the fluorescence could be modulated from the monomer state to the assembled state, displaying enhanced excimer emission upon aggregation accompanied by a large red-shift of approximately 100 nm. Next, NiR as an energy acceptor was loaded into the PYC12/COONa- γ -CD assembly, leading to an efficient energy-transfer process from PYC12/COONa- γ -CD to NiR. When the donor/acceptor ratio was 160 : 1, the energy-transfer efficiency was 83%. In addition, a photoresponsive diarylethylene derivative (DAE) could be loaded into the PYC12/COONa- γ -CD/NiR assembly as an energy acceptor, which endowed the light-harvesting system with excellent photocontrolled energy-transfer performance, and this process could be effectively adjusted under UV and visible light irradiation.

Molecular recognition

In the field of molecular recognition, Pettiwala and Singh reported a ratiometric sensor based on SCD and ThT for the selective detection and discrimination of lysine and arginine (Fig. 35a).³⁶⁰ In this system, ThT acted as a guest molecule to form H-aggregates on the surface of the polyanionic supramolecular host SCD *via* electrostatic interactions to construct the supramolecular assembly. Upon lysine- and arginine-induced dissociation of this supramolecular assembly, the fluorescence

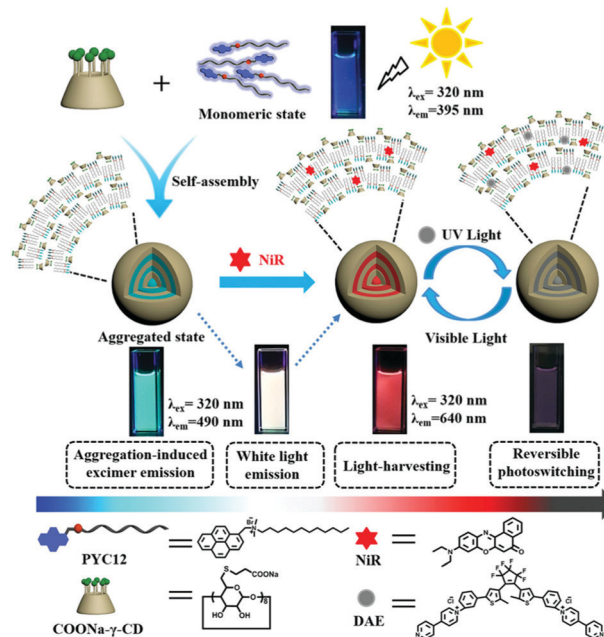


Fig. 34 Schematic illustration of a photocontrolled supramolecular artificial light-harvesting system based on a pyrene derivative (PYC12), polyanionic γ -CD (COONa- γ -CD), Nile red (NiR), and a diarylethylene derivative (DAE). Reproduced with permission from ref. 359. Copyright 2020, Wiley-VCH.

emission wavelength changed from 545 nm (ThT aggregate) to 490 nm (ThT monomer) with detection limits of 40 and 50 μ M, respectively. Recognition patterns for arginine and lysine were generated by monitoring the fluorescence changes at four different wavelengths (470, 490, 520, and 550 nm), which revealed that the two amino acids afforded entirely distinct patterns (Fig. 35b). With the help of principal component analysis (PCA), the two closely related basic amino acids could be successfully distinguished using their recognition patterns (Fig. 35c). This system could be used not only in aqueous solution but also in biological media such as serum samples.

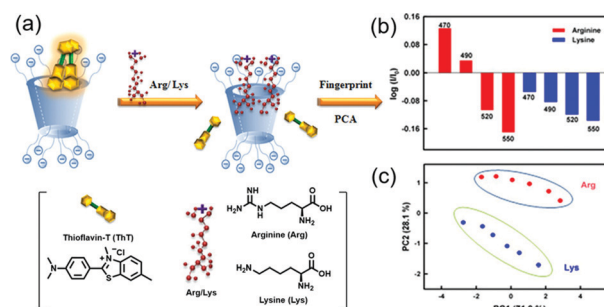


Fig. 35 (a) Chemical structures of thioflavin-T (ThT), arginine, and lysine, and schematic illustration of the lysine- and arginine-induced dissociation of ThT H-aggregates to monomers from the SCD surface. (b) Generation of recognition patterns for arginine and lysine by taking the logarithms of the emission intensity ratios at different wavelengths. (c) 2D principal component analysis (PCA) score plot for the sensor system response to different concentrations of arginine and lysine. Reproduced with permission from ref. 360. Copyright 2017, American Chemical Society.

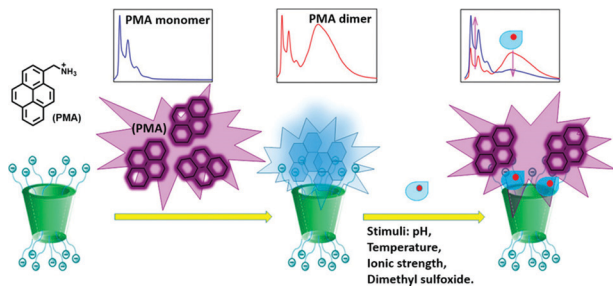


Fig. 36 Molecular structure of 1-pyrenemethylamine (PMA), and schematic illustration of the sensitivity of PMA-SCD from the PMA dimer to monomer in the presence of external chemical stimuli. Reproduced with permission from ref. 361. Copyright 2019, American Chemical Society.

Singh and co-workers reported a stimuli-responsive supramolecular assembly composed of cationic 1-pyrenemethylamine (PMA) and SCD through host-guest interactions (Fig. 36).³⁶¹ It is well known that pyrene and its derivatives exhibit strong fluorescence emission peaks at 375 and 395 nm in their monomeric forms, whereas the dimeric forms generally display red-shifted peaks at approximately 490 nm. In the highly negatively charged environment of the polyanionic SCD, PMA exhibited a highly red-shifted, broad, and structure-free emission band at approximately 490 nm, which was ascribed to the charge neutralization of the cationic PMA by the negatively charged sulfate groups, leading to their association due to the close proximity of the cyclodextrin edges, accompanied by the dimerization of the PMA molecules. This monomer/dimer equilibrium of PMA in the PMA-SCD system was found to be very sensitive to external chemical stimuli such as temperature, pH, ionic strength of the medium, and the presence of an organic solvent (dimethyl sulfoxide). Finally, the ratiometric detection of arginine was accomplished using the distinct fluorescence emission properties of the monomeric and dimeric forms of PMA-SCD.

In addition, CD-based host-guest interactions have significant advantages in the construction of FRET-type supramolecular optical probes. Wang and co-workers reported the use of supramolecular fluorescent nanoparticles for H_2O_2 sensing based on the interaction between β -CD and ferrocene in cancer cells.³⁶² The nanoparticles were prepared using FITC-modified β -CD (FITC- β -CD) as the host and rhodamine-B-modified ferrocene (Fc-RhB) as the guest through host-guest interactions (Fig. 37). In aqueous media, the self-assembled nanoparticles showed good stability under physiological conditions, and exhibited high sensitivity toward H_2O_2 . Based on the FRET effect, the addition of H_2O_2 resulted in an obvious fluorescence change from red (RhB) to green (FITC). *In vitro* experiments revealed that the nanoparticles could be efficiently internalized by cancer cells and then they reacted with endogenous H_2O_2 , accompanied by switching of the FRET process from “on” to “off.” This supramolecular strategy based on a combination of host-guest and hydrophilic/hydrophobic interactions may prove useful for molecular imaging and recognition in living systems.

The covalent modification of nanochannels with β -CD can lead to remarkable specificity in the chiral sensing of amino

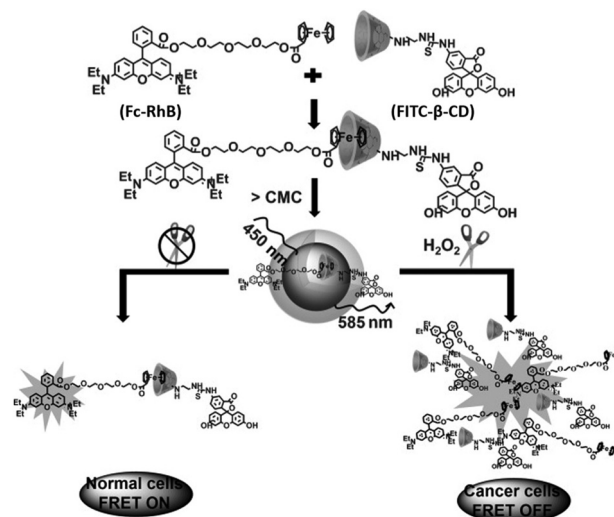


Fig. 37 Schematic illustration of the construction of FRET-type supramolecular optical probes based on FITC- β -CD/Fc-RhB and their H_2O_2 -activated behavior. Reproduced with permission from ref. 362. Copyright 2015, Wiley-VCH.

acids. Li and co-workers reported a nanochannel-based chiral analysis system for the highly enantioselective recognition of L-histidine (Fig. 38a).³⁶³ In this work, a single conical nanochannel was fabricated, which contained a single ion track in the center. The chemical etching process led to exposed carboxyl groups on the nanochannel surface, to which mono-6-amino- β -CD units were attached *via* an EDC/NHS coupling reaction. After exposing the β -CD-modified nanochannel to L-His solution, the amino acid became encapsulated within the chiral cavity of β -CD, and this was accompanied by a reduction in the transmembrane ionic current (Fig. 38b). In contrast, no significant changes in the ionic current were observed when the β -CD-modified nanochannel was exposed

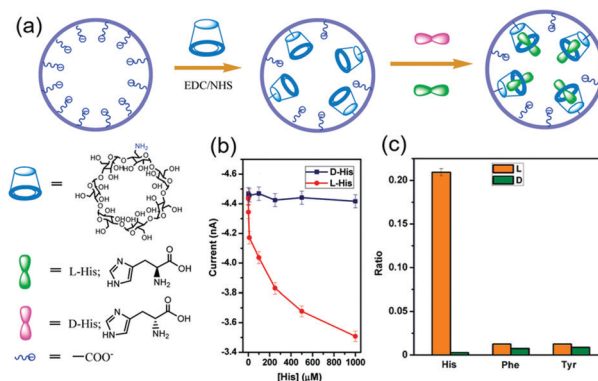


Fig. 38 (a) Schematic illustration of the preparation and application of a β -CD-modified single conical nanochannel for the enantioselective sensing of L-His over D-His. (b) Current-concentration plot for the single conical nanochannel after the attachment of β -CD to the inner wall. (c) Current change ratios in the β -CD-modified single conical nanochannel after addition of different amino acids (L- or D-His, L- or D-Phe, and L- or D-Tyr). Reproduced with permission from ref. 363. Copyright 2011, American Chemical Society.

to D-His or other aromatic amino acid solutions, such as phenylalanine and tyrosine (Fig. 38c). The ionic current in the nanochannel was hardly affected by Phe or Tyr, which may originate from the electrostatic repulsion between negatively charged Phe or Tyr at pH 7.2 and the channel surface. Therefore, the CD-functionalized nanochannel displayed excellent chiral recognition ability for histidine.

Construction of hydrogels

Slide-ring networks consisting of mobile crosslinkers (CD dimers) and polyethylene glycol shafts can increase the toughness and stretchability of hydrogels (Fig. 39a).^{364,365} In these systems, when the material is stretched or compressed, the mobile α -CD crosslinkers can translocate along the PEG axles.³⁶⁶ Instead of using covalent bonds to bridge the CDs, dynamic boronate esters have also been introduced to form the CD crosslinkers, adding self-healing properties to the slide-ring hydrogel (Fig. 39b).³⁶⁷ Recently, Lin and Ke used a partially carboxymethylated polyrotaxane and polyacrylamide to prepare stretchable, tough, and anti-freezing slide-ring hydrogels (Fig. 39c and d).³⁶⁸ The pseudo-slip-ring network was achieved through the hydrogen bonds between the carboxylic acid groups of the α -CD units in the polyrotaxane and the amide groups in polyacrylamide. The resulting multivalent hydrogen bonds greatly enhanced the strength and toughness of the hydrogel. The combination of the ring sliding motion and hydrogen bond site exchange improved the stretchability. Meanwhile, the sliding of the carboxymethylated α -CD rings inhibited ice crystallization by enabling the dynamic adjustment of the local network when ice crystals formed in the hydrogel, thereby

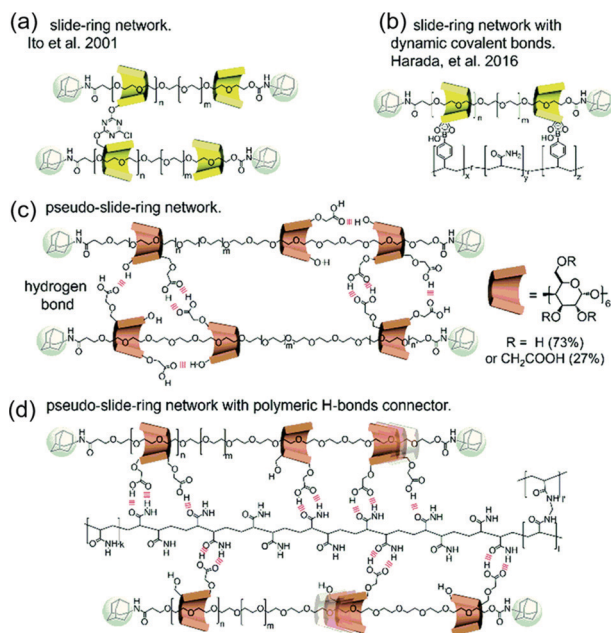


Fig. 39 Schematic illustration of (a) a slide-ring network reported by Ito and co-workers, (b) a slide-ring network based on dynamic covalent bonds reported by Harada and co-workers, and (c and d) pseudo-slide-ring networks constructed via multiple hydrogen-bonding interactions. Reproduced with permission from ref. 368. Copyright 2022, Royal Society of Chemistry.

slowing down ice-crystal propagation. In addition, the formed hydrogel remained stretchable and conductive at both room temperature and $-14\text{ }^{\circ}\text{C}$, facilitating the manufacture of low-temperature strain sensors.

Willner and co-workers used carboxymethyl cellulose (CMC) as the backbone matrix for preparing shape-memory and self-healing DNA-based hydrogels.³⁶⁹ In this work, two pairs of nucleic acids were employed for bridge formation, and a *trans*-Azo/ β -CD supramolecular crosslinking unit was used as the functional matrix for the shape-memory and self-healing properties. In the first system, self-complementary nucleic acid tethers (NAT1) were attached to Azo-CMC and β -CD-CMC to obtain P_A and P_B, respectively (Fig. 40a). Upon mixing P_A and P_B

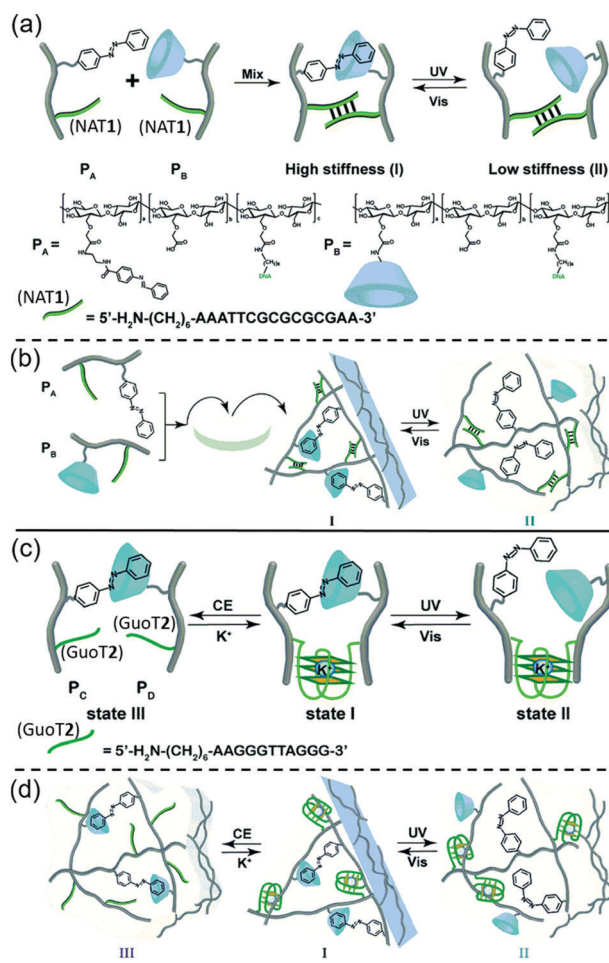


Fig. 40 (a) Schematic illustration of a photoresponsive CMC hydrogel crosslinked by self-complementary nucleic acid tethers (NAT1)/(NAT1) and *trans*-Azo/ β -CD complexes. (b) Schematic illustration of the preparation of a photoresponsive triangle-shaped CMC hydrogel from (a), and light-induced reversible transitions between the stiff triangle-shaped hydrogel and the quasi-liquid shapeless hydrogel. (c) Schematic illustration of a dual-signal-triggered CMC hydrogel crosslinked by *trans*-Azo/ β -CD complexes and K⁺-ion-stabilized G-quadruplexes (CE: 18-crown-6-ether). (d) Schematic illustration of the preparation of a stiff triangle-shaped CMC hydrogel from (c), and light-induced reversible transitions between the stiff triangle-shaped hydrogel and the quasi-liquid shapeless hydrogel. Reproduced with permission from ref. 369. Copyright 2018, Royal Society of Chemistry.

together, the hydrogel crosslinked by the *trans*-Azo/ β -CD complex and the (NAT1)/(NAT1) self-complementary strands exhibited high stiffness. However, photoisomerization of the *trans*-Azo moiety to the *cis* isomer led to lower stiffness of the hydrogel because of the separation of the Azo/ β -CD bridging units. Thus, through this photoinduced Azo isomerization, the hydrogel could be switched between high-stiffness and low-stiffness states. Therefore, shape-memory hydrogels could be developed by exploiting this photoinduced control over the stiffness properties (Fig. 40b). In the second system, the self-complementary nucleic acid tethers (NAT1) were replaced by guanosine-rich tethers (GuoT2) (Fig. 40c). This system could then be crosslinked by K^+ -ion-stabilized G-quadruplex units and by the *trans*-Azo/ β -CD complexes. In addition to the photoisomerization from *trans*-Azo to the *cis* isomer, the K^+ -stabilized G-quadruplexes could also be reversibly dissociated and reformed mediated by 18-crown-6-ether or K^+ ions. The resulting hydrogels crosslinked by both K^+ -ion-stabilized G-quadruplex units and *trans*-Azo/ β -CD complexes displayed high stiffness, whereas crosslinking by either the K^+ -ion-stabilized G-quadruplex or *trans*-Azo/ β -CD alone led to low stiffness. Therefore, the hydrogel also displayed photoinduced reversible shape-memory behavior (Fig. 40d). Furthermore, these hydrogels containing two types of stimuli-responsive crosslinking units could be used as self-healing matrices in which application of the stimulus triggers the self-healing process.

Recently, Fan and co-workers reported a semiconvertible hyaluronic acid hydrogel for red-photoresponsive reversible mechanics, adhesion, and self-healing based on tetra-*ortho*-methoxy-substituted Azo (mAzo)-grafted hyaluronic acid (mAzo-HA) and β -CD-grafted hyaluronic acid (HA-CD) (Fig. 41).³⁷⁰ In this report, electron-donating methoxy groups were attached to the benzene rings of Azo to realize photoresponsivity at 625 nm. Hyaluronic acid was selected as the macroscopic framework owing to its good cytocompatibility and strong intermolecular hydrogen-bonding ability from the hydroxy, carboxyl, and acetamido groups. Upon alternating irradiation at 625 and 470 nm,

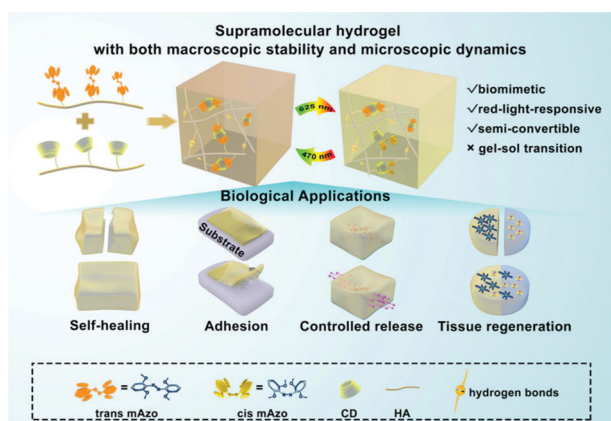


Fig. 41 Schematic illustration of the construction of red-photoresponsive semiconverting supramolecular biomimetic hydrogels and their biological applications. Reproduced with permission from ref. 370. Copyright 2022, American Chemical Society.

the mAzo-HA/HA-CD hydrogel exhibited reversible mechanical and structural dynamics, and the complete gel-sol transition was avoided. The foundation for the construction of this semiconvertible hydrogel system comes from the steric hindrance caused by the conformation of the HA polymer chains, which weakened the conformational overturn of mAzo between the *cis* and *trans* states and made isomerization-induced host-guest dissociation difficult. This supramolecular hydrogel system displayed spatiotemporal mechanical controllability, photoswitchable self-healing, reversible adhesion, and sustained drug delivery. Furthermore, its good cytocompatibility and manufacturability provide potential advantages for tissue engineering applications.

In the construction of organic-inorganic hybrid supramolecular hydrogels, CDs play an important role as building blocks. Li and co-workers reported remote control of reversible sol-gel phase transitions of robust luminescent hybrid hydrogels (Fig. 42).³⁷¹ In this system, α -CD is linked to 2,6-pyridinedicarboxylic acid (PDA) through a hydrophilic PEG (1000) chain as a spacer to form α -CD-PDA, and the azobenzene unit is modified with a guanidino group (Guazo). By using the coordination of PDA groups and Ln ions (Tb^{3+} and Eu^{3+}), and the host-guest interactions of α -CD and azobenzene, as well as the electrostatic interactions between guanidinium groups and negatively charged surfaces of sodium polyacrylate exfoliated LAPONITE[®] nanosheets (SPLNs), organic-inorganic hybrid luminescent supramolecular hydrogels were successfully achieved. Taking advantage of the conformation-dependent binding behavior of azobenzene to α -CD, the isomerization of azobenzene can induce the dissociation or association of inclusion complexes under UV irradiation (365 nm) and visible-light irradiation (450 nm), respectively, accompanied by sol-gel phase transition of luminescent hybrid hydrogels. In addition, supramolecular hydrogels possess high water content and

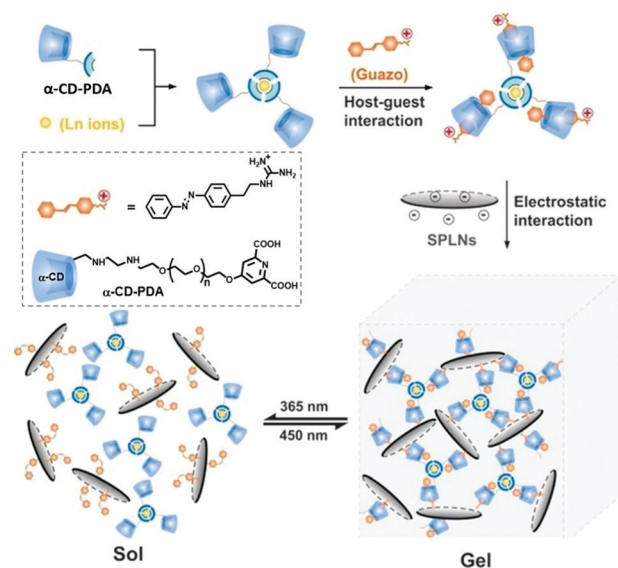


Fig. 42 Chemical structures of α -CD-PDA, guanidino-modified azobenzene (Guazo), and sodium polyacrylate exfoliated LAPONITE[®] nanosheets (SPLNs), as well as the photoinduced sol-gel phase transition of organic-inorganic hybrid luminescent supramolecular hydrogels. Reproduced with permission from ref. 371. Copyright 2018, Wiley-VCH.

excellent mechanical toughness, as well as color-tunable luminescence properties, which provide a good strategy for the design and preparation of smart luminescent materials.

Recently, photoresponsive hydrogels have attracted widespread interest as functional materials because of the ability to remotely and precisely control their properties.³⁷² However, despite its promise, altering the electrical conductivity of hydrogels *via* light-mediated ion transport is a challenging approach. Huang and co-workers reported the development of an ion-conducting supramolecular hydrogel based on the copolymerization of acrylic acid, an acrylic acid-modified azobenzene monomer (AC-Azo), an α -CD-acrylic acid monomer (AC- α -CD), an ionic liquid monomer (IL), and the crosslinker *N,N'*-methylenebisacrylamide (Fig. 43a).³⁷³ Because the order of the association constants for the functional groups bound by α -CD is *trans*-Azo > anion of the ionic liquid > *cis*-Azo, the concentration of free-moving anions can be adjusted by alternating 365 and 420 nm light irradiation. Upon irradiation with 365 nm light, α -CD preferentially complexed with the anionic moiety of the ionic liquid, leading to reduced ionic mobility and thus high resistance of the hydrogel. In contrast, upon 420 nm light irradiation, a more stable complex was formed between α -CD and *trans*-Azo, which released the bound anions to regenerate the low-resistivity hydrogel. As a result, remote control over the ionic conductivity of the hydrogel was achieved through host-guest chemistry. Incorporation of the hydrogel into a logic gate enabled an electric circuit to be reversibly switched on and off through irradiation with a light of

appropriate wavelength (Fig. 43b). The strategy of photoswitchable ionic conductivity mediated by competitive molecular recognition used in hydrogels holds great potential in optoelectronic device fabrication.

3. Assemblies of neutral CDs and charged guests

3.1 Assemblies of neutral CDs and positively charged guests

In contrast to positively/negatively charged CDs and their assemblies, supramolecular assemblies formed by the binding of parent CDs and positively charged guests mainly rely on using the CD cavity to encapsulate the hydrophobic moieties of charged guest molecules through host-guest interactions in either aqueous solution or the solid state (Scheme 3). Importantly, the exposed positive charges of these assemblies can be employed for co-assembly with negatively charged molecules *via* electrostatic interactions, as well as co-assembly with other supramolecular macrocycles, particularly cucurbit[*n*]urils (CB[*n*]s), which is useful for the construction of multilevel supramolecular assemblies. Therefore, multicharged interactions based on the secondary assembly of CDs can endow supramolecular structures with excellent performance and provide broad application prospects in fields such as functional supramolecular hydrogels, topological morphology control, luminescent materials, molecular recognition, pseudorotaxanes, and ionic organic-inorganic frameworks.

Stimuli-responsive materials

Amphiphilic surfactants can self-organize into various molecular assemblies, such as micelles, vesicles, and nanoparticles, and they have been widely applied as capsules for drug delivery.³⁷⁴ Unfortunately, the formed supramolecular assemblies often do not exhibit good responsiveness to stimuli.³⁷⁵ Therefore, it is interesting to construct stimuli-responsive supramolecular assemblies based on surfactants and CDs *via* host-guest interactions. In this regard, Zhang and co-workers reported the preparation of a photocontrolled reversible supramolecular assembly based on an Azo-containing surfactant (AzoC10) and α -CD.³⁷⁶ In this work, the Azo moiety at the end of the hydrophobic alkyl tail of AzoC10 underwent photoisomerization under irradiation at 365 and 450 nm (Fig. 44a). Driven by hydrophobic and van der Waals interactions, the *trans* isomer of AzoC10 could be well encapsulated by the α -CD unit, leading to dissociation of the assembly, accompanied by the disassembly of the vesicle-like aggregates of AzoC10 (Fig. 44b).

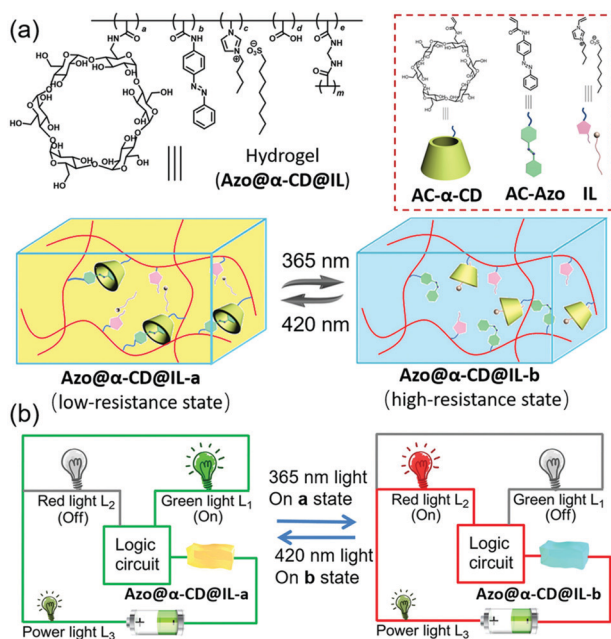
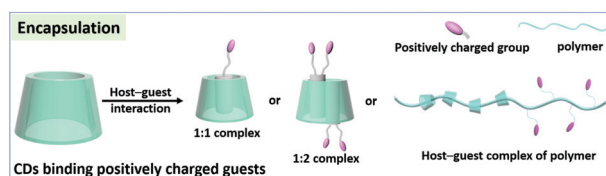


Fig. 43 (a) Chemical structures of polymer monomers AC- α -CD, AC-Azo, IL and hydrogel (Azo@ α -CD@IL), as well as the schematic illustration of guest molecule exchange in the hydrogel (Azo@ α -CD@IL) under irradiation with 365 or 420 nm light. (b) Reversible switching of green light L_1 and red light L_2 after incorporation of the hydrogel (Azo@ α -CD@IL) into a logic-gate circuit under irradiation with 365 or 420 nm light. Reproduced with permission from ref. 373. Copyright 2019, Wiley-VCH.



Scheme 3 Schematic diagram of various types of supramolecular assemblies formed by parent CDs binding positively charged guests.

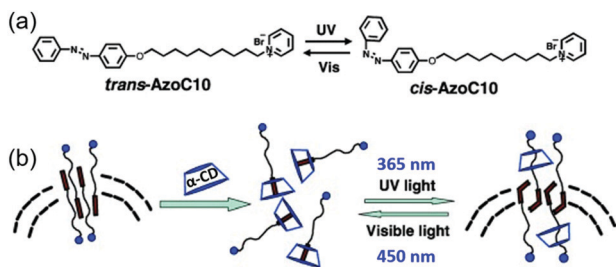


Fig. 44 (a) Reversible photoisomerization of AzoC10 under UV and visible light irradiation. (b) Schematic illustration of the construction of assemblies based on AzoC10 and α -CD, as well as their photocontrolled reversible assembly and disassembly process. Red bars: Azo moieties; blue circles: pyridinium groups. Reproduced with permission from ref. 376. Copyright 2007, Wiley-VCH.

However, when *trans*-AzoC10 was converted to its *cis* isomer by UV irradiation at 365 nm, the α -CD unit failed to encapsulate the bulkier *cis*-AzoC10 owing to the mismatch between the host and guest, resulting in re-formation of the vesicular aggregates. Subsequently, the CD-encapsulated AzoC10 state could be recovered by visible irradiation at 450 nm to regenerate the *trans* isomer. This photocontrolled host-guest assembly and disassembly process between Azo derivatives and α -CD units could serve as a driving force for the fabrication of molecular shuttles, motors, machines, and other devices.

Li and co-workers reported a light-driven linear helical supramolecular polymer based on a bipyridinium- and Azo-modified chiral 1,1'-binaphthyl monomer (M), bis(*p*-sulfonato-calix[4]arene) (bis-SC4A), and α -CD (Fig. 45).³⁷⁷ First, the Azo units of the monomer were encapsulated into the α -CD cavities to afford pseudo[3]rotaxanes (R), which enhanced the water solubility of the monomer. Subsequently, the 4,4'-bipyridinium moieties of the pseudo[3]rotaxanes were further encapsulated into the bis-SC4A cavities, resulting in the supramolecular polymer (P), which was accompanied by an obvious star-like multibranch morphology. However, the morphology of the polymer changed significantly upon UV irradiation, showing a linear band-like shape owing to the straighter structure of the *cis*-Azo-containing polymer compared with the *trans*-Azo-containing form. Interestingly, a single helical structure of the irradiated supramolecular polymer was observed owing to the axially chiral 1,1'-binaphthyl units. This work provides guidance for the construction of controllable supramolecular polymers.

Construction of pseudorotaxanes

By using the point chirality of CDs and the planar chirality of pillar[*n*]arenes, Wang and co-workers reported stoichiometry-controlled chirality induced by a co-assembly based on an amphiphilic tetraphenylethylene derivative (TPEA), γ -CD, and negatively charged pillar[5]arene (WP5) (Fig. 46).³⁷⁸ The tetraphenylethylene unit of TPEA could be encapsulated into the chiral cavity of γ -CD through hydrophobic interactions and lead to obvious negative induced circular dichroism (ICD₁). During the addition of WP5 (0.05–0.20 equiv.) to γ -CD \supset TPEA, the

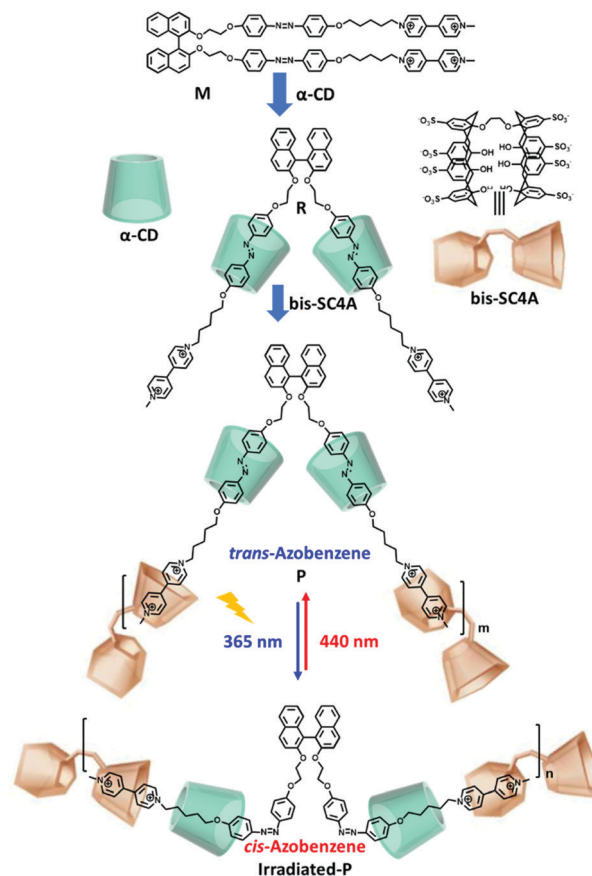


Fig. 45 Chemical structures of the monomer (M) and bis-SC4A, as well as the schematic illustration of the self-assembly process of α -CD-based pseudo[3]rotaxane (R), the formation of a supramolecular polymer (P) based on bis-SC4A and R with the *trans*-Azo configuration, and the corresponding UV-irradiated polymer (irradiated-P) with the *cis*-Azo configuration. Reproduced with permission from ref. 377. Copyright 2013, American Chemical Society.

induced negative signal intensity from TPEA gradually decreased, and with the addition of 0.20 equiv. of WP5 in total, ICD₁ was completely silenced. This behavior occurred because a small amount of WP5 induced the self-assembly of TPEA, resulting in the formation of vesicles from the tightly packed structure. When 2 equiv. of WP5 was added to the γ -CD \supset TPEA solution to form pseudo[4]rotaxane, dual chiral induction from γ -CD to TPEA (negative ICD₁) and continuous dynamic racemic WP5 (positive ICD₂) was observed. Therefore, stoichiometric changes of WP5 were an effective strategy for inducing topological transitions from the vesicular form to pseudo[4]rotaxane, triggering chiral induction of both γ -CD and WP5.

Construction of hydrogels

For functional polymeric materials with reversible non-covalent bonds, the association and dissociation of these bonds can increase the fracture energy of the material. Recently, Takashima and co-workers reported a general strategy for designing supramolecular polymeric materials based on the host-guest interactions between α -CD and charged alkyl chains and explored the relationship between the relaxation time and the fracture energy

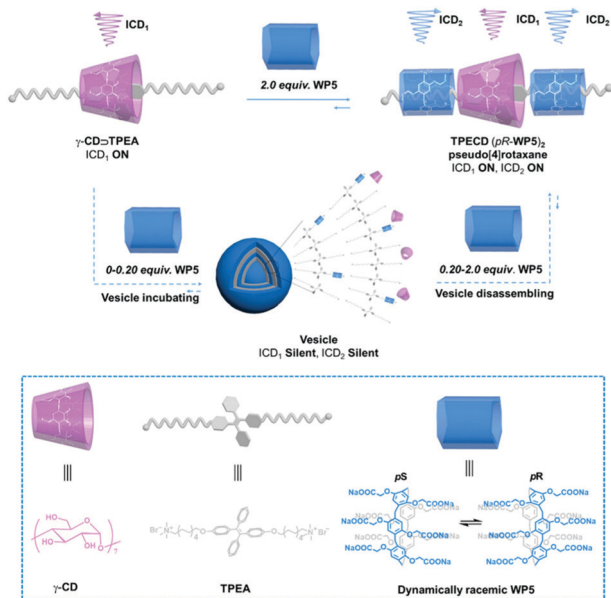
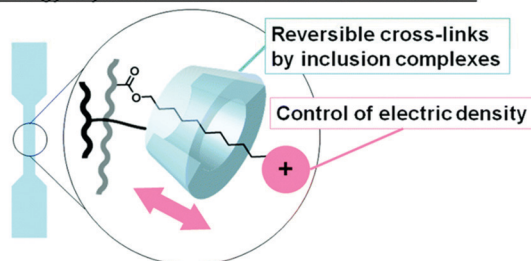


Fig. 46 Schematic illustration of a co-assembly based on γ -CD, a tetraphenylethylene derivative (TPEA), and pillar[5]arene (WPS), as well as its application for stoichiometrically controlled chirality induction. Reproduced with permission from ref. 378. Copyright 2021, American Chemical Society.

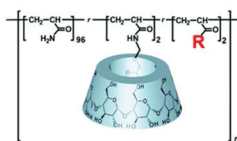
(a) Molecular design for tough materials

Strategy: Dynamic control of reversible cross-links



Relaxation time \leftrightarrow Fracture energy

(b) Chemical structures of α CD-R hydrogels



α CD-R hydrogels

Chemical structures of guest monomers (R)

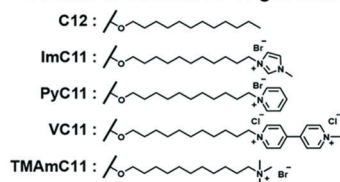


Fig. 47 (a) Schematic illustration of the reversible crosslinking points in supramolecular polymeric materials. (b) Chemical structures of the α -CD-R hydrogels and the guest monomers. Reproduced with permission from ref. 379. Copyright 2020, Royal Society of Chemistry.

(Fig. 47a).³⁷⁹ Five reversibly crosslinked supramolecular hydrogels (α -CD-R hydrogels) were constructed with cation-terminated or nonionic linear alkyl chain guests on the polymer side chains (Fig. 47b). Among them, the linear alkyl units served as molecular recognition sites for α -CD, while the cationic groups functioned as electrical traps. Notably, the second-order average relaxation time ($\langle\tau\rangle_w$) of the hydrogel linearly increased with the restrained electrostatic potential charges on N^+ (ImC11 < TMAmC11 < PyC11 < VC11). In contrast to the other species, the absence of a cationic unit in the α -CD-C12 hydrogel led to fast threading/dethreading motions with a smaller $\langle\tau\rangle_w$ value. Therefore, the viscoelastic behavior of the reversible crosslinking points can be tuned by the positively charged functional groups, thereby increasing the fracture energy of supramolecular hydrogels.

Adjust optical performance

Realizing multicolor photoluminescence based on a single fluorescent compound would be of great value. Tian and co-workers reported a single host-guest complex displaying multicolor photoluminescence, including white-light emission.³⁸⁰ This system consisted of coumarin-modified binaphthyl (BPC) as a two-armed fluorescent guest and γ -CD as the host (Fig. 48a). In this system, γ -CD could form host-guest complexes with BPC molecules in a 1:1 stoichiometric ratio (BPC- γ -CD) in aqueous solution, accompanied by the self-folding of BPC, resulting in obvious changes in optical behavior. Under specific conditions, the complex BPC- γ -CD displays three different emission wavelengths, and by orthogonal modulation of the excitation wavelength and γ -CD, multicolor photoluminescence could be achieved, including red, green, blue, and various intermediate colors (Fig. 48b). In this manner, almost pure white-light emission with CIE coordinates of (0.33, 0.34) could be realized (Fig. 48c). The mechanism underlying the multicolor luminescence of the complex BPC- γ -CD in response to stimulation involves a combination of host-enhanced intramolecular

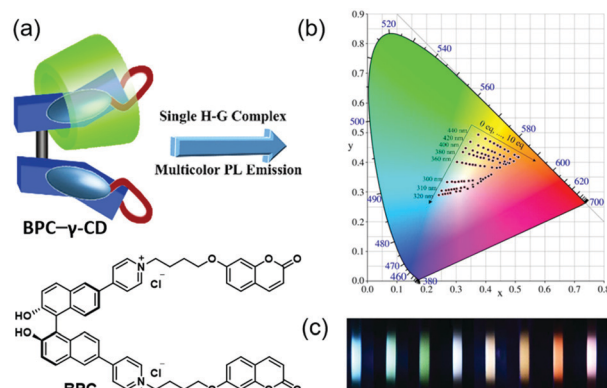


Fig. 48 (a) Chemical structure of BPC and its host-guest complex with γ -CD (BPC- γ -CD). (b) CIE 1931 chromaticity diagram. The black dots indicate the luminescent color coordinates for BPC in the presence of various amounts of γ -CD at different excitation wavelengths. (c) Representative fluorescence photographs of BPC solutions according to (b). Reproduced with permission from ref. 380. Copyright 2016, American Chemical Society.

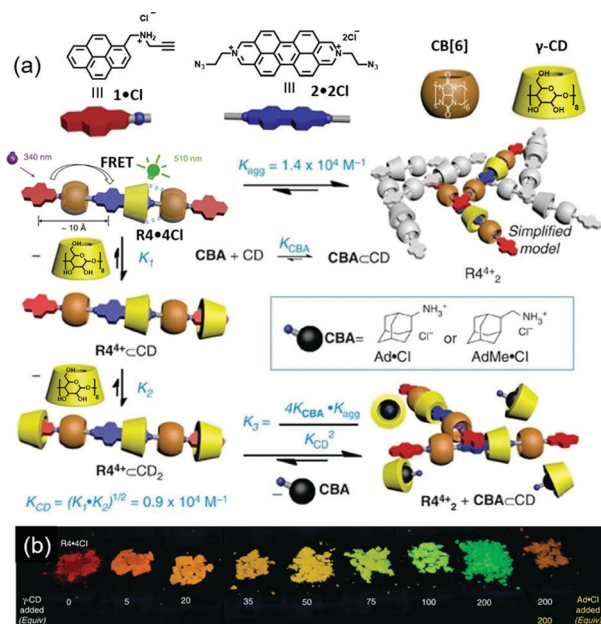


Fig. 49 (a) Chemical structures of pyrene stopper 1-Cl and dumbbell precursor 2-2Cl, and the schematic illustration of heterorotaxanes R4-4Cl with the assistance of CB[6] and γ -CD, as well as the equilibria involving R4-4Cl in the presence of γ -CD and competitive binding agent (CBA) Ad-Cl or AdMe-Cl. (b) Photographs showing the powders achieved from homogeneous mixtures of R4-4Cl with different amounts (0–200 equiv.) of γ -CD and Ad-Cl (200 equiv.) under UV light. Reproduced with permission from ref. 381. Copyright 2015, Springer Nature.

charge transfer and host-restricted intramolecular rotation. These supramolecular complexes with excellent multicolor emission capability may have a wide range of applications in display media and information processing.

The host-guest recognition strategy can also be used in the construction of solid-state fluorescent hetero[n]rotaxanes. For example, Ke and co-workers reported tunable solid-state fluorescent materials for supramolecular encryption based on γ -CD, cucurbit[8]uril (CB[6]), the diazaperopyrenium (DAPP) dication, and two pyrene stoppers.³⁸¹ Hetero[4]rotaxane R4-4Cl was synthesized by a cooperative capture strategy, in which γ -CD encircled the DAPP unit (Fig. 49a). A FRET process was observed from the pyrene to DAPP in R4-4Cl. In addition, R4-4Cl aggregated at high concentrations owing to the intermolecular π - π stacking between the pyrene and DAPP units at room temperature, and it de-aggregated into the monomeric form when heated to 80 °C. Therefore, the addition of excessive γ -CD prevented the aggregation because of the encapsulation of the pyrene moiety. The resulting $R4^{4+} \subset CD$ and $R4^{4+} \subset CD_2$ complexes underwent dissociation upon the introduction of the competitive binding agent (CBA) Ad-Cl or AdMe-Cl, followed by the formation of $R4^{4+}$ aggregates. As a result of this dynamic aggregation and de-aggregation, the solid-state fluorescence of $R4^{4+}$ could be reversibly tuned over a wide wavelength range (approximately 100 nm) to afford various colors from green to red (Fig. 49b), and this was successfully applied in fluorescent security inks.

Molecular recognition

The use of rotaxanes for molecular recognition through their 3D topological binding sites has recently been developed. Yang and co-workers reported γ -CD-CB[6]-coveheded hetero[4]rotaxanes with RTP emission for the specific sensing of tryptophan.³⁸² The hetero[4]rotaxanes were synthesized *via* CB[6]-templated azide-alkyne 1,3-dipolar cycloaddition from aqueous solutions of the guest and γ -CD, using selected naphthalene or biphenyl derivatives as the rotaxane axis (Fig. 50a). Among the synthesized rotaxanes **Rot0–Rot4**, **Rot2–Rot4** exhibited obvious RTP properties, with **Rot3** displaying the highest phosphorescence quantum yield. In addition, **Rot3** was highly sensitive to Trp, exhibiting significant quenching at Trp concentrations as low as 0.5 μ M, whereas no RTP quenching was observed in the presence of other major physiological amino acids or the Trp-containing protein human serum albumin, indicating the highly specific sensing of Trp by **Rot3**. The recognition mechanism involved the integration of free Trp into the remaining space of the γ -CD cavity of **Rot3** and its interaction with the naphthalene axis to form a co-inclusion complex *via* π - π interactions, as well as the dipole-charge interactions provided by the CB[6] opening, resulting in severe quenching of the phosphorescence (Fig. 50b). In this work, the supramolecular probe enabled convenient and specific high-throughput detection of free Trp in serum samples.

Supramolecular diagnosis and treatment

Molecules displaying aggregation-induced emission (AIE) have drawn widespread attention, and this phenomenon was officially selected by the International Union of Pure and Applied Chemistry (IUPAC) as one of the “Top Ten Emerging Technologies in Chemistry” in 2020.³⁸³ In contrast to conventional light-emitting molecules, AIE molecules possess a non-planar configuration. They are like miniature propellers that keep rotating. However, when they aggregate, this rotation is greatly

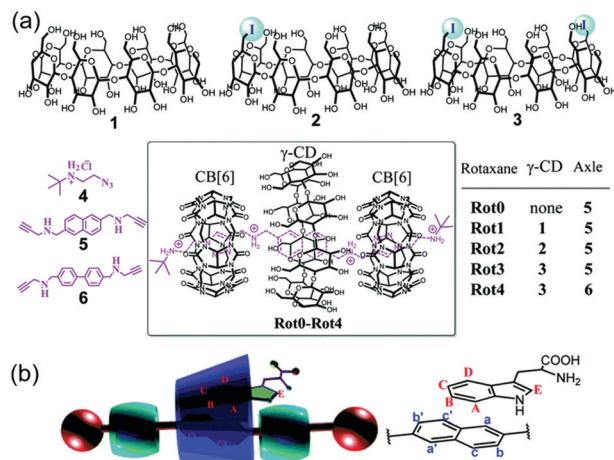


Fig. 50 (a) Structures of γ -CD-CB[6]-coveheded [4]rotaxanes **Rot0–Rot4**. (b) Schematic illustration of the complexation of **Rot3** with tryptophan. Reproduced with permission from ref. 382. Copyright 2019, Royal Society of Chemistry.

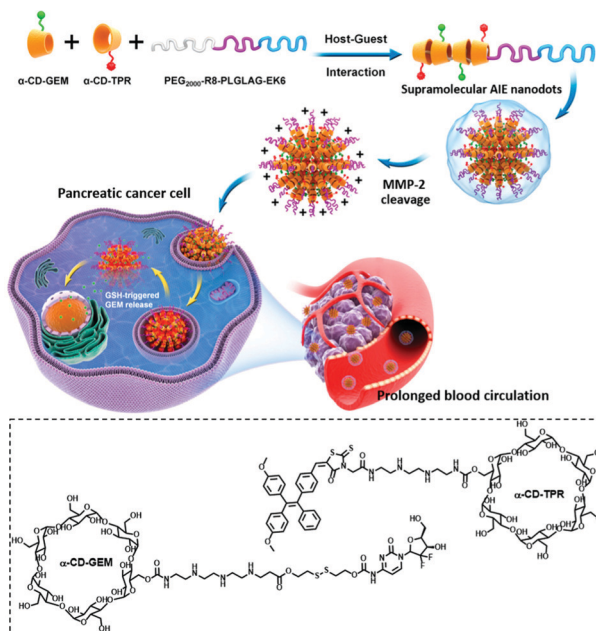


Fig. 51 Schematic illustration of the construction of supramolecular AIE dots based on α -CD-TPR, α -CD-GEM, and PEG₂₀₀₀-R8-PLGLAG-EK6 via host-guest assembly, and the tumor-microenvironment-activated targeting and GSH-triggered gemcitabine (GEM) release processes. Reproduced with permission from ref. 384. Copyright 2020, American Chemical Society.

suppressed and energy is released in the form of light. Therefore, the attachment of AIE molecules to CDs has promoted the development of supramolecular luminescent materials. Recently, Ding and co-workers reported supramolecular AIE nanodots for image-guided *in situ* pancreatic cancer therapy based on CD derivatives (Fig. 51).³⁸⁴ Two functional α -CDs were modified with the anticancer drug gemcitabine (GEM) via disulfide bond formation (α -CD-GEM) and the AIE luminescent agent (α -CD-TPR). Supramolecular AIE dots were then formed by the co-assembly of the matrix metalloproteinase-2 (MMP-2)-sensitive PEG-peptide (PEG₂₀₀₀-RRRRRRRR (R8)-PLGLAG-EKEKEKEKEKEK (EK6); PEG₂₀₀₀-R8-PLGLAG-EK6), α -CD-GEM, and α -CD-TPR through host-guest interactions between PEG and α -CD. The presence of the cell-penetrating peptide R8 and the zwitterionic stealth sequence EK6 allowed the AIE dots to exhibit both “stealth” and cell-penetrating capabilities in one system, accompanied by a long blood circulation time. *In vivo* tumor experiments demonstrated that the supramolecular AIE dots could respond sequentially to tumor-overexpressed MMP-2 and the intracellular reducing microenvironment for enhanced cancer cell uptake and selective GEM release, resulting in superior tumor suppression in subcutaneous and orthotopic pancreatic tumor models. This strategy combines the advantages of AIE and CD-based supramolecular nanomaterials to provide a new platform for drug delivery.

Nano-size separation

In the construction of CD-based supramolecular frameworks, Wu and co-workers reported flexible single-layer two-dimensional

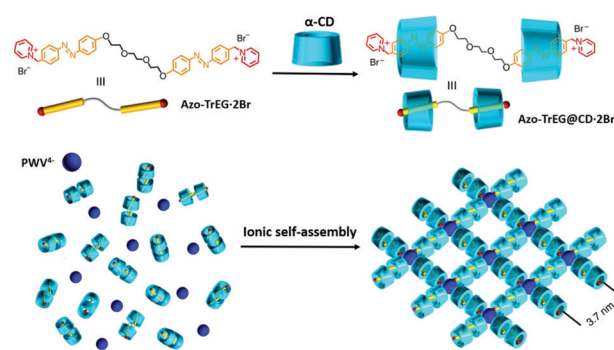
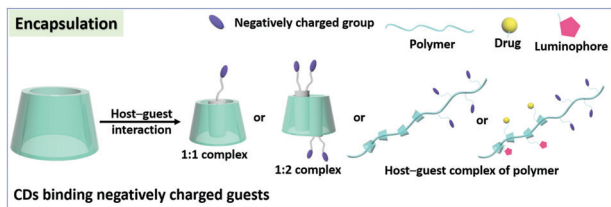


Fig. 52 Chemical structure of Azo-TrEG-2Br, its interaction with α -CD, and the spontaneous formation of 2D supramolecular frameworks via ionic self-assembly based on cationic pseudorotaxane units (Azo-TrEG@CD²⁺) and POM clusters (PWV⁴⁻). Reproduced with permission from ref. 385. Copyright 2016, Springer Nature.

(2D) ionic organic-inorganic frameworks (IOIFs) for precise nano-size separation (Fig. 52).³⁸⁵ An azo-modified pyridinium derivative (Azo-TrEG-2Br) was designed as the guest and then complexed with two α -CD rings to generate the corresponding pseudo[3]rotaxane (Azo-TrEG@CD-2Br). Further co-assembly with anionic PW₁₁VO₄₀⁴⁻ (PWV⁴⁻) clusters via electrostatic interactions afforded free-standing single-layer IOIFs in water. The introduced α -CD provided steric guidance and lateral hydrogen bonding for the 2D arrangement of the cation rods around the polyanion nodes. In addition, the PWV⁴⁻ clusters acted as both a crosslinker to bind the cation of Azo-TrEG@CD-2Br and a capping agent to lock the pseudorotaxane rods. The layer thickness of the obtained IOIFs was approximately 1.4 nm, and this soft supramolecular polymer framework possessed a uniform and tunable ortho-tetragonal nanoporous structure with pore sizes of 3.4–4.1 nm in addition to having good solution processability. Importantly, it could be used to fabricate stable supramolecular membranes with good durability and reusability for the precise size-selective separation of semiconductor quantum dots with an accuracy of 0.1 nm, requiring only rapid filtration under reduced pressure. Such supramolecular membranes with 2D IOIF assemblies are expected to find practical applications in selective transport, molecular separation, and dialysis systems.

3.2 Assemblies of neutral CDs and negatively charged guests

In addition to their encapsulation of positively charged guest molecules, CDs can encapsulate both hydrophobic and negatively charged moieties of negatively charged guest molecules to form tight supramolecular assemblies (Scheme 4). These different encapsulation modes can enable different applications, such as encapsulating negatively charged fluorescent dyes to significantly enhance their luminescence properties. When the ability of a CD to encapsulate the hydrophobic part exceeds its ability to encapsulate the negatively charged part, the exposed negative charge can be exploited for co-assembly with positively charged molecules through electrostatic interactions, as well as co-assembly with other supramolecular macrocycles



Scheme 4 Schematic diagram of various types of supramolecular assemblies formed by CDs binding negatively charged guests.

such as charged calixarenes and pillar[*n*]arenes. Therefore, multilevel supramolecular assemblies with excellent performance may be achieved.

Supramolecular diagnosis and treatment

The construction of supramolecular nanomaterials based on CDs binding negatively charged guests has attracted increasing attention in the development of drug carriers owing to the inherent advantages of these systems, such as their high stability, strong inclusion ability, and facile modification of the parent CDs.³⁸⁶ Chen and co-workers reported supramolecular polymer nanomedicines with good therapeutic properties and negligible long-term immunotoxicity (Fig. 53).³⁸⁷ First, β -CD and camptothecin (CPT) were linked *via* a disulfide bond to form a prodrug (CD-SS-CPT) that was responsive to glutathione. The formation of an inclusion complex through host-guest interactions between β -CD and CPT not only significantly improved the solubility of CPT but also effectively inhibited the opening of its lactone ring under physiological conditions, thus maintaining

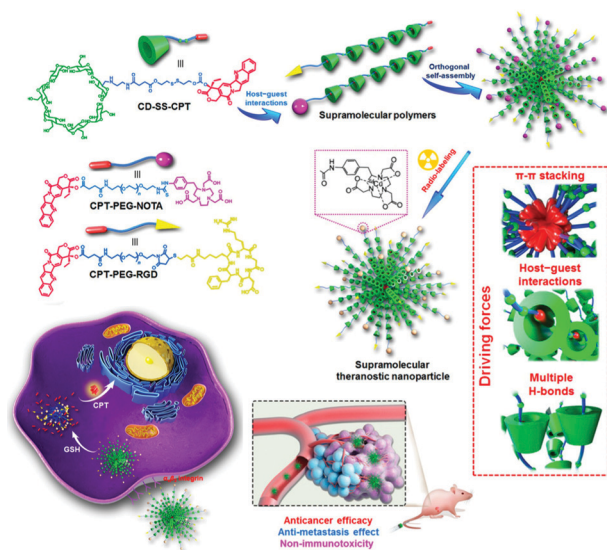


Fig. 53 Schematic illustration of the construction of supramolecular polymer nanomedicines based on self-assembly of β -CD-modified camptothecin (CD-SS-CPT); the driving force comes from the π - π stacking of CPT, host-guest complexation of CPT and β -CD, and multiple hydrogen bonds from β -CD. The nanomedicines can be dissociated in the presence of intracellular glutathione (GSH), exhibiting excellent anticancer efficacy, antimetastatic effect, and non-immunotoxicity. Reproduced with permission from ref. 387. Copyright 2018, American Chemical Society.

its anticancer activity. In order to improve the stability of CD-SS-CPT and install targeting and imaging capabilities, CPT-PEG-RGD or CPT-PEG-NOTA was introduced by orthogonal self-assembly to incorporate a targeting ligand (cRGDFK) and a positron emission tomography tracer (^{64}Cu). Meanwhile, by using PEG to link CPT and RGD, CPT and NOTA, the formed assembly can avoid being adsorbed by proteins due to the PEG shell on the outside. Stabilized by a combination of π - π stacking interactions, host-guest complexation, and multiple hydrogen bonds, these supramolecular polymer nanomedicines exhibited excellent anticancer efficacy and antimetastatic effects both *in vitro* and *in vivo*, accompanied by negligible systemic or long-term immunotoxicity. This work combined the advantages of supramolecular chemistry and the dynamic nature of nanotechnology to provide a novel method for cancer therapeutics.

Wang and co-workers reported a supramolecular polymerization-induced nanoparticle mediated by platinum(IV) complex-modified β -CD-ferrocene (Cis-CD-Fc) as the supramolecular monomer and ferrocene-modified PEG (PEG-Fc) as the terminal unit (Fig. 54).³⁸⁸ As a result of the host-guest interactions between β -CD and Fc, Cis-CD-Fc could form linear supramolecular polymers with Fc located in the CD cavity, followed by self-assembly driven by colloidal amphiphilicity into nanoassemblies. The introduced PEG-Fc not only allowed control over the length of the supramolecular polymers by modulating the ratio of PEG-Fc to the supramolecular monomers but also generated steric hindrance in the presence of plasma proteins, thereby improving the *in vivo* stability of the nanoassemblies and prolonging their blood circulation. The resulting supramolecular nanoassemblies dissociated rapidly when exposed to endogenous hydrogen peroxide (H_2O_2), releasing hydroxyl radicals through a Fenton-like reaction with Fc. Meanwhile, the released platinum(IV) prodrugs were reduced to cisplatin, further promoting the generation of H_2O_2 in tumor tissues. This cascade production of ROS and burst release of platinum(IV) complexes enhanced the antitumor efficacy.

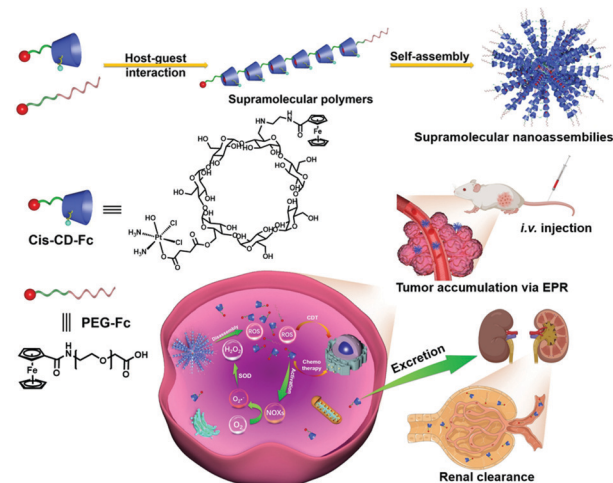


Fig. 54 Schematic illustration of the construction of H_2O_2 -responsive supramolecular nanoassemblies and a self-enhancing chemo/chemokinetic cancer therapy process with rapid renal clearance. Reproduced with permission from ref. 388. Copyright 2021, Wiley-VCH.

Furthermore, the dissociated supramolecular nanoassemblies were easily excreted from the body through renal clearance, thus effectively avoiding systemic toxicity and ensuring long-term biocompatibility of the nanomedicines. This work provides new approaches for the design and development of novel supramolecular nanoassemblies for cascade chemical and chemodynamic therapy.

As a class of important biomolecules, peptides can be exploited both as targeting agents and for the assembly of biomaterials. For example, He and co-workers reported CD-based peptide self-assembly for enhanced peptide-based fluorescence imaging and antimicrobial efficacy.³⁸⁹ β -CD was modified with hepta-dicyanomethylene-4*H*-pyran (DCM₇- β -CD) and used as the host to encapsulate 1-bromonaphthalene-modified peptides (**P1**–**P4**) to form multiple building blocks (Fig. 55a), which were then passed through second-stage ordered assembly to prepare supramolecular peptide dots (Fig. 55b). When the probes **P1**–**P3** were bound to DCM₇- β -CD, the fluorescence emission was suppressed owing to FRET between the fluorescein isothiocyanate (FITC) fluorophores on the probes and the DCM fluorophores on DCM₇- β -CD. The addition of caspase-3 to DCM₇- β -CD-**P1**/DCM₇- β -CD-**P2** resulted in an obvious increase in the FITC-derived fluorescence intensity. It is the process by which **P1**/**P2** undergoes enzymatic cleavage that disrupts FRET by releasing free FITC. In addition, DCM₇- β -CD-**P3** showed recovery of fluorescence intensity

because the probe **P3** could bind to tubulin, resulting in the disassembly of DCM₇- β -CD-**P3** and the interruption of the FRET process. Cellular imaging revealed that the supramolecular peptide dots possessed superior cell permeability than the fluorescent peptides **P1**–**P3** alone, which facilitated the intracellular delivery of the constituent probes and had a positive effect on apoptosis biomarkers (caspase-3) and mitosis for spatiotemporal imaging. Interestingly, the therapeutic effect of DCM₇- β -CD-**P4** against Gram-positive and Gram-negative bacteria was enhanced compared to **P4** alone owing to the improved through-membrane transport. The fluorescent DCM₇- β -CD-**P4**-FITC also showed enhanced bacterial cellular uptake in *E. coli* (ATCC 25922) and *S. aureus* (ATCC 25923), which was greater than that of the peptide alone (**P4**-FITC). This CD-based assembly strategy is anticipated to provide new approaches for the development of more effective peptide-based diagnostics and therapeutics.

Adjust optical performance

In the construction of CD-based chemiluminescent materials, Ma and co-workers reported efficient cascade resonance energy transfer for intensive and long-lasting multicolor chemiluminescence in a CD-based dynamic nanoassembly.³⁹⁰ Upon choosing luminol (LUM) as the energy-transfer donor, the luminescent intermediate 3-aminophthalate (3-AP) generated from LUM could be encapsulated into the β -CD cavity, and this was accompanied by greatly enhanced chemiluminescence intensity (Fig. 56a and b). In addition, β -CD could also bind numerous other fluorophores including fluorescein, erythrosin B, eosin Y, phloxine B, and rhodamine B. Thus, the nanoassembly of β -CD could bring the encapsulated 3-AP and fluorophore into close proximity and proper alignment, because β -CD can form dynamic nanoassemblies by itself or with inclusion complexes above a critical concentration (2–3 mM). This dynamic nanoassembly exhibited both enhanced chemiluminescence intensity and highly efficient cascade FRET from 3-AP to various fluorophores (Fig. 56c), leading to strong chemiluminescence with an adjustable emission wavelength in the range of 410–610 nm. Interestingly, diffusion was slowed to prolong the chemiluminescence emission upon using hydroxypropyl methylcellulose as a thickener and solid Ca(OH)₂ as a buffer to maintain an optimal pH, and the nanoassembled system enabled slow diffusion-controlled catalytic chemiluminescence reactions to achieve visible and durable multicolor chemiluminescence in aqueous solution for more than 20 h (Fig. 56d). This multicolor chemiluminescence system was employed to prepare transformable 2D multicolor codes for encryption applications (Fig. 56e).

It has been reported that γ -CD can self-assemble with alkali-metal ions to form γ -CD-MOF.^{391–394} In γ -CD-MOF, the formed supramolecular cubic box with a size of 1.7 nm is larger than the intrinsic void (0.95 nm) of γ -CD. To take advantage of this property of γ -CD-MOF, Liu and co-workers developed crystalline circularly polarized luminescent (CPL) materials based on γ -CD-MOF and luminophores.³⁹⁵ In this work, the cubic voids of γ -CD-MOF surrounded by six- γ -CD faces were also chiral, and

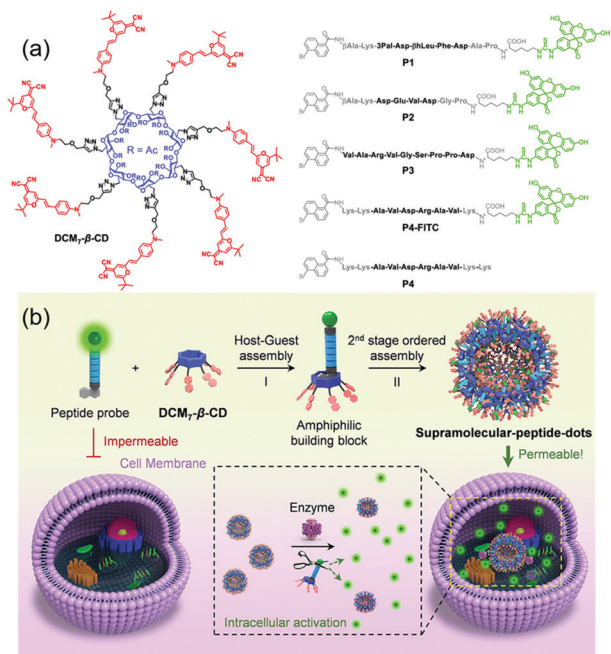


Fig. 55 (a) Chemical structures of the hepta-dicyanomethylene-4*H*-pyran-appended β -CD (DCM₇- β -CD) host and different guests of fluorescent (**P1**–**P3**, **P4**-FITC) and antimicrobial (**P4**) peptide probes. (b) Schematic illustration of the supramolecular peptide dots based on the sequential host–guest and second-stage ordered self-assembly between peptide probes and DCM₇- β -CD with enhanced cellular uptake. Reproduced with permission from ref. 389. Copyright 2020, American Chemical Society.

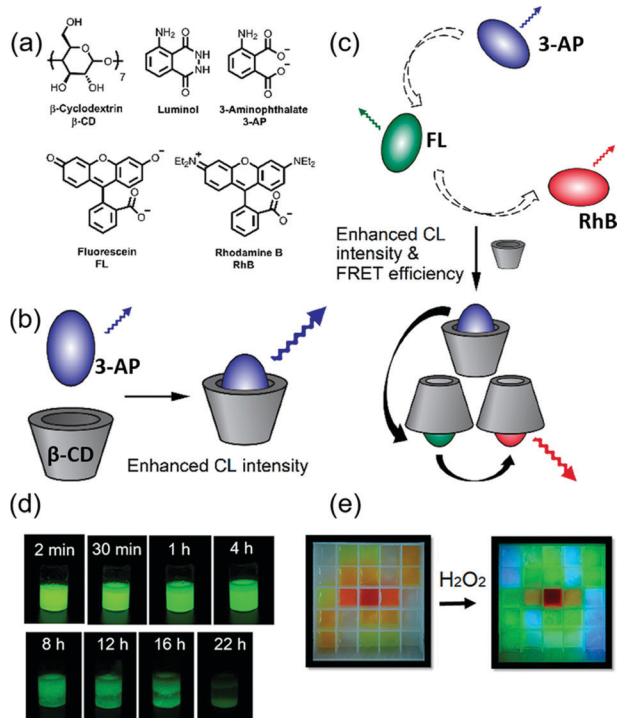


Fig. 56 (a) Chemical structures of β -CD, CL reagents, and some fluorophores used in the nanoassembly. (b) CL intensity of 3-aminophthalate (3-AP) can be greatly enhanced in the presence of β -CD. (c) Both the CL intensity and the cascade FRET efficiency can be greatly enhanced in the presence of β -CD. (d) Optical images of a β -CD-LUM-FL CL sample recorded at various time points. (e) Preparation of H_2O_2 stimuli-responsive switchable multicolor 2D codes based on multicolor CL systems. Reproduced with permission from ref. 390. Copyright 2020, American Chemical Society.

CPL crystalline materials could be prepared by integrating achiral luminophores into the γ -CD-MOF by means of the size effect and cubic chirality (Fig. 57a). That means the achiral luminophores, including neutral, positively and negatively charged, aggregation-induced quenching (ACQ), and AIE molecules could be integrated into γ -CD-MOF which emitted significantly enhanced CPL. Importantly, a size-matching effect was observed in terms of CPL induction in the cubic voids of γ -CD-MOF (Fig. 57b). When the size of the luminophore approached that of the cubic void, the luminophore could be well confined within the void, thus specifically inducing a strong negative CPL signal. However, when the luminophore was smaller than the cubic void, the interaction between the luminophore and the void was insufficient, resulting in positive or negative induced CPL. In addition, the authors found that γ -CD could hardly induce CPL in aqueous solution, while the CPL signal was also weak in amorphous powders of the luminophores and γ -CD, demonstrating that the crystalline γ -CD-MOF was far more efficient for CPL induction. Notably, the dissymmetry factor g_{lum} was also greatly improved for many luminophores. This work revealed the unique features of the cubic chirality of γ -CD-MOF, providing an excellent versatile platform for the fabrication of crystalline CPL materials from a diverse variety of achiral luminophores.

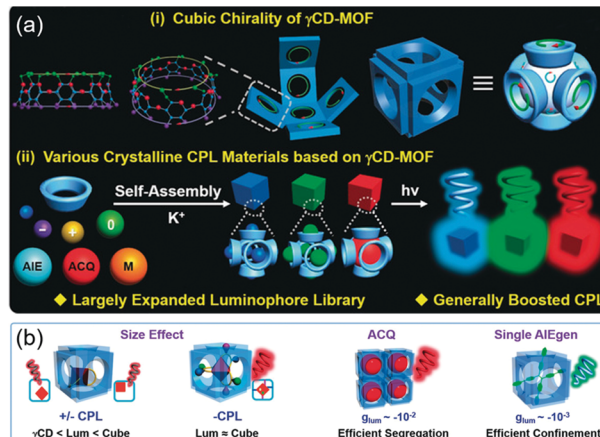


Fig. 57 (a) Schematic illustration of (i) the cubic chirality of γ -CD-MOF and (ii) various crystalline CPL materials based on γ -CD-MOF and boosted CPL for achiral luminophores. (b) Schematic illustration of the size effect and induced CPL mechanism based on the cubic chirality of γ -CD-MOF for ACQ and AIE molecules. Reproduced with permission from ref. 395. Copyright 2020, Wiley-VCH.

In the construction of rare-earth luminescent materials, Liu and co-workers reported a photoresponsive supramolecular assembly based on γ -CD-wrapped anthracene dimers for application in tunable photochromic multicolor cell labels and fluorescent inks (Fig. 58a).³⁹⁶ In this work, two anthracene-modified dipicolinic acid (AnDA) molecules were non-covalently encapsulated inside a single γ -CD cavity, and then coordination polymerization with $\text{Eu}(\text{III})$ afforded the photoresponsive assembly $\text{Eu}^{3+} \subset \gamma\text{-CD} \cdot (\text{AnDA})_2$. Irradiation of this assembly at 365 nm caused the anthracene moieties to dimerize within the γ -CD cavity, resulting in fluorescence emission ranging from cyan to red according to the different irradiation time (Fig. 58b). This supramolecular assembly was successfully applied for labeling living cells with white fluorescence and tunable photochromic fluorescent inks (Fig. 58c), representing a good approach for multicolor biological imaging and information processing.

In contrast to one γ -CD unit encapsulating two molecules of anthracene to afford a dimer, the larger size of pyrene can lead to excimer formation with γ -CD in a 2:2 binding ratio. In 2014, Inouye and co-workers reported a doubly alkynylpyrene-threaded [4]rotaxane that exhibited intense CPL from a spatially confined excimer.³⁹⁷ In this work, alkynylpyrene (Alkp) was used as the axle component of the [4]rotaxane, while γ -CD served as a wheel because its cavity can accommodate two pyrene rings to form a double-threaded inclusion complex $(\text{Alkp})_2 \subset (\gamma\text{-CD})_2$ in a 2:2 ratio (Fig. 59a). A terphenylcarboxylic acid derivative (TPCA) was used as a terminator and it reacted with the $(\text{Alkp})_2 \subset (\gamma\text{-CD})_2$ complex *via* Sonogashira coupling to afford the [4]rotaxane $(\text{Alkp} \subset \gamma\text{-CD-TPCA})$ (Fig. 59b), which displayed strong yellow-green excimer emission and a high fluorescence quantum yield because of the spatially restricted excimer. Importantly, the excimer emission was hardly affected by self-quenching and was circularly polarized with a high g_{lum} value of -1.5×10^{-2} . This strong CPL may be attributable to the presence of the two stacked

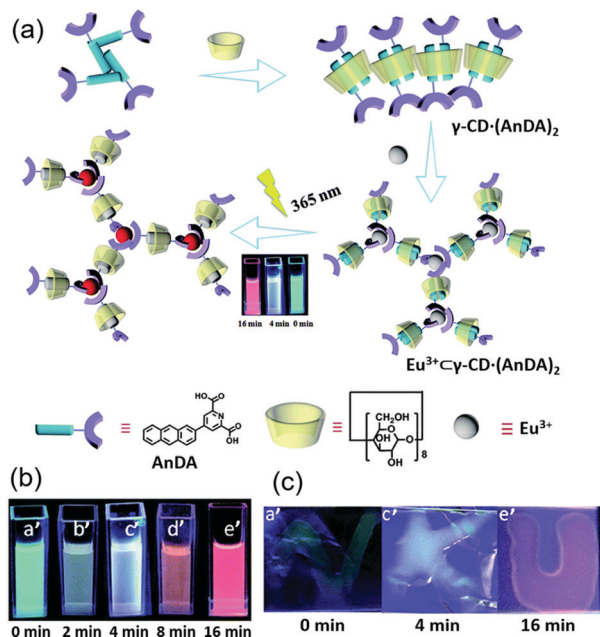


Fig. 58 (a) Schematic illustration of the construction of supramolecular assembly $\text{Eu}^{3+} \cdot \gamma\text{-CD} \cdot (\text{AnDA})_2$ and tunable lanthanide luminescence based on reversible photoinduced cyclodimerization. (b) $\text{Eu}^{3+} \cdot \gamma\text{-CD} \cdot (\text{AnDA})_2$ after photoirradiation for 0, 2, 4, 8, and 16 min in aqueous solution at pH 9.0. (c) Fluorescent inks based on $\text{Eu}^{3+} \cdot \gamma\text{-CD} \cdot (\text{AnDA})_2$ -doped PVA film under UV irradiation. Reproduced with permission from ref. 396. Copyright 2019, Royal Society of Chemistry.

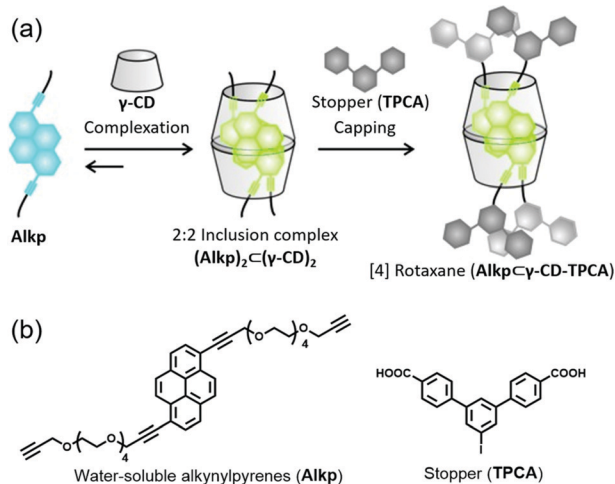


Fig. 59 (a) Schematic illustration of the construction of [4]rotaxane ($\text{Alkp} \cdot \gamma\text{-CD} \cdot \text{TPCA}$). (b) Chemical structures of the alkylnylpyrene (Alkp) and stopper (TPCA). Reproduced with permission from ref. 397. Copyright 2014, Wiley-VCH.

pyrenes in the rotaxane in an asymmetrically twisted manner. This strategy was also extended to achieve CPL from [4]rotaxane based on the excimer derived from two perylene cores.³⁹⁸

Molecular recognition

In the field of molecular recognition and imaging, Liu and co-workers reported a fluorescent β -CD supramolecular assembly

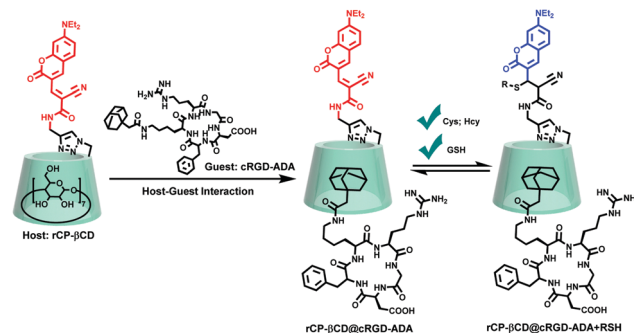


Fig. 60 Schematic illustration of the construction of rCP- β -CD@cRGD-ADA and its reversible Michael addition–elimination reactions with biothiols.

for the highly efficient dynamic sensing of biothiols in cancer cells.³¹⁵ This unique fluorescent supramolecular assembly (CP- β -CD@cRGD-ADA) was constructed using a coumarin-modified β -CD (rCP- β -CD) as a reversible ratiometric probe and an adamantane-modified cyclic Arg-Gly-Asp-containing peptide (cRGD-ADA) as a cancer-targeting agent through host-guest interactions (Fig. 60). Importantly, as a result of the numerous hydroxy groups on the β -CD surface, rCP- β -CD displayed higher sensitivity for biothiols than the parent coumarin derivative, which was accompanied by a micromolar dissociation constant. In addition, the hydrophobic cavity provided a useful means of encapsulating the cancer-targeting agent. The supramolecular assembly displayed a reversible and rapid response to biothiols alongside excellent cancer-cell permeability, which could be used to efficiently monitor biothiols in cancer cells in real time. Thus, this supramolecular strategy involving modified CDs can endow fluorescent probes with superior performance for the dynamic sensing of biothiols, and it could also be used to covalently connect other types of fluorescent probes to improve their detection sensitivity.

Chemiluminescence-based supramolecular assemblies of CDs exhibit significantly high signal-to-noise ratios for molecular recognition because of their low background, lack of interference from autofluorescence, and high sensitivity.³⁹⁹ As IUPAC officially announced the “Top Ten Emerging Technologies in Chemistry” in 2021, the water-soluble dioxetane was selected because it improved the speed and sensitivity of biological detection.⁴⁰⁰ Therefore, in order to further improve the chemiluminescence efficiency of adamantane-dioxetane chemiluminescent probes, Shabat and co-workers reported several 1:1 host-guest complexes for enhanced bioimaging based on chemiluminescent phenoxy-adamantyl-1,2-dioxetane probes as the guests and trimethyl β -CD (TMCD) as the host.⁴⁰¹ In aqueous solution, the alkaline-phosphatase-activated probe **1** displayed minimal light emission, whereas the formed host-guest complex **1**/TMCD emitted bright light with an intensity approximately 60 times greater than that from the probe alone (Fig. 61a). This emission enhancement originated from the hydrophobic environment of the CD cavity, which reduced water-induced quenching. Subsequently, fluorescein was covalently attached to TMCD to obtain TMCD-FITC, which encapsulated probe **1** to afford a

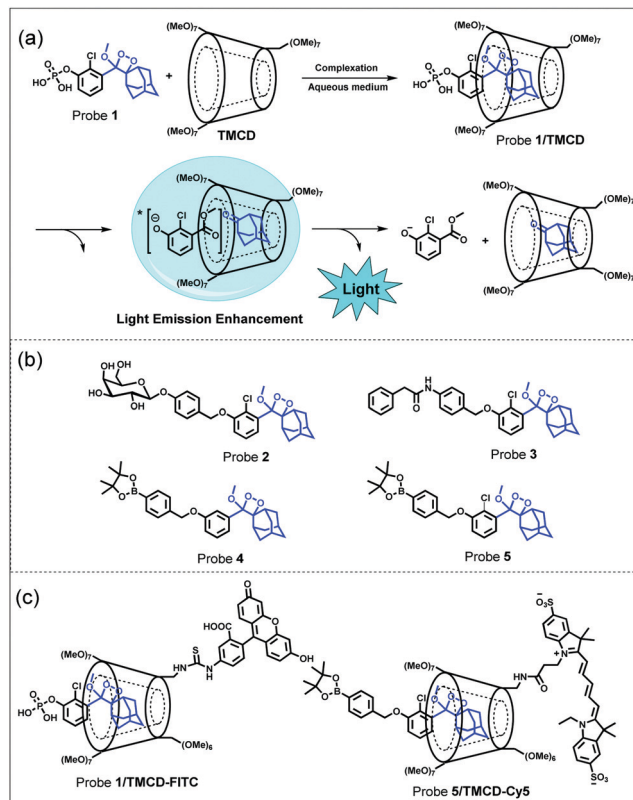


Fig. 61 (a) Encapsulation of probe **1** by permethylated β -CD (TMCD) and activation pathway of the triggerable **1**/TMCD complex. (b) Molecular structures of probes **2–4**. (c) Molecular structures of the **1**/TMCD-FITC and **5**/TMCD-Cy5 complexes.

new supramolecular complex probe denoted **1**/TMCD-FITC. In aqueous solution, the luminescence intensity of the **1**/TMCD-FITC complex was approximately 1500 times that of probe **1** alone. Furthermore, three additional probes (**2–4**) were synthesized for the detection of β -galactosidase, penicillin G amidase, and H_2O_2 , respectively (Fig. 61b). All three probes exhibited enhanced chemiluminescence signals after complexation with TMCD-FITC. For live-cell imaging, the **2**/TMCD-FITC complex was incubated with HEK-293-LacZ cells, leading to a strong chemiluminescence signal with an approximately 400-fold enhancement relative to probe **2** alone and a 15-fold enhancement relative to TMCD. For *in vivo* applications, TMCD was modified with the dye Cy5, and probe **5** was used to image ROS (Fig. 61c). In lipopolysaccharide-treated mice, the observed NIR light emission intensity from the **5**/TMCD-Cy5 complex was approximately threefold greater than that in untreated mice, and no significant change was observed after treatment with probe **5** alone. This work provides guidance for developing chemiluminescent supramolecular dioxetane-based probes for various biological applications.

By using the susceptibility of CDs to specific hydrolysis in the presence of α -amylase,⁴⁰² Zhang and co-workers developed an enzyme-responsive supra-amphiphile based on a γ -CD and a tetraphenylethylene–sodium glycyrrhetinate conjugate (TPE-SGA) through host–guest recognition (Fig. 62).⁴⁰³ The amphiphile

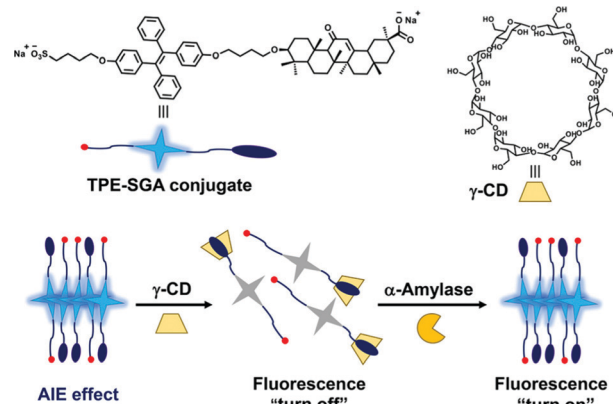


Fig. 62 Schematic illustration of the construction and α -amylase responsiveness of the supra-amphiphile based on the TPE-SGA conjugate and γ -CD. Reproduced with permission from ref. 403. Copyright 2021, American Chemical Society.

TPE-SGA exhibited strong fluorescence due to AIE in aqueous solution. Upon the addition of γ -CD, the aggregation of TPE-SGA was prevented owing to the host–guest recognition by γ -CD, which effectively quenched the fluorescence of TPE-SGA. In contrast, α - and β -CD exerted no effect on the assembly behavior because of their weaker host–guest interactions. In the presence of α -amylase, γ -CD underwent hydrolysis, resulting in a gradual turn-on of the fluorescence of the supra-amphiphile, and the fluorescence intensity was linearly correlated with the α -amylase activity. This study has enriched the field of CD-based supra-amphiphiles and provided a new strategy for constructing fluorescent functional assembly, which is expected to lead to potential applications in biological analysis and the diagnosis of pancreatic diseases.

Liquid crystal materials based on CDs can also display specific molecular-recognition abilities. By using the host–guest complex of sodium dodecyl sulfate (SDS) and β -CD, Munir and Park reported a cholesterol biosensor based on the liquid crystal/aqueous interface in a solution (Fig. 63).⁴⁰⁴ The liquid crystal/aqueous interface consisted of the mesogen 4-cyano-4'-pentylbiphenyl (5CB) and was arranged in a transmission electron microscopy (TEM) grid cell. Upon the addition

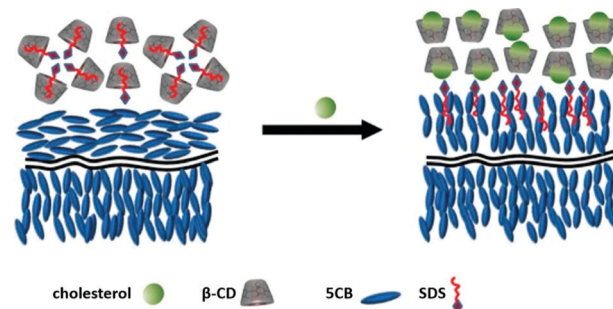


Fig. 63 Schematic illustration of a cholesterol biosensor based on the mesogen 4-cyano-4'-pentylbiphenyl (5CB) liquid crystal/aqueous interface mediated by the host–guest complex of SDS and β -CD in solution. Reproduced with permission from ref. 404. Copyright 2015, Elsevier.

of an excess concentration of cholesterol solution into the TEM cell, the guest SDS molecules enclosed in the β -CD cavities were completely replaced with cholesterol molecules. The excluded SDS altered the planar orientation of the 5CB/aqueous interface to a homeotropic orientation. This planar-to-homeotropic transition at the 5CB/aqueous interface could be detected optically using a polarizing optical microscopy system equipped with crossed polarizers. The TEM grid cell sensor system can be used to determine the cholesterol concentrations in human blood.

CD-POM complexes

The hydrophobic cavities of CDs can also form complexes with hydrophilic guests, especially polyoxometalates (POMs). For example, Stoddart and co-workers reported the complexation of β - and γ -CDs with the archetypal POM trianion $[\text{PMo}_{12}\text{O}_{40}]^{3-}$, leading to the formation of two organic-inorganic hybrid 2:1 CD-POM complexes (Fig. 64a).⁴⁰⁵ The main driving force governing the formation of these hybrid assemblies is the molecular recognition encoded by the remarkable complementarity of molecular structure, including size-fitness, pre-organization, and hydrogen bonding. Single-crystal diffraction analysis revealed that these pre-assembled complexes further self-organized into one-dimensional (1D) tubular arrays in a solid-state superstructure (Fig. 64b). Importantly, the redox properties of the trianion were largely retained in the CD-POM complexes, with additional chemical/electrochemical stabilization. The constructed CD-POM complexes have potential applications in the fields of catalysis and biomedical materials.

As novel modified CD macrocycles, partially oxidized β -CD aldehydes can also be complexed with POMs. Mao and co-workers reported a sensing platform consisting of cross-linked cyclodextrin (CL-CD) and lanthanide-ion-containing polyoxometalate clusters (LnPOM) for the selective detection of inorganic and organic phosphates.⁴⁰⁶ In this system, β -CD was first partially oxidized to obtain the aldehyde-containing β -CD, which afforded improved water solubility and higher

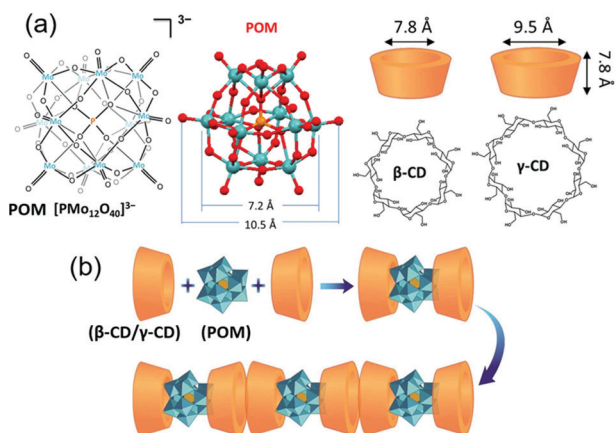


Fig. 64 (a) Chemical structures of the $[\text{PMo}_{12}\text{O}_{40}]^{3-}$ trianion and its X-ray crystal structure (color code: Mo, cyan; O, red; P, orange), β -CD, and γ -CD. (b) Schematic illustration of the formation of CD-POM complexes. Reproduced with permission from ref. 405. Copyright 2015, American Chemical Society.

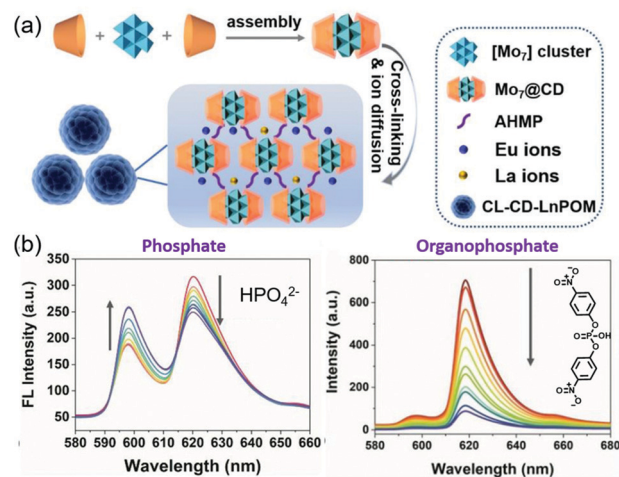


Fig. 65 (a) Schematic illustration of CL-CD-LnPOM formation through the host-guest interaction between β -CD and POM, crosslinking, and post-diffusion of lanthanide ions including Eu^{3+} and La^{3+} ions. (b) Fluorescence spectra of CL-CD-LnPOM with HPO_4^{2-} and bis(*p*-nitrophenyl) phosphate. Reproduced with permission from ref. 406. Copyright 2021, Wiley-VCH.

reactivity with crosslinkers. Then, the $\text{Mo}_7\text{O}_{24}^{6-}$ $[\text{Mo}_7]$ anion was locked in the CD molecular torus with the molar ratio of 2:1 ($\text{Mo}_7@CD$) owing to the size-fitness. Finally, CL-CD-LnPOM was prepared using 4-amino-6-hydroxy-2-mercaptopyrimidine (AHMP) as a crosslinker followed by the post-diffusion of Ln^{3+} (Eu^{3+} and La^{3+}) ions (Fig. 65a). CL-CD-LnPOM exhibited an excellent ratiometric fluorescence response and good selectivity for inorganic phosphate, as well as high tolerance to complex analyte mixtures due to the strong affinity of POM and the unique interactions between La^{3+} , Eu^{3+} , and phosphate ions (Fig. 65b). Furthermore, it exhibited a “signal-off” fluorescence response to nitrophenyl-substituted organophosphates, which displayed a stronger interaction with POM owing to the encapsulation of the nitrophenyl group by the hydrophobic CD cavity. The different responses of CL-CD-LnPOM to inorganic and organic phosphates provide new insights into the detection of inorganic and organic phases by POM-based supramolecular optical probes.

CD-COF porous materials

CDs can also be used to construct covalent organic frameworks (COFs), since hydroxy groups can serve as efficient chelating and nucleophilic sites. Feng and co-workers reported the construction of three-dimensional anionic CD-based COFs using γ -CD as organic struts and trimethyl borate ($\text{B}(\text{OMe})_3$) as tetrahedral linkages under basic conditions with microwave assistance (Fig. 66).¹⁶⁷ In the presence of LiOH , the 3D anionic COF (CD-COF-Li) was achieved with Li^+ as the counterion, accompanied by a highly crystalline structure. Due to the properties of flexible building blocks, charged skeleton and high porosity, CD-COF-Li shows Li ion conductivity as high as 2.7 mS cm^{-1} at 30°C and a Brunauer-Emmett-Teller (BET) surface area of $760 \text{ m}^2\text{g}^{-1}$. In addition, the counterions of CD-COFs can be

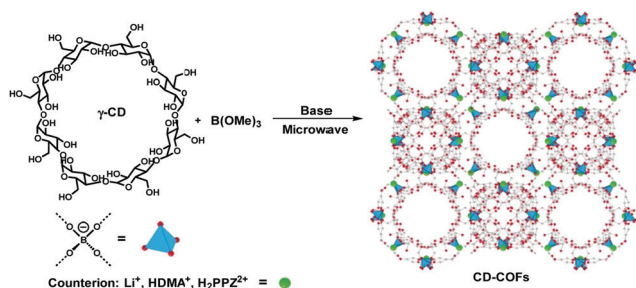


Fig. 66 Synthesis of CD-COFs based on γ -CD and $\text{B}(\text{OMe})_3$ in the presence of LiOH , DMA , or PPZ under microwave conditions with different counterions. Reproduced with permission from ref. 167. Copyright 2017, Wiley-VCH.

converted to dimethylamine (DMA) or piperazine (PPZ), so the inner charged pore surface environment can be regulated. In the application of CO_2 adsorption, CD-COF-Li exhibited high uptake and selectivity because of the ionic nature, hydroxy groups and microporosity, indicating that it has carbon capture potential. This strategy of constructing CD-based COFs holds great promise in developing crystalline porous solids for energy, medical, and environmental applications.

Topological morphology regulation

The supramolecular assemblies obtained by covalently linking CDs and Azo derivatives can exhibit highly efficient stimuli responsiveness with a controlled topological morphology. Liu and co-workers reported the tunable supramolecular assembly and photoconversion switching of 1D and 2D nanostructures based on azobenzene-bridged bis(β -CD) (**H**) and adamantanyl-modified diphenylalanine (Ada-FF) (Fig. 67a).⁴⁰⁷ Ada-FF can self-assemble into 1D nanofibers with a length of several micrometers. After assembly with *trans*-**H**, Ada-FF@trans-H formed numerous 2D planar nanosheets with a length and width of several micrometers. Because **H** can undergo reversible photoisomerization between its *trans* isomer (*trans*-**H**) and *cis* isomer (*cis*-**H**) upon external photostimulation with UV light at 365 nm and visible light at 450 nm, the Ada-FF@cis-H assembly displayed many curved tubular structures with open ends. On account of the different Brunauer–Emmett–Teller surface areas of the nanosheets and nanotubes, distinct adsorption capacities for Nile red were observed. Fluorescence microscopy images revealed that the 2D nanosheets loaded with Nile red displayed stronger fluorescence emission than the similarly loaded 1D nanotubes, indicating that the 2D nanosheets provided superior adsorption and fluorescence enhancement (Fig. 67b). These results provide a convenient approach for controlling assembly and morphological transition processes by using different wavelengths of light.

For a guest whose chromophore is located within the CD cavity, it has been found that the dipole–dipole interaction between the CD and the chromophore leads to a positive induced circular dichroism (ICD) spectrum.⁴⁰⁸ Conversely, a negative ICD spectrum should be expected if the chromophore is located outside of the CD cavity.⁴⁰⁹ Therefore, in an effort to

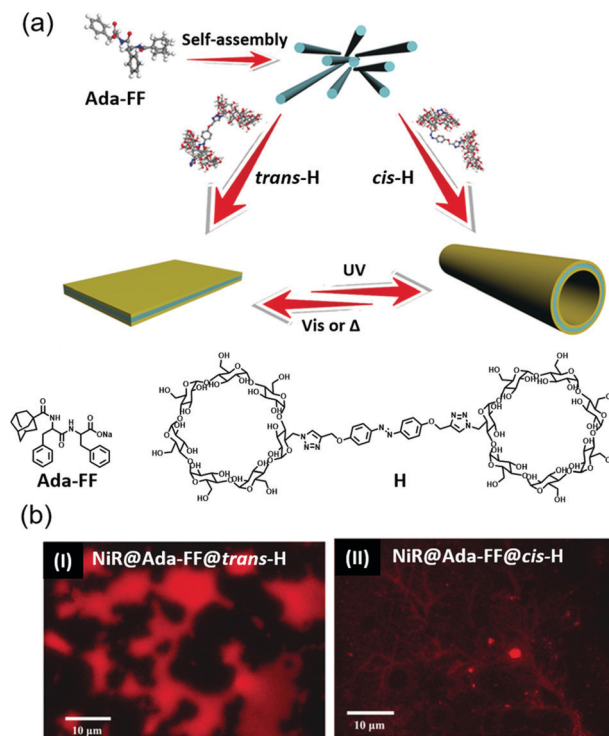


Fig. 67 (a) Chemical structures of adamantanyl-modified diphenylalanine (Ada-FF) and azobenzene-bridged bis(β -CD) (**H**), and schematic illustration of their assembly. (b) Fluorescence microscopy images of $\text{NiR@Ada-FF@trans-H}$ and NiR@Ada-FF@cis-H . Reproduced with permission from ref. 407. Copyright 2017, Wiley-VCH.

control the supramolecular chirality of self-assembled structures, Yan and co-workers reported symmetry breaking and precise regulation of chirality in supramolecular self-assembly catalyzed by α -CD (Fig. 68).⁴¹⁰ The studied achiral alkylazo-benzene derivative (C4AZO) was able to simultaneously form coordination complexes with Zn^{2+} through strong self-assembly ability and hollow cone shell structures exhibiting both left- and right-handed chirality. Notably, the C4 chain was critical

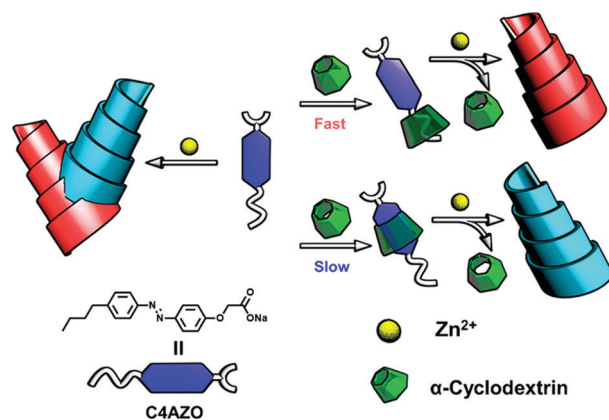


Fig. 68 Schematic illustration of α -CD-catalyzed symmetry breaking in the coordinating self-assembly system of $\text{Zn}(\text{C4AZO})_2$ cone shells. Reproduced with permission from ref. 410. Copyright 2021, American Chemical Society.

for the formation of the helical structure; when it was removed or shortened to C2, only plate-like structures were formed, suggesting that the C4 alkyl chains in the bilayer may create steric hindrance that hinders the azobenzene groups during the coordinated self-assembly of $\text{Zn}(\text{C4AZO})_2$, such that they must form some dislocations during their assembly with Zn^{2+} . In addition, because C4AZO forms a host-guest complex with α -CD, the further addition of Zn^{2+} resulted in drastic symmetry breaking of the cone shell self-assembly. The mechanism may involve C4AZO entering the α -CD cavity from both the wider and narrower rim together with butyl and azobenzene groups, resulting in diverse conformations. Because of the small difference in formation energy, these conformations were in dynamic equilibrium with each other. However, after the addition of metal ions, the conformation near the narrower edge of the polar head became dominant because it may have encountered less steric hindrance as it packed further into a bilayer. Since the coordination reduced the electrostatic repulsion between C4AZO molecules, the π - π stacking was significantly enhanced. Consequently, α -CD was extruded from the system, but leaving the induced chirality to the coordinative self-assembly of $\text{Zn}(\text{C4AZO})_2$.

Chiral π -gelators with photoresponsive emitters are ideal platforms for reversibly modulating CPL materials. However, the photoinduced configuration transformation of luminophores often does not proceed smoothly or sufficiently owing to tight π - π -stacking-induced aggregation or self-assembly. The large inner cavity of CDs may provide sufficient space for photoisomerization while maintaining self-assembly ability and avoiding the compact packing of chromophores, enabling improved photoresponsive properties. Recently, Liu and co-workers integrated a cyanostilbene hydrogel (CG) into γ -CD *via* host-guest interactions to obtain an efficient and durable photoswitchable CPL-active supra-gelator (CG \subset γ -CD) (Fig. 69).⁴¹¹ Supra-gelators can also be prepared using CG with α - or β -CDs; although photo-switching cannot be achieved, these gels exhibit enhanced CPL because the cyanostilbene moiety is fixed in the CD cavity. In particular, photoresponsiveness was observed in the case of the γ -CD supra-gelator because of the large cavity of γ -CD. Because both (*Z*)- and (*E*)-cyanostilbene always remain encapsulated within the inner cavity of γ -CD, *Z*-*E* isomerization becomes more fatigue resistant. Under UV irradiation, the CPL from the CG \subset γ -CD hydrogel disappeared and subsequently recovered upon heating with excellent reversibility, which provides insights for designing CD-based photoresponsive CPL materials. In this work, the chiral sign of the supra-gelator was determined by the molecular chirality of the CG components; the CD itself only enhanced the chiral signal intensity but did not control the chiral sign during the formation of the assembled nanostructures. However, during the assembly process, although the addition of the CD did not alter the bilayer structure of the CG molecules, the large size of the CD resulted in the destruction of the non-covalent interactions between the amide bonds, leading to slight changes in the spatial arrangement of the chromophores that resulted in enhanced circular dichroism and CPL.

Huang and co-workers reported a 2:1 complex between β -CD and sodium dodecyl sulfate (SDS) that could self-assemble

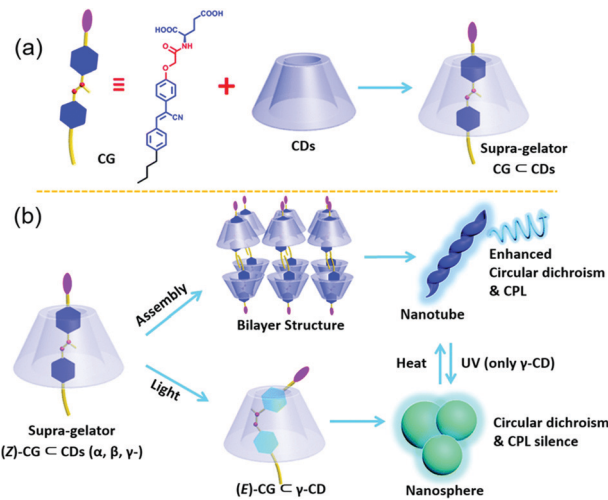


Fig. 69 (a) Schematic illustration of a supra-gelator CG \subset CDs based on host-guest interactions of cyanostilbene hydrogelator (CG) and CDs. (b) Schematic illustration of photoregulated reversible self-assembly of CG \subset CDs, as well as the activity of circular dichroism and CPL. Reproduced with permission from ref. 411. Copyright 2019, Royal Society of Chemistry.

into lamellar and vesicular structures in aqueous solutions of different concentrations.²⁴⁶ The 2:1 inclusion complex of SDS and β -CD could self-assemble into lamellar structures in concentrated aqueous solution, accompanied by classical lamellar liquid-crystalline ordering and in-plane solid-crystalline ordering, which can be regarded as an intermediate phase between a liquid crystal and a solid. After that, the aggregates can transform from lamellae *via* microtubes to vesicles upon dilution (Fig. 70). In this system, the source of driving force for assembly is hydrogen bonding and electrostatic interactions rather than the hydrophobic effect. The nonamphiphilic self-assembly of the 2:1 inclusion complex provides a valuable research basis for self-assembly chemistry.

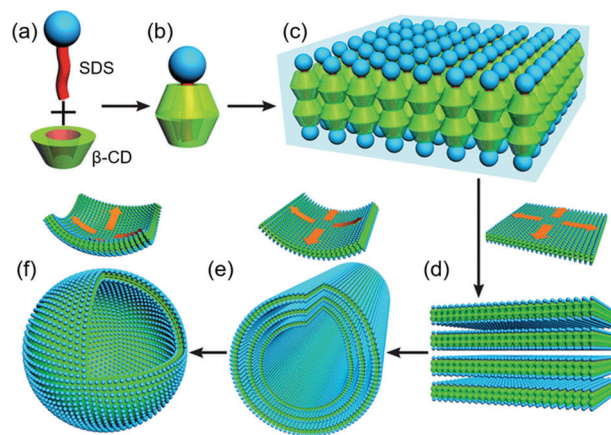


Fig. 70 Schematic illustration of the self-assembly process of β -CD and SDS. (a) SDS and β -CD monomers. (b) 2:1 inclusion complex of β -CD and SDS. (c) β -CD-SDS bilayer membrane with channel-type crystal structure. (d-f) Schematic illustration of the transformation of aggregates from lamellae *via* microtubes to vesicles upon dilution. Reproduced with permission from ref. 246. Copyright 2011, Royal Society of Chemistry.

4. Summary and outlook

In summary, supramolecular assemblies based on multicharged CDs and parent CDs encapsulating charged guests have been extensively applied in chemistry, materials science, medicine, biological science, catalysis, and other fields. By comparing the studies discussed throughout this review, it can be seen that multicharged CDs are important macrocyclic compounds that not only enrich CD-based chemistry but also promote the development of supramolecular chemistry and related disciplines in general. For example, positively charged CDs can be used to enhance antibacterial activity, while negatively charged CDs can be applied to improve antiviral activity and inhibit protein fibrosis. Negatively charged CDs are often exploited in co-assemblies with fluorescent dyes to realize excellent luminescence properties with applications in light-harvesting energy transfer and molecular recognition. In particular, the modification of hyaluronic acid with β -CD not only allows the encapsulation of drugs or fluorophores for targeted delivery to cancer cells but also serves as a framework for the construction of supramolecular hydrogels. In the preparation of rotaxanes and hydrogels, the introduction of positive charges can alter the threading and dethreading rates, while the introduction of negative charges can lead to a large number of hydrogen bonds, significantly improving hydrogel strength and toughness. In CD-based host-guest assemblies, negative charges are mainly used as terminators to form supramolecular rotaxanes and for coordination with metal ions to construct multilevel supramolecular assemblies, while positive charges are primarily exploited for co-assembly with polyanionic clusters, *etc.* Notably, the assembly of CDs and negatively charged surfactants facilitates the construction of ordered assemblies such as liquid crystals, which can be applied in molecular recognition and regulation of assembly morphology. In addition, the host-guest interactions of CDs in luminescent supramolecular assemblies can significantly enhance the luminescence and induce purely organic room-temperature phosphorescence, circularly polarized luminescence, intramolecular folding, and dimer formation, endowing raw materials with novel functions.

The key challenge for the future with respect to the construction of supramolecular assemblies based on multicharged CDs is to develop more efficient and versatile luminescent assemblies, such as those operating in the near-infrared II window and two- or three-photon excitation assemblies for molecular recognition and imaging *in vivo*. In addition to developing supramolecular fluorescent or phosphorescent materials with higher quantum yields and longer lifetimes, attention should be devoted to the introduction of photoisomeric groups such as spiropyran and diarylethene derivatives, which can be used not only for anti-counterfeiting and encryption applications but also in photostimulated release for *in situ* monitoring and drug-release applications. Furthermore, for the construction of pH-triggered surface-charge-switchable nanomaterials, CDs can be directly modified with reagents such as 2,3-dimethylmaleic anhydride, thereby enabling efficient drug delivery and controllable release. Zwitterionic or ionic liquids

can be appropriately introduced into supramolecular assemblies and combined with the host-guest interactions of CDs to construct multistimuli-responsive supramolecular functional materials. CD-based selective catalytic systems and liquid crystal materials also warrant extensive study by using the selective host-guest interactions of CDs and their hydroxy groups. Meanwhile, partial oxidation yields aldehyde-containing CDs, which not only improve aqueous solubility but can also be used for crosslinking and encapsulation of larger molecules due to the more spacious cavity. Multicharged polyrotaxanes will also be used to construct soft materials with potential applications in polymer science. Supramolecular assemblies of multicharged CDs formed by cavity confinement and multicharge interactions are expected to become more widely used in fields such as supercatalysis, superassembly, and confined luminescence. Overall, we believe that the construction of functional materials based on multicharged CD supramolecular assemblies will surely promote their rapid development in luminescent materials, information anti-counterfeiting and encryption, soft robotics, 3D printing, flexible electronic devices, information processing, molecular recognition, soft materials, and other scientific and technological fields.

Conflicts of interest

There are no conflicts to declare.

Acknowledgements

This work was supported by the National Natural Science Foundation of China (grant no. 22131008, 21807038, 21772099) and the China Postdoctoral Science Foundation (grant no. 2019M651006). We thank the Haihe Laboratory of Sustainable Chemical Transformations for financial support.

References

- 1 L. Szente and J. Szeman, *Anal. Chem.*, 2013, **85**, 8024–8030.
- 2 C. B. Lebrilla, *Acc. Chem. Res.*, 2001, **34**, 653–661.
- 3 J. P. Quirino, W. Grochocki and M. J. Markuszewski, *Anal. Chem.*, 2017, **89**, 13422–13428.
- 4 X. Du, Y. Wang, S. Zhang, P. Fan, S. Yan, P. Zhang, H. Y. Chen and S. Huang, *Anal. Chem.*, 2021, **93**, 14161–14168.
- 5 S. Li and W. C. Purdy, *Chem. Rev.*, 1992, **92**, 1457–1470.
- 6 T. Huang, G. Sheng, P. Manchanda, A. H. Emwas, Z. Lai, S. P. Nunes and K. V. Peinemann, *Sci. Adv.*, 2019, **5**, eaax6976.
- 7 Y. Zhao, Y. Huang, H. Zhu, Q. Zhu and Y. Xia, *J. Am. Chem. Soc.*, 2016, **138**, 16645–16654.
- 8 C. Blaszkiewicz, H. Bricout, E. Leonard, C. Len, D. Landy, C. Cezard, F. Djedaini-Pilard, E. Monflier and S. Tilloy, *Chem. Commun.*, 2013, **49**, 6989–6991.
- 9 M. Guitet, P. Zhang, F. Marcelo, C. Tugny, J. Jimenez-Barbero, O. Buriez, C. Amatore, V. Mouries-Mansuy, J. P. Goddard, L. Fensterbank, Y. Zhang, S. Roland, M. Menand

- and M. Sollogoub, *Angew. Chem., Int. Ed.*, 2013, **52**, 7213–7218.
- 10 F. Ortega-Caballero, C. Rousseau, B. Christensen, T. E. Petersen and M. Bols, *J. Am. Chem. Soc.*, 2005, **127**, 3238–3239.
 - 11 D. Prochowicz, A. Kornowicz and J. Lewinski, *Chem. Rev.*, 2017, **117**, 13461–13501.
 - 12 X.-B. Li, J.-X. Jian, X.-Z. Wang, Y. Wang, S.-G. Xia, C.-H. Tung and L.-Z. Wu, *Sol. RRL*, 2020, **5**, 2000474.
 - 13 A. Harada, Y. Takashima and H. Yamaguchi, *Chem. Soc. Rev.*, 2009, **38**, 875–882.
 - 14 M. Votava and B. J. Ravoo, *Chem. Soc. Rev.*, 2021, **50**, 10009–10024.
 - 15 X. Ma and Y. Zhao, *Chem. Rev.*, 2015, **115**, 7794–7839.
 - 16 J. Wankar, N. G. Kotla, S. Gera, S. Rasala, A. Pandit and Y. A. Rochev, *Adv. Funct. Mater.*, 2020, **30**, 1909049.
 - 17 C. Alvarez-Lorenzo, C. A. Garcia-Gonzalez and A. Concheiro, *J. Controlled Release*, 2017, **268**, 269–281.
 - 18 R. Liao, P. Lv, Q. Wang, J. Zheng, B. Feng and B. Yang, *Biomater. Sci.*, 2017, **5**, 1736–1745.
 - 19 C. Ortiz Mellet, J. M. Garcia Fernandez and J. M. Benito, *Chem. Soc. Rev.*, 2011, **40**, 1586–1608.
 - 20 G. Chen and M. Jiang, *Chem. Soc. Rev.*, 2011, **40**, 2254–2266.
 - 21 R. Villalonga, R. Cao and A. Fragoso, *Chem. Rev.*, 2007, **107**, 3088–3116.
 - 22 A. Douhal, *Chem. Rev.*, 2004, **104**, 1955–1976.
 - 23 S. Monti and S. Sortino, *Chem. Soc. Rev.*, 2002, **31**, 287–300.
 - 24 D. Xia, P. Wang, X. Ji, N. M. Khashab, J. L. Sessler and F. Huang, *Chem. Rev.*, 2020, **120**, 6070–6123.
 - 25 S. Pan, R. Guo, N. Bertleff-Zieschang, S. Li, Q. A. Besford, Q. Z. Zhong, G. Yun, Y. Zhang, F. Cavalieri, Y. Ju, E. Goudeli, J. J. Richardson and F. Caruso, *Angew. Chem., Int. Ed.*, 2020, **59**, 275–280.
 - 26 B. Schmidt and C. Barner-Kowollik, *Angew. Chem., Int. Ed.*, 2017, **56**, 8350–8369.
 - 27 Y. He, Y. J. Yoon, Y. W. Harn, G. V. Biesold-McGee, S. Liang, C. H. Lin, V. V. Tsukruk, N. Thadhani, Z. Kang and Z. Lin, *Sci. Adv.*, 2019, **5**, eaax4424.
 - 28 Y. Chen, F. Huang, Z.-T. Li and Y. Liu, *Sci. China: Chem.*, 2018, **61**, 979–992.
 - 29 G. Crini, *Chem. Rev.*, 2014, **114**, 10940–10975.
 - 30 Z. Liu, X. Dai, Y. Sun and Y. Liu, *Aggregate*, 2020, **1**, 31–44.
 - 31 T. Matsunaga, J. Kanazawa, T. Ichikawa, M. Harada, Y. Nishiyama, N. T. Duong, T. Matsumoto, K. Miyamoto and M. Uchiyama, *Angew. Chem., Int. Ed.*, 2021, **60**, 2578–2582.
 - 32 X. Wang, J. Ji, M. Rao, W. Wu and C. Yang, *Chem. – Asian J.*, 2021, **16**, 3091–3096.
 - 33 H. Shigemitsu, K. Kawakami, Y. Nagata, R. Kajiwara, S. Yamada, T. Mori and T. Kida, *Angew. Chem., Int. Ed.*, 2022, **61**, e202114700.
 - 34 I. Krabicova, S. L. Appleton, M. Tannous, G. Hoti, F. Caldera, A. Rubin Pedrazzo, C. Ceccone, R. Cavalli and F. Trotta, *Polymers*, 2020, **12**, 1122.
 - 35 D. Ikuta, Y. Hirata, S. Wakamori, H. Shimada, Y. Tomabechi, Y. Kawasaki, K. Ikeuchi, T. Hagimori, S. Matsumoto and H. Yamada, *Science*, 2019, **364**, 674–677.
 - 36 T. Takaha, M. Yanase, H. Takata, S. Okada and S. M. Smith, *J. Biol. Chem.*, 1996, **271**, 2902–2908.
 - 37 W. W. Li, T. D. Claridge, Q. Li, M. R. Wormald, B. G. Davis and H. Bayley, *J. Am. Chem. Soc.*, 2011, **133**, 1987–2001.
 - 38 T. Kureha, D. Aoki, S. Hiroshige, K. Iijima, D. Aoki, T. Takata and D. Suzuki, *Angew. Chem., Int. Ed.*, 2017, **56**, 15393–15396.
 - 39 W. C. Geng, J. L. Sessler and D. S. Guo, *Chem. Soc. Rev.*, 2020, **49**, 2303–2315.
 - 40 Y. Chen and Y. Liu, *Chem. Soc. Rev.*, 2010, **39**, 495–505.
 - 41 F. Bellia, D. La Mendola, C. Pedone, E. Rizzarelli, M. Saviano and G. Vecchio, *Chem. Soc. Rev.*, 2009, **38**, 2756–2781.
 - 42 M. Řezanka, *Environ. Chem. Lett.*, 2018, **17**, 49–63.
 - 43 A. R. Khan, P. Forgo, K. J. Stine and V. T. D'Souza, *Chem. Rev.*, 1998, **98**, 1977–1996.
 - 44 A. Martinez, C. Ortiz Mellet and J. M. Garcia Fernandez, *Chem. Soc. Rev.*, 2013, **42**, 4746–4773.
 - 45 S. Guieu, E. Zaborova, Y. Bleriot, G. Poli, A. Jutand, D. Madec, G. Prestat and M. Sollogoub, *Angew. Chem., Int. Ed.*, 2010, **49**, 2314–2318.
 - 46 E. Zaborova, M. Guitet, G. Prencipe, Y. Bleriot, M. Menand and M. Sollogoub, *Angew. Chem., Int. Ed.*, 2013, **52**, 639–644.
 - 47 J. Liu, B. Wang, C. Przybylski, O. Bistri-Aslanoff, M. Menand, Y. Zhang and M. Sollogoub, *Angew. Chem., Int. Ed.*, 2021, **60**, 12090–12096.
 - 48 T. Tominaga, K. Fukuda, K. Koga, M. Fukudome and D. Q. Yuan, *Chem. – Eur. J.*, 2022, **28**, e202103940.
 - 49 P. Zhang, A. Wang, L. Cui and C. C. Ling, *Org. Lett.*, 2012, **14**, 1612–1615.
 - 50 M. Řezanka, *Eur. J. Org. Chem.*, 2016, 5322–5334.
 - 51 P. L. Champagne, D. Ester, D. Polan, V. E. Williams, V. Thangadurai and C. C. Ling, *J. Am. Chem. Soc.*, 2019, **141**, 9217–9224.
 - 52 P. Falvey, C. W. Lim, R. Darcy, T. Revermann, U. Karst, M. Giesbers, A. T. Marcelis, A. Lazar, A. W. Coleman, D. N. Reinhoudt and B. J. Ravoo, *Chem. – Eur. J.*, 2005, **11**, 1171–1180.
 - 53 P.-L. Champagne, D. Ester, M. Zeeman, C. Zellman, V. E. Williams and C.-C. Ling, *J. Mater. Chem. C*, 2017, **5**, 9247–9254.
 - 54 S. Ward, O. Calderon, P. Zhang, M. Sobchuk, S. N. Keller, V. E. Williams and C.-C. Ling, *J. Mater. Chem. C*, 2014, **2**, 4928–4936.
 - 55 D. Larsen, P. M. Bjerre and S. R. Beeren, *Chem. Commun.*, 2019, **55**, 15037–15040.
 - 56 S. G. Bolton and M. D. Pluth, *Chem. Sci.*, 2020, **11**, 11777–11784.
 - 57 C. M. Yau, S. I. Pascu, S. A. Odom, J. E. Warren, E. J. Klotz, M. J. Frampton, C. C. Williams, V. Coropceanu, M. K. Kuimova, D. Phillips, S. Barlow, J. L. Bredas, S. R. Marder, V. Millar and H. L. Anderson, *Chem. Commun.*, 2008, 2897–2899.
 - 58 T. Oshikiri, Y. Takashima, H. Yamaguchi and A. Harada, *Chem. – Eur. J.*, 2007, **13**, 7091–7098.
 - 59 G. Fang, X. Yang, S. Chen, Q. Wang, A. Zhang and B. Tang, *Coord. Chem. Rev.*, 2022, **454**, 214352.

- 60 H. Xu, C. Zhou, C. Jian, S. Yang, M. Liu, X. Huang, W. Gao and H. Wu, *Chin. Chem. Lett.*, 2020, **31**, 369–372.
- 61 A. Miyawaki, M. Miyauchi, Y. Takashima, H. Yamaguchi and A. Harada, *Chem. Commun.*, 2008, 456–458.
- 62 M. M. Sartin, M. Osawa, S. Takeuchi and T. Tahara, *Chem. Commun.*, 2022, **58**, 961–964.
- 63 S. S. Liow, H. Zhou, S. Sugiarto, S. Guo, M. L. Chalasani, N. K. Verma, J. Xu and X. J. Loh, *Biomacromolecules*, 2017, **18**, 886–897.
- 64 M. Guo, M. Jiang, S. Pispas, W. Yu and C. Zhou, *Macromolecules*, 2008, **41**, 9744–9749.
- 65 Y. Liu, C. Yu, H. Jin, B. Jiang, X. Zhu, Y. Zhou, Z. Lu and D. Yan, *J. Am. Chem. Soc.*, 2013, **135**, 4765–4770.
- 66 Z. Hu, D. Zhang, F. Lu, W. Yuan, X. Xu, Q. Zhang, H. Liu, Q. Shao, Z. Guo and Y. Huang, *Macromolecules*, 2018, **51**, 5294–5303.
- 67 Y. M. Zhang, N. Y. Zhang, K. Xiao, Q. Yu and Y. Liu, *Angew. Chem., Int. Ed.*, 2018, **57**, 8649–8653.
- 68 G. Xie, P. Li, Z. Zhao, Z. Zhu, X. Y. Kong, Z. Zhang, K. Xiao, L. Wen and L. Jiang, *J. Am. Chem. Soc.*, 2018, **140**, 4552–4559.
- 69 A. Harada, M. Okada, J. Li and M. Kamachi, *Macromolecules*, 2002, **28**, 8406–8411.
- 70 T. Higashi, K. Morita, X. Song, J. L. Zhu, A. Tamura, N. Yui, K. Motoyama, H. Arima and J. Li, *Commun. Chem.*, 2019, **2**, 78.
- 71 O. Peters and H. Ritter, *Angew. Chem., Int. Ed.*, 2013, **52**, 8961–8963.
- 72 X. Huan, D. Wang, R. Dong, C. Tu, B. Zhu, D. Yan and X. Zhu, *Macromolecules*, 2012, **45**, 5941–5947.
- 73 X. Dai, X. Dong, Z. Liu, G. Liu and Y. Liu, *Biomacromolecules*, 2020, **21**, 5369–5379.
- 74 E. Wajcs, A. Molina-Ontoria, T. T. Nielsen, L. Echegoyen and A. Fragoso, *Langmuir*, 2015, **31**, 535–541.
- 75 Y. Han, K. Cheng, K. A. Simon, Y. Lan, P. Sejwal and Y. Y. Luk, *J. Am. Chem. Soc.*, 2006, **128**, 13913–13920.
- 76 Y. Li, Z. Xu, Y. Liu, S. Jin, E. M. Fell, B. Wang, R. G. Gordon, M. J. Aziz, Z. Yang and T. Xu, *ChemSusChem*, 2021, **14**, 745–752.
- 77 F. van de Manakker, M. van der Pot, T. Vermonden, C. F. van Nostrum and W. E. Hennink, *Macromolecules*, 2008, **41**, 1766–1773.
- 78 Y. Takechi-Haraya, K. Tanaka, K. Tsuji, Y. Asami, H. Izawa, A. Shigenaga, A. Otaka, H. Saito and K. Kawakami, *Bioconjugate Chem.*, 2015, **26**, 572–581.
- 79 Y.-G. Jia and X. X. Zhu, *Chem. Mater.*, 2014, **27**, 387–393.
- 80 C. Yu, C.-F. Wang and S. Chen, *Adv. Funct. Mater.*, 2014, **24**, 1235–1242.
- 81 T. Trelenkamp and H. Ritter, *Macromolecules*, 2010, **43**, 5538–5543.
- 82 J. W. Park, S. Y. Lee, H. J. Song and K. K. Park, *J. Org. Chem.*, 2005, **70**, 9505–9513.
- 83 Z. Deng, Y. Guo, X. Zhao, P. X. Ma and B. Guo, *Chem. Mater.*, 2018, **30**, 1729–1742.
- 84 Y. Wu, B. Guo and P. X. Ma, *ACS Macro Lett.*, 2014, **3**, 1145–1150.
- 85 Y. Zhang, D. Yang, J. Han, J. Zhou, Q. Jin, M. Liu and P. Duan, *Langmuir*, 2018, **34**, 5821–5830.
- 86 H. Tian, X. Yu, J. Yao, G. Gao, W. Wu and C. Yang, *Chem. Commun.*, 2021, **57**, 1806–1809.
- 87 Q. Wang, Q. Zhang, Q.-W. Zhang, X. Li, C.-X. Zhao, T.-Y. Xu, D.-H. Qu and H. Tian, *Nat. Commun.*, 2020, **11**, 158.
- 88 Q. Wang, W. Liang, X. Wei, W. Wu, Y. Inoue, C. Yang and Y. Liu, *Org. Lett.*, 2020, **22**, 9757–9761.
- 89 W. Saenger, J. Jacob, K. Gessler, T. Steiner, D. Hoffmann, H. Sanbe, K. Koizumi, S. M. Smith and T. Takaha, *Chem. Rev.*, 1998, **98**, 1787–1802.
- 90 G. Yu, K. Jie and F. Huang, *Chem. Rev.*, 2015, **115**, 7240–7303.
- 91 Z. Xu, S. Jia, W. Wang, Z. Yuan, B. Jan Ravoo and D. S. Guo, *Nat. Chem.*, 2019, **11**, 86–93.
- 92 L. Xu, W. Zhang, H. Cai, F. Liu, Y. Wang, Y. Gao and W. Zhang, *J. Mater. Chem. B*, 2015, **3**, 7417–7426.
- 93 J. Guo, D. Li, H. Tao, G. Li, R. Liu, Y. Dou, T. Jin, L. Li, J. Huang, H. Hu and J. Zhang, *Adv. Mater.*, 2019, **31**, 1904607.
- 94 Y. Sugita, D. Aoki, M. Tokita and H. Otsuka, *Chem. Commun.*, 2022, **58**, 3067–3070.
- 95 J. N. Silva, A. M. Silva, J. P. Tome, A. O. Ribeiro, M. R. Domingues, J. A. Cavaleiro, A. M. Silva, M. G. Neves, A. C. Tome, O. A. Serra, F. Bosca, P. Filipe, R. Santus and P. Morliere, *Photochem. Photobiol. Sci.*, 2008, **7**, 834–843.
- 96 H. Yang, F. Lu, Y. Sun, Z. Yuan and C. Lu, *Anal. Chem.*, 2018, **90**, 12846–12853.
- 97 M. Gomez-Garcia, J. M. Benito, A. P. Butera, C. Ortiz Mellet, J. M. Garcia Fernandez and J. L. Jimenez Blanco, *J. Org. Chem.*, 2012, **77**, 1273–1288.
- 98 Q. Zhang, Y. Cai, X. J. Wang, J. L. Xu, Z. Ye, S. Wang, P. H. Seeberger and J. Yin, *ACS Appl. Mater. Interfaces*, 2016, **8**, 33405–33411.
- 99 G. Xu, S. Leloux, P. Zhang, J. Mejjide Suarez, Y. Zhang, E. Derat, M. Menand, O. Bistri-Aslanoff, S. Roland, T. Leysens, O. Riant and M. Sollogoub, *Angew. Chem., Int. Ed.*, 2020, **59**, 7591–7597.
- 100 P. Zhang, J. Mejjide Suarez, T. Driant, E. Derat, Y. Zhang, M. Menand, S. Roland and M. Sollogoub, *Angew. Chem., Int. Ed.*, 2017, **56**, 10821–10825.
- 101 Y. Liu, C.-C. You, H.-Y. Zhang and Y.-L. Zhao, *Eur. J. Org. Chem.*, 2003, 1415–1422.
- 102 P. Xin, H. Kong, Y. Sun, L. Zhao, H. Fang, H. Zhu, T. Jiang, J. Guo, Q. Zhang, W. Dong and C. P. Chen, *Angew. Chem., Int. Ed.*, 2019, **58**, 2779–2784.
- 103 J. Ji, W. Wu, X. Wei, M. Rao, D. Zhou, G. Cheng, Q. Gong, K. Luo and C. Yang, *Chem. Commun.*, 2020, **56**, 6197–6200.
- 104 Y. G. Jia, J. Jin, S. Liu, L. Ren, J. Luo and X. X. Zhu, *Biomacromolecules*, 2018, **19**, 626–632.
- 105 X. Ma, N. Zhou, T. Zhang, W. Hu and N. Gu, *Mater. Sci. Eng., C*, 2017, **73**, 357–365.
- 106 H. Xuan, W. Dai, Y. Zhu, J. Ren, J. Zhang and L. Ge, *Sens. Actuators, B*, 2018, **257**, 1110–1117.
- 107 C. B. Rodell, C. B. Highley, M. H. Chen, N. N. Dusaj, C. Wang, L. Han and J. A. Burdick, *Soft Matter*, 2016, **12**, 7839–7847.
- 108 Y. Akae, H. Sogawa and T. Takata, *Angew. Chem., Int. Ed.*, 2018, **57**, 14832–14836.

- 109 S. Zhang, C. Zhang, H. Chen, S. J. Kieffer, F. Neubrech, H. Giessen, A. G. Alleyne and P. V. Braun, *Angew. Chem., Int. Ed.*, 2019, **58**, 18165–18170.
- 110 K. Wei, M. Zhu, Y. Sun, J. Xu, Q. Feng, S. Lin, T. Wu, J. Xu, F. Tian, J. Xia, G. Li and L. Bian, *Macromolecules*, 2016, **49**, 866–875.
- 111 D. Prochowicz, A. Kornowicz, I. Justyniak and J. Lewinski, *Coord. Chem. Rev.*, 2016, **306**, 331–345.
- 112 X. Dai, B. Zhang, Q. Yu and Y. Liu, *ACS Appl. Bio Mater.*, 2021, **4**, 8536–8542.
- 113 S. T. Jones, V. Cagno, M. Janecek, D. Ortiz, N. Gasilova, J. Piret, M. Gasbarri, D. A. Constant, Y. Han, L. Vukovic, P. Kral, L. Kaiser, S. Huang, S. Constant, K. Kirkegaard, G. Boivin, F. Stellacci and C. Tapparel, *Sci. Adv.*, 2020, **6**, eaax9318.
- 114 M. N. Shinde, R. Khurana, N. Barooah, A. C. Bhasikuttan and J. Mohanty, *J. Phys. Chem. C*, 2017, **121**, 20057–20065.
- 115 W. Han, W. Xiang, Q. Li, H. Zhang, Y. Yang, J. Shi, Y. Ji, S. Wang, X. Ji, N. M. Khashab and J. L. Sessler, *Chem. Soc. Rev.*, 2021, **50**, 10025–10043.
- 116 X. Li, S. Lee and J. Yoon, *Chem. Soc. Rev.*, 2018, **47**, 1174–1188.
- 117 L. Voorhaar and R. Hoogenboom, *Chem. Soc. Rev.*, 2016, **45**, 4013–4031.
- 118 H. X. Zhou and X. Pang, *Chem. Rev.*, 2018, **118**, 1691–1741.
- 119 M. Nakahata, Y. Takashima and A. Harada, *Angew. Chem., Int. Ed.*, 2014, **53**, 3617–3621.
- 120 A. Nonat, S. Bahamyirou, A. Lecointre, F. Przybilla, Y. Mely, C. Platas-Iglesias, F. Camerel, O. Jeannin and L. J. Charbonniere, *J. Am. Chem. Soc.*, 2019, **141**, 1568–1576.
- 121 Q. Zhang, C. Liu, G. Ju, M. Cheng and F. Shi, *Macromol. Rapid Commun.*, 2018, **39**, 1800180.
- 122 G. Izzet, B. Abecassis, D. Brouri, M. Piot, B. Matt, S. A. Serapian, C. Bo and A. Proust, *J. Am. Chem. Soc.*, 2016, **138**, 5093–5099.
- 123 Y. Wang, X. Li, F. Li, W. Y. Sun, C. Zhu and Y. Cheng, *Chem. Commun.*, 2017, **53**, 7505–7508.
- 124 R.-J. Shi, Y. Chen, X.-F. Hou and Y. Liu, *RSC Adv.*, 2016, **6**, 15175–15179.
- 125 Y. Matsui and A. Okimoto, *Bull. Chem. Soc. Jpn.*, 1978, **51**, 3030–3034.
- 126 J. Wang, Y. Chen, N. Cheng, L. Feng, B.-H. Gu and Y. Liu, *ACS Appl. Bio Mater.*, 2019, **2**, 5898–5904.
- 127 N. Mourtzis, K. Eliadou, C. Aggelidou, V. Sophianopoulou, I. M. Mavridis and K. Yannakopoulou, *Org. Biomol. Chem.*, 2007, **5**, 125–131.
- 128 J. Junthip, N. Tabary, M. Maton, S. Ouerghemmi, J. N. Staelens, F. Cazaux, C. Neut, N. Blanchemain and B. Martel, *Int. J. Pharm.*, 2020, **587**, 119730.
- 129 D. Maffeo, L. Leondiadis, I. M. Mavridis and K. Yannakopoulou, *Org. Biomol. Chem.*, 2006, **4**, 1297–1304.
- 130 H. L. Sun, Y. M. Zhang, Y. Chen and Y. Liu, *Sci. Rep.*, 2016, **6**, 27.
- 131 N. Mourtzis, K. Eliadou and K. Yannakopoulou, *Supramol. Chem.*, 2010, **16**, 587–593.
- 132 Ó. López and M. Bols, *Tetrahedron*, 2008, **64**, 7587–7593.
- 133 A. Pineiro, J. Pipkin, V. Antle and R. Garcia-Fandino, *J. Mol. Liq.*, 2021, **343**, 117588.
- 134 G. Singh and P. K. Singh, *J. Mol. Liq.*, 2020, **305**, 112840.
- 135 G. Chakraborty, V. S. Pillai and R. K. Chittela, *J. Photochem. Photobiol., A*, 2021, **419**, 113454.
- 136 J. Wankar, F. Bonvicini, G. Benkovics, V. Marassi, M. Malanga, E. Fenyvesi, G. A. Gentilomi, P. Reschiglian, B. Roda and I. Manet, *Mol. Pharmaceutics*, 2018, **15**, 3823–3836.
- 137 L. Yue, W. Jin, S. Chi, T. Yang, Z. Lei, H. Zhu and Y. Zhao, *Polym. Eng. Sci.*, 2020, **60**, 2403–2413.
- 138 N. H. Mudliar and P. K. Singh, *Chem. – Eur. J.*, 2016, **22**, 7394–7398.
- 139 Y. Zhang and Y. Liu, *Chin. J. Org. Chem.*, 2020, **40**, 3802.
- 140 Y. C. Pan, X. Y. Hu and D. S. Guo, *Angew. Chem., Int. Ed.*, 2021, **60**, 2768–2794.
- 141 R. Kumar, A. Sharma, H. Singh, P. Suating, H. S. Kim, K. Sunwoo, I. Shim, B. C. Gibb and J. S. Kim, *Chem. Rev.*, 2019, **119**, 9657–9721.
- 142 H. L. Sun, H. Y. Zhang, Z. Dai, X. Han and Y. Liu, *Chem. – Asian J.*, 2017, **12**, 265–270.
- 143 P. Branna, M. Rouchal, Z. Pruckova, L. Dastychova, R. Lenobel, T. Pospisil, K. Malac and R. Vicha, *Chem. – Eur. J.*, 2015, **21**, 11712–11718.
- 144 R. Liu, Y. Zhang, W. Wu, W. Liang, Q. Huang, X. Yu, W. Xu, D. Zhou, N. Selvapalam and C. Yang, *Chin. Chem. Lett.*, 2019, **30**, 577–581.
- 145 C. Ke, R. A. Smaldone, T. Kikuchi, H. Li, A. P. Davis and J. F. Stoddart, *Angew. Chem., Int. Ed.*, 2013, **52**, 381–387.
- 146 T. Ogoshi, T. Kakuta and T. A. Yamagishi, *Angew. Chem., Int. Ed.*, 2019, **58**, 2197–2206.
- 147 T. Ogoshi, T. A. Yamagishi and Y. Nakamoto, *Chem. Rev.*, 2016, **116**, 7937–8002.
- 148 L. Zalewski, J. M. Mativetsky, S. Brovelli, M. Bonini, N. Crivillers, T. Breiner, H. L. Anderson, F. Cacialli and P. Samori, *Small*, 2012, **8**, 1835–1839.
- 149 D. H. Qu, Q. C. Wang and H. Tian, *Angew. Chem., Int. Ed.*, 2005, **44**, 5296–5299.
- 150 E. J. Klotz, T. D. Claridge and H. L. Anderson, *J. Am. Chem. Soc.*, 2006, **128**, 15374–15375.
- 151 G. Liu, Q. Yuan, G. Hollett, W. Zhao, Y. Kang and J. Wu, *Polym. Chem.*, 2018, **9**, 3436–3449.
- 152 H. Chen, X. Ma, S. Wu and H. Tian, *Angew. Chem., Int. Ed.*, 2014, **53**, 14149–14152.
- 153 W. Deng, H. Yamaguchi, Y. Takashima and A. Harada, *Angew. Chem., Int. Ed.*, 2007, **46**, 5144–5147.
- 154 X. Liao, G. Chen, X. Liu, W. Chen, F. Chen and M. Jiang, *Angew. Chem., Int. Ed.*, 2010, **49**, 4409–4413.
- 155 S. Tamesue, Y. Takashima, H. Yamaguchi, S. Shinkai and A. Harada, *Angew. Chem., Int. Ed.*, 2010, **49**, 7461–7464.
- 156 J. Boonleang and J. F. Stobaugh, *Electrophoresis*, 2013, **34**, 1232–1240.
- 157 T. Schmitt and H. Engelhardt, *Chromatographia*, 1993, **37**, 475–481.
- 158 B. Chankvetadze, G. Endresz and G. Blaschke, *Electrophoresis*, 1994, **15**, 804–807.
- 159 M. L. Konjaria and G. K.-E. Scriba, *J. Chromatogr. A*, 2020, **1632**, 461585.
- 160 J. P. Quirino, *J. Sep. Sci.*, 2017, **40**, 4835–4838.

- 161 C. M. Rudzinski, W. K. Hartmann and D. G. Nocera, *Coord. Chem. Rev.*, 1998, **171**, 115–123.
- 162 F. Hapiot, S. Tilloy and E. Monflier, *Chem. Rev.*, 2006, **106**, 767–781.
- 163 I. Roy and J. F. Stoddart, *Acc. Chem. Res.*, 2021, **54**, 1440–1453.
- 164 X. Han, C. Yuan, B. Hou, L. Liu, H. Li, Y. Liu and Y. Cui, *Chem. Soc. Rev.*, 2020, **49**, 6248–6272.
- 165 R. Q. Wang, X. B. Wei and Y. Q. Feng, *Chem. – Eur. J.*, 2018, **24**, 10979–10983.
- 166 C. Yuan, X. Wu, R. Gao, X. Han, Y. Liu, Y. Long and Y. Cui, *J. Am. Chem. Soc.*, 2019, **141**, 20187–20197.
- 167 Y. Zhang, J. Duan, D. Ma, P. Li, S. Li, H. Li, J. Zhou, X. Ma, X. Feng and B. Wang, *Angew. Chem., Int. Ed.*, 2017, **56**, 16313–16317.
- 168 C. J. Brown, F. D. Toste, R. G. Bergman and K. N. Raymond, *Chem. Rev.*, 2015, **115**, 3012–3035.
- 169 K. Takahashi, *Chem. Rev.*, 1998, **98**, 2013–2034.
- 170 X. Hou, C. Ke and J. Fraser Stoddart, *Chem. Soc. Rev.*, 2016, **45**, 3766–3780.
- 171 Y. M. Zhang, Y. H. Liu and Y. Liu, *Adv. Mater.*, 2020, **32**, 1806158.
- 172 D. H. Qu, Q. C. Wang, Q. W. Zhang, X. Ma and H. Tian, *Chem. Rev.*, 2015, **115**, 7543–7588.
- 173 S. Yagai and A. Kitamura, *Chem. Soc. Rev.*, 2008, **37**, 1520–1529.
- 174 A. Harada, Y. Takashima and M. Nakahata, *Acc. Chem. Res.*, 2014, **47**, 2128–2140.
- 175 L. Yang, X. Tan, Z. Wang and X. Zhang, *Chem. Rev.*, 2015, **115**, 7196–7239.
- 176 X. Ji, M. Ahmed, L. Long, N. M. Khashab, F. Huang and J. L. Sessler, *Chem. Soc. Rev.*, 2019, **48**, 2682–2697.
- 177 A. Harada, *Coord. Chem. Rev.*, 1996, **148**, 115–133.
- 178 N. Bognanni, F. Bellia, M. Viale, N. Bertola and G. Vecchio, *Molecules*, 2021, **26**, 1724.
- 179 Z. Liu, L. Ye, J. Xi, J. Wang and Z.-G. Feng, *Prog. Polym. Sci.*, 2021, **118**, 101408.
- 180 B. V.-K. J. Schmidt, M. Hetzer, H. Ritter and C. Barner-Kowollik, *Prog. Polym. Sci.*, 2014, **39**, 235–249.
- 181 X. Yao, P. Huang and Z. Nie, *Prog. Polym. Sci.*, 2019, **93**, 1–35.
- 182 M. Mohamadhoseini and Z. Mohamadnia, *Coord. Chem. Rev.*, 2021, **432**, 213711.
- 183 G. Varan, C. Varan, N. Erdogar, A. A. Hincal and E. Bilensoy, *Int. J. Pharm.*, 2017, **531**, 457–469.
- 184 Y. Zhou, K. Jie, R. Zhao and F. Huang, *Adv. Mater.*, 2020, **32**, 1904824.
- 185 G. Wenz, B. H. Han and A. Muller, *Chem. Rev.*, 2006, **106**, 782–817.
- 186 S. A. Nepogodiev and J. F. Stoddart, *Chem. Rev.*, 1998, **98**, 1959–1976.
- 187 K. L. Liu, Z. Zhang and J. Li, *Soft Matter*, 2011, **7**, 11290.
- 188 A. Hashidzume, H. Yamaguchi and A. Harada, *Eur. J. Org. Chem.*, 2019, 3344–3357.
- 189 M. Xue, Y. Yang, X. Chi, X. Yan and F. Huang, *Chem. Rev.*, 2015, **115**, 7398–7501.
- 190 X. Ma and H. Tian, *Chem. Soc. Rev.*, 2010, **39**, 70–80.
- 191 Q. D. Hu, G. P. Tang and P. K. Chu, *Acc. Chem. Res.*, 2014, **47**, 2017–2025.
- 192 T. Irie, *Adv. Drug Delivery Rev.*, 1999, **36**, 101–123.
- 193 H. B. Cheng, Y. M. Zhang, Y. Liu and J. Y. Yoon, *Chem*, 2019, **5**, 553–574.
- 194 K. Uekama, F. Hirayama and T. Irie, *Chem. Rev.*, 1998, **98**, 2045–2076.
- 195 R. N. Dsouza, U. Pischel and W. M. Nau, *Chem. Rev.*, 2011, **111**, 7941–7980.
- 196 W. F. Lai, A. L. Rogach and W. T. Wong, *Chem. Soc. Rev.*, 2017, **46**, 6379–6419.
- 197 T. L. Mako, J. M. Racicot and M. Levine, *Chem. Rev.*, 2019, **119**, 322–477.
- 198 E. Rizzarelli and G. Vecchio, *Coord. Chem. Rev.*, 1999, **188**, 343–364.
- 199 X. Y. Lou, N. Song and Y. W. Yang, *Molecules*, 2017, **22**, 1640.
- 200 A. Harada, *Acc. Chem. Res.*, 2001, **34**, 456–464.
- 201 M. Hussain Asim, M. Ijaz, A. C. Rösch and A. Bernkop-Schnürch, *Coord. Chem. Rev.*, 2020, **420**, 213433.
- 202 M. Kryjewski, T. Goslinski and J. Mielcarek, *Coord. Chem. Rev.*, 2015, **300**, 101–120.
- 203 Y. Liu, Y. Chen, X. Gao, J. Fu and L. Hu, *Crit. Rev. Food Sci. Nutr.*, 2022, **62**, 2627–2640.
- 204 J. M. Lopez-Nicolas, P. Rodriguez-Bonilla and F. Garcia-Carmona, *Crit. Rev. Food Sci. Nutr.*, 2014, **54**, 251–276.
- 205 C. Guo and Y. Xiao, *Carbohydr. Polym.*, 2021, **256**, 117517.
- 206 B. Tian, Y. Liu and J. Liu, *Carbohydr. Polym.*, 2021, **251**, 116871.
- 207 M. Agnes, A. Thanassoulas, P. Stavropoulos, G. Nounesis, G. Miliotis, V. Miriagou, E. Athanasiou, G. Benkovics, M. Malanga and K. Yannakopoulou, *Int. J. Pharm.*, 2017, **531**, 480–491.
- 208 M. Másson, T. Loftsson, S. D. Jónsdóttir, H. Fridriksdóttir and D. S. Petersen, *Int. J. Pharm.*, 1998, **164**, 45–55.
- 209 J. Junthip, N. Tabary, F. Chai, L. Leclercq, M. Maton, F. Cazaux, C. Neut, L. Paccou, Y. Guinet, J. N. Staelens, M. Bria, D. Landy, A. Hedoux, N. Blanchemain and B. Martel, *J. Biomed. Mater. Res. A*, 2016, **104**, 1408–1424.
- 210 C. Wang, J. Wang, X. Chen, X. Zheng, Z. Xie, L. Chen and X. Chen, *Macromol. Biosci.*, 2017, **17**, 1600227.
- 211 J. Mosinger, L. Slavetinska, K. Lang, P. Coufal and P. Kubat, *Org. Biomol. Chem.*, 2009, **7**, 3797–3804.
- 212 V. Rodriguez-Ruiz, A. Maksimenko, G. Salzano, M. Lampropoulou, Y. G. Lazarou, V. Agostoni, P. Couvreur, R. Gref and K. Yannakopoulou, *Sci. Rep.*, 2017, **7**, 8353.
- 213 L. Yue, T. Sun, K. Yang, Q. Cheng, J. Li, Y. Pan, S. Wang and R. Wang, *Nanoscale*, 2021, **13**, 9570–9576.
- 214 J. Liu, T. Luo, Y. Xue, L. Mao, P. J. Stang and M. Wang, *Angew. Chem., Int. Ed.*, 2021, **60**, 5429–5435.
- 215 J. W. Fredy, J. Scelle, G. Ramniceanu, B. T. Doan, C. S. Bonnet, E. Toth, M. Menand, M. Sollogoub, G. Vives and B. Hasenknopf, *Org. Lett.*, 2017, **19**, 1136–1139.
- 216 P. Xiao, C. Liu, T. Ma, X. Lu, L. Jing, Y. Hou, P. Zhang, G. Huang and M. Gao, *Adv. Sci.*, 2021, **8**, 2004044.
- 217 F. F. Shen, Y. Chen, X. Xu, H. J. Yu, H. Wang and Y. Liu, *Small*, 2021, **17**, 2101185.

- 218 J.-L. Xu, Y. Quan, Q.-Y. Li, H. Lu, H. Wu, J. Yin, X.-J. Wang and Q. Zhang, *RSC Adv.*, 2015, **5**, 88176–88180.
- 219 Y. Guo, F. Jian and X. Kang, *RSC Adv.*, 2017, **7**, 15315–15320.
- 220 G. Xie, W. Tian, L. Wen, K. Xiao, Z. Zhang, Q. Liu, G. Hou, P. Li, Y. Tian and L. Jiang, *Chem. Commun.*, 2015, **51**, 3135–3138.
- 221 K. Kanagaraj, A. Affrose, S. Sivakolunthu and K. Pitchumani, *Biosens. Bioelectron.*, 2012, **35**, 452–455.
- 222 J. G. Cheng, H. J. Yu, Y. Chen and Y. Liu, *Bioorg. Med. Chem. Lett.*, 2018, **26**, 2287–2290.
- 223 Y. Liu and C.-C. You, *Chin. J. Chem.*, 2010, **19**, 533–544.
- 224 T. Kraus, *Curr. Org. Chem.*, 2011, **15**, 802–814.
- 225 H. Yao, J. Wang, Y.-Q. Fan, Q. Zhou, X.-W. Guan, X.-T. Kan, Y.-M. Zhang, Q. Lin and T.-B. Wei, *Dye. Pig.*, 2019, **167**, 16–21.
- 226 M. Rezanka, M. J. Langton and P. D. Beer, *Chem. Commun.*, 2015, **51**, 4499–4502.
- 227 T. Ogoshi and A. Harada, *Sensors*, 2008, **8**, 4961–4982.
- 228 G. Chakraborty, J. N. Malegaonkar, S. V. Bhosale, P. K. Singh and H. Pal, *J. Phys. Chem. B*, 2021, **125**, 11122–11133.
- 229 M. J. Langton, I. Marques, S. W. Robinson, V. Felix and P. D. Beer, *Chem. – Eur. J.*, 2016, **22**, 185–192.
- 230 L. Feng, C. Tong, Y. He, B. Liu, C. Wang, J. Sha and C. Lü, *J. Lumin.*, 2014, **146**, 502–507.
- 231 X. P. He, R. H. Li, S. Maisonneuve, Y. Ruan, G. R. Chen and J. Xie, *Chem. Commun.*, 2014, **50**, 14141–14144.
- 232 S. Zhang, I. Boussouar and H. Li, *Chin. Chem. Lett.*, 2021, **32**, 642–648.
- 233 N. Liu, C. Li, T. Zhang, R. Hou, Z. Xiong, Z. Li, B. Wei, Z. Yang, P. Gao, X. Lou, X. Zhang, W. Guo and F. Xia, *Small*, 2017, **13**, 1600287.
- 234 Q. W. Zhang, J. Zajicek and B. D. Smith, *Org. Lett.*, 2018, **20**, 2096–2099.
- 235 B. Zhao, L. Jiang and Q. Jia, *Chin. Chem. Lett.*, 2022, **33**, 11–21.
- 236 J. Liu, C. Zhang, S. Zhang, H. Yu and W. Xie, *Chin. Chem. Lett.*, 2020, **31**, 539–542.
- 237 H. T. Le, J. W. Lee, S. C. Park, J. W. Jeong, W. Jung, C. W. Lim, K. P. Kim and T. W. Kim, *Chem. Commun.*, 2017, **53**, 10459–10462.
- 238 F. Schluter, M. M. Bela, D. Glikman, B. Braunschweig and B. J. Ravoo, *Chem. Commun.*, 2020, **56**, 15434–15437.
- 239 W. Xu, Y. Chen, B. Zhang, W. Xu, J. Niu and Y. Liu, *Biomacromolecules*, 2021, **22**, 4434–4445.
- 240 H. Che and J. Yuan, *J. Mater. Chem. B*, 2021, **10**, 8–19.
- 241 S.-S. Jia, W.-S. Xu, Y. Chen and Y. Liu, *Chin. Chem. Lett.*, 2021, **32**, 2773–2776.
- 242 C. Falaise, M. A. Moussawi, S. Floquet, P. A. Abramov, M. N. Sokolov, M. Haouas and E. Cadot, *J. Am. Chem. Soc.*, 2018, **140**, 11198–11201.
- 243 M. A. Moussawi, M. Haouas, S. Floquet, W. E. Shepard, P. A. Abramov, M. N. Sokolov, V. P. Fedin, S. Cordier, A. Ponchel, E. Monflier, J. Marrot and E. Cadot, *J. Am. Chem. Soc.*, 2017, **139**, 14376–14379.
- 244 M. A. Moussawi, N. Leclerc-Laronze, S. Floquet, P. A. Abramov, M. N. Sokolov, S. Cordier, A. Ponchel, E. Monflier, H. Bricout, D. Landy, M. Haouas, J. Marrot and E. Cadot, *J. Am. Chem. Soc.*, 2017, **139**, 12793–12803.
- 245 P. Yang, W. Zhao, A. Shkurenko, Y. Belmabkhout, M. Eddaoudi, X. Dong, H. N. Alshareef and N. M. Khashab, *J. Am. Chem. Soc.*, 2019, **141**, 1847–1851.
- 246 L. Jiang, Y. Peng, Y. Yan and J. Huang, *Soft Matter*, 2011, **7**, 1726–1731.
- 247 X. Ma and H. Tian, *Acc. Chem. Res.*, 2014, **47**, 1971–1981.
- 248 P. Kuad, A. Miyawaki, Y. Takashima, H. Yamaguchi and A. Harada, *J. Am. Chem. Soc.*, 2007, **129**, 12630–12631.
- 249 Y. Su, J. Dang, H. Zhang, Y. Zhang and W. Tian, *Langmuir*, 2017, **33**, 7393–7402.
- 250 A. Wu, P. Sun, N. Sun and L. Zheng, *Chem. – Eur. J.*, 2018, **24**, 10452–10459.
- 251 Y. Zhang, F. Gong, Y. Wu, S. Hou, L. Xue, Z. Su and C. Zhang, *Nano Lett.*, 2021, **21**, 9736–9745.
- 252 G. Chakraborty, P. K. Singh and H. Pal, *J. Mol. Liq.*, 2021, **321**, 114499.
- 253 J. Scelle, H. Vervoitte, L. Bouteiller, L. M. Chamoreau, M. Sollogoub, G. Vives and B. Hasenknopf, *Chem. Sci.*, 2022, **13**, 2218–2225.
- 254 J. Shi, Y. Chen, Q. Wang and Y. Liu, *Adv. Mater.*, 2010, **22**, 2575–2578.
- 255 W. H. Chen, G. F. Luo, W. X. Qiu, Q. Lei, L. H. Liu, S. B. Wang and X. Z. Zhang, *Biomaterials*, 2017, **117**, 54–65.
- 256 H. Murakami, A. Kawabuchi, R. Matsumoto, T. Ido and N. Nakashima, *J. Am. Chem. Soc.*, 2005, **127**, 15891–15899.
- 257 Q. C. Wang, D. H. Qu, J. Ren, K. Chen and H. Tian, *Angew. Chem., Int. Ed.*, 2004, **43**, 2661–2665.
- 258 X. Li, H. Bai, Y. Yang, J. Yoon, S. Wang and X. Zhang, *Adv. Mater.*, 2019, **31**, 1805092.
- 259 Y. Zhu, C. Xu, N. Zhang, X. Ding, B. Yu and F.-J. Xu, *Adv. Funct. Mater.*, 2018, **28**, 1706709.
- 260 F. Ding, H. Deng, Y. Du, X. Shi and Q. Wang, *Nanoscale*, 2014, **6**, 9477–9493.
- 261 C. Zhou, D. Wang, M. Cao, Y. Chen, Z. Liu, C. Wu, H. Xu, S. Wang and Y. Wang, *ACS Appl. Mater. Interfaces*, 2016, **8**, 30811–30823.
- 262 Z. Huang, H. Zhang, H. Bai, Y. Bai, S. Wang and X. Zhang, *ACS Macro Lett.*, 2016, **5**, 1109–1113.
- 263 S. Yan, S. Chen, X. Gou, J. Yang, J. An, X. Jin, Y. W. Yang, L. Chen and H. Gao, *Adv. Funct. Mater.*, 2019, **29**, 1904683.
- 264 S. Guo, Q. Huang, Y. Chen, J. Wei, J. Zheng, L. Wang, Y. Wang and R. Wang, *Angew. Chem., Int. Ed.*, 2021, **60**, 618–623.
- 265 S. Li, N. Jiang, W. Zhao, Y. F. Ding, Y. Zheng, L. H. Wang, J. Zheng and R. Wang, *Chem. Commun.*, 2017, **53**, 5870–5873.
- 266 C. Zhou, H. Wang, H. Bai, P. Zhang, L. Liu, S. Wang and Y. Wang, *ACS Appl. Mater. Interfaces*, 2017, **9**, 31657–31666.
- 267 J. Kim, G. Saravanakumar, H. W. Choi, D. Park and W. J. Kim, *J. Mater. Chem. B*, 2014, **2**, 341–356.
- 268 S. Sortino, *Chem. Soc. Rev.*, 2010, **39**, 2903–2913.
- 269 A. W. Carpenter and M. H. Schoenfish, *Chem. Soc. Rev.*, 2012, **41**, 3742–3752.

- 270 D. A. Riccio and M. H. Schoenfish, *Chem. Soc. Rev.*, 2012, **41**, 3731–3741.
- 271 H. Jin, L. Yang, M. J.-R. Ahonen and M. H. Schoenfish, *J. Am. Chem. Soc.*, 2018, **140**, 14178–14184.
- 272 X. Chen, H. Li, W. Xu, K. Huang, B. Zhai and X. He, *J. Agric. Food Chem.*, 2020, **68**, 11144–11150.
- 273 W. Yang, C. Yu, C. Wu, S. Q. Yao and S. Wu, *Polym. Chem.*, 2017, **8**, 4043–4051.
- 274 P. Y. Li, Y. Chen, C. H. Chen and Y. Liu, *Chem. Commun.*, 2019, **55**, 11790–11793.
- 275 S. Behzadi, V. Serpooshan, W. Tao, M. A. Hamaly, M. Y. Alkawareek, E. C. Dreaden, D. Brown, A. M. Alkilany, O. C. Farokhzad and M. Mahmoudi, *Chem. Soc. Rev.*, 2017, **46**, 4218–4244.
- 276 V. S. Trubetskoy, S. C. Wong, V. Subbotin, V. G. Budker, A. Loomis, J. E. Hagstrom and J. A. Wolff, *Gene Ther.*, 2003, **10**, 261–271.
- 277 Y. J. Ooi, Y. Wen, J. Zhu, X. Song and J. Li, *Biomacromolecules*, 2020, **21**, 1136–1148.
- 278 J. Z. Du, T. M. Sun, W. J. Song, J. Wu and J. Wang, *Angew. Chem., Int. Ed.*, 2010, **49**, 3621–3626.
- 279 Y. Y. Yuan, C. Q. Mao, X. J. Du, J. Z. Du, F. Wang and J. Wang, *Adv. Mater.*, 2012, **24**, 5476–5480.
- 280 P. Hu, Y. Chen, J. J. Li and Y. Liu, *Chem. – Asian J.*, 2016, **11**, 505–511.
- 281 P. Hu, Y. Chen and Y. Liu, *Chem. Commun.*, 2015, **51**, 10839–10842.
- 282 P. Evenou, J. Rossignol, G. Pembouong, A. Gothland, D. Colesnic, R. Barbeyron, S. Rudiuk, A. G. Marcelin, M. Menand, D. Baigl, V. Calvez, L. Bouteiller and M. Sollogoub, *Angew. Chem., Int. Ed.*, 2018, **57**, 7753–7758.
- 283 D. K. Hoover, E. W. Chan and M. N. Yousaf, *J. Am. Chem. Soc.*, 2008, **130**, 3280–3281.
- 284 T. Ooya, M. Eguchi and N. Yui, *J. Am. Chem. Soc.*, 2003, **125**, 13016–13017.
- 285 H. Hyun and N. Yui, *Macromol. Biosci.*, 2011, **11**, 765–771.
- 286 J. H. Seo, S. Kakinoki, Y. Inoue, T. Yamaoka, K. Ishihara and N. Yui, *J. Am. Chem. Soc.*, 2013, **135**, 5513–5516.
- 287 Y. M. Zhang, X. Xu, Q. Yu, Y. H. Liu, Y. H. Zhang, L. X. Chen and Y. Liu, *J. Med. Chem.*, 2017, **60**, 3266–3274.
- 288 Y. Zhang, Y. Su, H. Wu, Z. Wang, C. Wang, Y. Zheng, X. Zheng, L. Gao, Q. Zhou, Y. Yang, X. Chen, C. Yang and Y. Zhao, *J. Am. Chem. Soc.*, 2021, **143**, 13675–13685.
- 289 S. Cai, H. Ma, H. Shi, H. Wang, X. Wang, L. Xiao, W. Ye, K. Huang, X. Cao, N. Gan, C. Ma, M. Gu, L. Song, H. Xu, Y. Tao, C. Zhang, W. Yao, Z. An and W. Huang, *Nat. Commun.*, 2019, **10**, 4247.
- 290 M. Baroncini, G. Bergamini and P. Ceroni, *Chem. Commun.*, 2017, **53**, 2081–2093.
- 291 D. Li, F. Lu, J. Wang, W. Hu, X. M. Cao, X. Ma and H. Tian, *J. Am. Chem. Soc.*, 2018, **140**, 1916–1923.
- 292 P. Alam, N. L.-C. Leung, J. Liu, T. S. Cheung, X. Zhang, Z. He, R. T.-K. Kwok, J. W.-Y. Lam, H. H.-Y. Sung, I. D. Williams, C. C.-S. Chan, K. S. Wong, Q. Peng and B. Z. Tang, *Adv. Mater.*, 2020, **32**, 2001026.
- 293 F. Xiao, H. Gao, Y. Lei, W. Dai, M. Liu, X. Zheng, Z. Cai, X. Huang, H. Wu and D. Ding, *Nat. Commun.*, 2022, **13**, 186.
- 294 Z. Xie, X. Zhang, H. Wang, C. Huang, H. Sun, M. Dong, L. Ji, Z. An, T. Yu and W. Huang, *Nat. Commun.*, 2021, **12**, 3522.
- 295 D. Wang, Y. Xie, X. Wu, Y. Lei, Y. Zhou, Z. Cai, M. Liu, H. Wu, X. Huang and Y. Dong, *J. Phys. Chem. Lett.*, 2021, **12**, 1814–1821.
- 296 Y. Lei, J. Yang, W. Dai, Y. Lan, J. Yang, X. Zheng, J. Shi, B. Tong, Z. Cai and Y. Dong, *Chem. Sci.*, 2021, **12**, 6518–6525.
- 297 B. Chen, W. Huang, H. Su, H. Miao, X. Zhang and G. Zhang, *Angew. Chem., Int. Ed.*, 2020, **59**, 10023–10026.
- 298 X. Zhang, L. Du, W. Zhao, Z. Zhao, Y. Xiong, X. He, P. F. Gao, P. Alam, C. Wang, Z. Li, J. Leng, J. Liu, C. Zhou, J. W.-Y. Lam, D. L. Phillips, G. Zhang and B. Z. Tang, *Nat. Commun.*, 2019, **10**, 5161.
- 299 X. Lin, Q. Xu and X. Ma, *Adv. Opt. Mater.*, 2021, **10**, 2101646.
- 300 H. Chen, L. Xu, X. Ma and H. Tian, *Polym. Chem.*, 2016, **7**, 3989–3992.
- 301 X. K. Ma and Y. Liu, *Acc. Chem. Res.*, 2021, **54**, 3403–3414.
- 302 W. W. Xu, Y. Chen, Y. L. Lu, Y. X. Qin, H. Zhang, X. Xu and Y. Liu, *Angew. Chem., Int. Ed.*, 2022, **61**, e202115265.
- 303 X. Ma, J. Wang and H. Tian, *Acc. Chem. Res.*, 2019, **52**, 738–748.
- 304 F. F. Shen, Y. Chen, X. Dai, H. Y. Zhang, B. Zhang, Y. Liu and Y. Liu, *Chem. Sci.*, 2020, **12**, 1851–1857.
- 305 Y. Wu, L. Chen, Y. Chen and Y. Liu, *ACS Appl. Mater. Interfaces*, 2021, **13**, 59126–59131.
- 306 X. Zhou, S. Lee, Z. Xu and J. Yoon, *Chem. Rev.*, 2015, **115**, 7944–8000.
- 307 D. Cao, Z. Liu, P. Verwilt, S. Koo, P. Jangjili, J. S. Kim and W. Lin, *Chem. Rev.*, 2019, **119**, 10403–10519.
- 308 X. Wu, R. Wang, N. Kwon, H. Ma and J. Yoon, *Chem. Soc. Rev.*, 2022, **51**, 450–463.
- 309 Z. Mao, J. Xiong, P. Wang, J. An, F. Zhang, Z. Liu and J. Seung Kim, *Coord. Chem. Rev.*, 2022, **454**, 214356.
- 310 Z. Liu, X. Zhou, Y. Miao, Y. Hu, N. Kwon, X. Wu and J. Yoon, *Angew. Chem., Int. Ed.*, 2017, **56**, 5812–5816.
- 311 Y. Yue, F. Huo, P. Ning, Y. Zhang, J. Chao, X. Meng and C. Yin, *J. Am. Chem. Soc.*, 2017, **139**, 3181–3185.
- 312 Y. Zhang, G. Zhang, Z. Zeng and K. Pu, *Chem. Soc. Rev.*, 2022, **51**, 566–593.
- 313 L. Wu, J. Liu, X. Tian, R. R. Groleau, B. Feng, Y. Yang, A. C. Sedgwick, H. H. Han, Y. Wang, H. M. Wang, F. Huang, S. D. Bull, H. Zhang, C. Huang, Y. Zang, J. Li, X. P. He, P. Li, B. Tang, T. D. James and J. L. Sessler, *J. Am. Chem. Soc.*, 2022, **144**, 174–183.
- 314 Z. Liu, X. Dai, Q. Xu, X. Sun and Y. Liu, *Chin. J. Chem.*, 2022, **40**, 493–499.
- 315 Z. Liu, W. Zhou, J. Li, H. Zhang, X. Dai, Y. Liu and Y. Liu, *Chem. Sci.*, 2020, **11**, 4791–4800.
- 316 J. Huang, J. Li, Y. Lyu, Q. Miao and K. Pu, *Nat. Mater.*, 2019, **18**, 1133–1143.

- 317 J. Huang, Y. Lyu, J. Li, P. Cheng, Y. Jiang and K. Pu, *Angew. Chem., Int. Ed.*, 2019, **58**, 17796–17804.
- 318 J. Huang, Y. Jiang, J. Li, S. He, J. Huang and K. Pu, *Angew. Chem., Int. Ed.*, 2020, **59**, 4415–4420.
- 319 S. S. Liew, Z. Zeng, P. Cheng, S. He, C. Zhang and K. Pu, *J. Am. Chem. Soc.*, 2021, **143**, 18827–18831.
- 320 Y. Jiao, W. L. Li, J. F. Xu, G. Wang, J. Li, Z. Wang and X. Zhang, *Angew. Chem., Int. Ed.*, 2016, **55**, 8933–8937.
- 321 S. Wu, Y. Li, S. Xie, C. Ma, J. Lim, J. Zhao, D. S. Kim, M. Yang, D. K. Yoon, M. Lee, S. O. Kim and Z. Huang, *Angew. Chem., Int. Ed.*, 2017, **56**, 11511–11514.
- 322 N. Dai, R. Qi, H. Zhao, L. Liu, F. Lv and S. Wang, *Chem. – Eur. J.*, 2021, **27**, 11567–11573.
- 323 Y. Zhao, B. Lei, M. Wang, S. Wu, W. Qi, R. Su and Z. He, *J. Mater. Chem. B*, 2018, **6**, 2444–2449.
- 324 L. Chen, Y. Chen, Y. Zhang and Y. Liu, *Angew. Chem., Int. Ed.*, 2021, **60**, 7654–7658.
- 325 H. Bouas-Laurent, J.-P. Desvergne, A. Castellan and R. Lapouyade, *Chem. Soc. Rev.*, 2001, **30**, 248–263.
- 326 H. Bouas-Laurent, J.-P. Desvergne, A. Castellan and R. Lapouyade, *Chem. Soc. Rev.*, 2000, **29**, 43–55.
- 327 X. Wei, W. Wu, R. Matsushita, Z. Yan, D. Zhou, J. J. Chruma, M. Nishijima, G. Fukuhara, T. Mori, Y. Inoue and C. Yang, *J. Am. Chem. Soc.*, 2018, **140**, 3959–3974.
- 328 X. Wei, A. M. Raj, J. Ji, W. Wu, G. B. Veerakanellore, C. Yang and V. Ramamurthy, *Org. Lett.*, 2019, **21**, 7868–7872.
- 329 A. Nakamura and Y. Inoue, *J. Am. Chem. Soc.*, 2005, **127**, 5338–5339.
- 330 A. Nakamura and Y. Inoue, *J. Am. Chem. Soc.*, 2003, **125**, 966–972.
- 331 J. Yi, W. Liang, X. Wei, J. Yao, Z. Yan, D. Su, Z. Zhong, G. Gao, W. Wu and C. Yang, *Chin. Chem. Lett.*, 2018, **29**, 87–90.
- 332 K. Kanagaraj, W. Liang, M. Rao, J. Yao, W. Wu, G. Cheng, J. Ji, X. Wei, C. Peng and C. Yang, *Org. Lett.*, 2020, **22**, 5273–5278.
- 333 M. Nakahata, Y. Takashima, A. Hashidzume and A. Harada, *Angew. Chem., Int. Ed.*, 2013, **52**, 5731–5735.
- 334 Y. Takashima, S. Hatanaka, M. Otsubo, M. Nakahata, T. Kakuta, A. Hashidzume, H. Yamaguchi and A. Harada, *Nat. Commun.*, 2012, **3**, 1270.
- 335 H. Aramoto, M. Osaki, S. Konishi, C. Ueda, Y. Kobayashi, Y. Takashima, A. Harada and H. Yamaguchi, *Chem. Sci.*, 2020, **11**, 4322–4331.
- 336 Z. Li, Y.-M. Zhang, H.-Y. Wang, H. Li and Y. Liu, *Macromolecules*, 2017, **50**, 1141–1146.
- 337 S. Cherraben, J. Scelle, B. Hasenknopf, G. Vives and M. Sollogoub, *Org. Lett.*, 2021, **23**, 7938–7942.
- 338 L. Yue, H. Ai, Y. Yang, W. Lu and L. Wu, *Chem. Commun.*, 2013, **49**, 9770–9772.
- 339 R. Anand, S. Nayyar, J. Pitha and C. R. Merril, *Antiviral Chem. Chemother.*, 1990, **1**, 41–46.
- 340 T. Otake, D. Schols, M. Witvrouw, L. Naesens, H. Nakashima, T. Moriya, H. Kurita, K. Matsumoto, N. Ueba and E. De Clercq, *Antiviral Chem. Chemother.*, 1994, **5**, 155–161.
- 341 T. Moriya, H. Kurita, K. Matsumoto, T. Otake, H. Mori, M. Morimoto, N. Ueba and N. Kunita, *J. Med. Chem.*, 1991, **34**, 2301–2304.
- 342 T. Moriya, K. Saito, H. Kurita, K. Matsumoto, T. Otake, H. Mori, M. Morimoto, N. Ueba and N. Kunita, *J. Med. Chem.*, 1993, **36**, 1674–1677.
- 343 X. Guan, Y. Chen, X. Wu, P. Li and Y. Liu, *Chem. Commun.*, 2019, **55**, 953–956.
- 344 X.-M. Chen, Y. Chen, X.-F. Hou, X. Wu, B.-H. Gu and Y. Liu, *ACS Appl. Mater. Interfaces*, 2018, **10**, 24987–24992.
- 345 Q. Yu, Y. M. Zhang, Y. H. Liu, X. Xu and Y. Liu, *Sci. Adv.*, 2018, **4**, eaat2297.
- 346 X. Dai, B. Zhang, W. Zhou and Y. Liu, *Biomacromolecules*, 2020, **21**, 4998–5007.
- 347 D. Hu, Y. Deng, F. Jia, Q. Jin and J. Ji, *ACS Nano*, 2020, **14**, 347–359.
- 348 Y. Tang, X. Lu, C. Yin, H. Zhao, W. Hu, X. Hu, Y. Li, Z. Yang, F. Lu, Q. Fan and W. Huang, *Chem. Sci.*, 2019, **10**, 1401–1409.
- 349 C. Zhao, Y. Jin, J. Wang, X. Cao, X. Ma and H. Tian, *Chem. Commun.*, 2019, **55**, 5355–5358.
- 350 X. M. Chen, Q. Cao, H. K. Bisoyi, M. Wang, H. Yang and Q. Li, *Angew. Chem., Int. Ed.*, 2020, **59**, 10493–10497.
- 351 M. Hao, G. Sun, M. Zuo, Z. Xu, Y. Chen, X. Y. Hu and L. Wang, *Angew. Chem., Int. Ed.*, 2020, **59**, 10095–10100.
- 352 W. J. Li, X. Q. Wang, D. Y. Zhang, Y. X. Hu, W. T. Xu, L. Xu, W. Wang and H. B. Yang, *Angew. Chem., Int. Ed.*, 2021, **60**, 18761–18768.
- 353 L. Xu, Z. Wang, R. Wang, L. Wang, X. He, H. Jiang, H. Tang, D. Cao and B. Z. Tang, *Angew. Chem., Int. Ed.*, 2020, **59**, 9908–9913.
- 354 Q. Song, S. Goia, J. Yang, S. C.-L. Hall, M. Staniforth, V. G. Stavros and S. Perrier, *J. Am. Chem. Soc.*, 2021, **143**, 382–389.
- 355 Z. Liu, X. Sun, X. Dai, J. Li, P. Li and Y. Liu, *J. Mater. Chem. C*, 2021, **9**, 1958–1965.
- 356 S. Garain, B. C. Garain, M. Eswaramoorthy, S. K. Pati and S. J. George, *Angew. Chem., Int. Ed.*, 2021, **60**, 19720–19724.
- 357 K. Wang, K. Velmurugan, B. Li and X. Y. Hu, *Chem. Commun.*, 2021, **57**, 13641–13654.
- 358 J. J. Li, Y. Chen, J. Yu, N. Cheng and Y. Liu, *Adv. Mater.*, 2017, **29**, 1701905.
- 359 J. J. Li, H. Y. Zhang, G. Liu, X. Dai, L. Chen and Y. Liu, *Adv. Opt. Mater.*, 2020, **9**, 2001702.
- 360 A. M. Pettiwala and P. K. Singh, *ACS Omega*, 2017, **2**, 8779–8787.
- 361 G. Singh and P. K. Singh, *Langmuir*, 2019, **35**, 14628–14638.
- 362 X. Wei, R. Dong, D. Wang, T. Zhao, Y. Gao, P. Duffy, X. Zhu and W. Wang, *Chem. – Eur. J.*, 2015, **21**, 11427–11434.
- 363 C. Han, X. Hou, H. Zhang, W. Guo, H. Li and L. Jiang, *J. Am. Chem. Soc.*, 2011, **133**, 7644–7647.
- 364 Y. Okumura and K. Ito, *Adv. Mater.*, 2001, **13**, 485–487.
- 365 C. Liu, N. Morimoto, L. Jiang, S. Kawahara, T. Noritomi, H. Yokoyama, K. Mayumi and K. Ito, *Science*, 2021, **372**, 1078–1081.
- 366 Y. Yasuda, Y. Hidaka, K. Mayumi, T. Yamada, K. Fujimoto, S. Okazaki, H. Yokoyama and K. Ito, *J. Am. Chem. Soc.*, 2019, **141**, 9655–9663.
- 367 M. Nakahata, S. Mori, Y. Takashima, H. Yamaguchi and A. Harada, *Chem*, 2016, **1**, 766–775.
- 368 Q. Lin and C. Ke, *Chem. Commun.*, 2021, **58**, 250–253.

- 369 C. Wang, M. Fadeev, J. Zhang, M. Vazquez-Gonzalez, G. Davidson-Rozenfeld, H. Tian and I. Willner, *Chem. Sci.*, 2018, **9**, 7145–7152.
- 370 K. Wu, X. Wu, Y. Zhang, S. Chen, Z. Qiao, D. Wei, J. Sun and H. Fan, *Biomacromolecules*, 2022, **23**, 1030–1040.
- 371 Z. Li, G. Wang, Y. Wang and H. Li, *Angew. Chem., Int. Ed.*, 2018, **57**, 2194–2198.
- 372 Z. Qi and C. A. Schalley, *Acc. Chem. Res.*, 2014, **47**, 2222–2233.
- 373 H. Wang, C. N. Zhu, H. Zeng, X. Ji, T. Xie, X. Yan, Z. L. Wu and F. Huang, *Adv. Mater.*, 2019, **31**, 1807328.
- 374 R. Guagliardo, J. Perez-Gil, S. De Smedt and K. Raemdonck, *J. Controlled Release*, 2018, **291**, 116–126.
- 375 D. S. Guo, K. Wang, Y. X. Wang and Y. Liu, *J. Am. Chem. Soc.*, 2012, **134**, 10244–10250.
- 376 Y. Wang, N. Ma, Z. Wang and X. Zhang, *Angew. Chem., Int. Ed.*, 2007, **46**, 2823–2826.
- 377 R. Sun, C. Xue, X. Ma, M. Gao, H. Tian and Q. Li, *J. Am. Chem. Soc.*, 2013, **135**, 5990–5993.
- 378 Y. Chen, S. Pangannaya, B. Sun, C. Qian, G. Sun, M. Cheng, C. Lin, X. Lu, J. Jiang and L. Wang, *ACS Appl. Bio Mater.*, 2020, **4**, 2066–2072.
- 379 S. Konishi, Y. Kashiwagi, G. Watanabe, M. Osaki, T. Katashima, O. Urakawa, T. Inoue, H. Yamaguchi, A. Harada and Y. Takashima, *Polym. Chem.*, 2020, **11**, 6811–6820.
- 380 Q. W. Zhang, D. Li, X. Li, P. B. White, J. Mecinovic, X. Ma, H. Agren, R. J.-M. Nolte and H. Tian, *J. Am. Chem. Soc.*, 2016, **138**, 13541–13550.
- 381 X. Hou, C. Ke, C. J. Bruns, P. R. McGonigal, R. B. Pettman and J. F. Stoddart, *Nat. Commun.*, 2015, **6**, 6884.
- 382 X. Yu, W. Liang, Q. Huang, W. Wu, J. J. Chruma and C. Yang, *Chem. Commun.*, 2019, **55**, 3156–3159.
- 383 F. Gomollón-Bel, *Chem. Int.*, 2020, **42**, 3–9.
- 384 X. Chen, H. Gao, Y. Deng, Q. Jin, J. Ji and D. Ding, *ACS Nano*, 2020, **14**, 5121–5134.
- 385 L. Yue, S. Wang, D. Zhou, H. Zhang, B. Li and L. Wu, *Nat. Commun.*, 2016, **7**, 10742.
- 386 J. Zhou, L. Rao, G. Yu, T. R. Cook, X. Chen and F. Huang, *Chem. Soc. Rev.*, 2021, **50**, 2839–2891.
- 387 G. Yu, X. Zhao, J. Zhou, Z. Mao, X. Huang, Z. Wang, B. Hua, Y. Liu, F. Zhang, Z. He, O. Jacobson, C. Gao, W. Wang, C. Yu, X. Zhu, F. Huang and X. Chen, *J. Am. Chem. Soc.*, 2018, **140**, 8005–8019.
- 388 K. Yang, G. Yu, Z. Yang, L. Yue, X. Zhang, C. Sun, J. Wei, L. Rao, X. Chen and R. Wang, *Angew. Chem., Int. Ed.*, 2021, **60**, 17570–17578.
- 389 J. B. Jiao, G. Z. Wang, X. L. Hu, Y. Zang, S. Maisonneuve, A. C. Sedgwick, J. L. Sessler, J. Xie, J. Li, X. P. He and H. Tian, *J. Am. Chem. Soc.*, 2020, **142**, 1925–1932.
- 390 Q. Song, X. Yan, H. Cui and M. Ma, *ACS Nano*, 2020, **14**, 3696–3702.
- 391 S. Han, Y. Wei, C. Valente, R. S. Forgan, J. J. Gassensmith, R. A. Smaldone, H. Nakanishi, A. Coskun, J. F. Stoddart and B. A. Grzybowski, *Angew. Chem., Int. Ed.*, 2011, **50**, 276–279.
- 392 R. A. Smaldone, R. S. Forgan, H. Furukawa, J. J. Gassensmith, A. M. Slawin, O. M. Yaghi and J. F. Stoddart, *Angew. Chem., Int. Ed.*, 2010, **49**, 8630–8634.
- 393 X. Y. Chen, H. Chen, L. Dordevic, Q. H. Guo, H. Wu, Y. Wang, L. Zhang, Y. Jiao, K. Cai, H. Chen, C. L. Stern, S. I. Stupp, R. Q. Snurr, D. Shen and J. F. Stoddart, *J. Am. Chem. Soc.*, 2021, **143**, 9129–9139.
- 394 K. J. Hartlieb, A. W. Peters, T. C. Wang, P. Deria, O. K. Farha, J. T. Hupp and J. F. Stoddart, *Chem. Commun.*, 2017, **53**, 7561–7564.
- 395 L. Hu, K. Li, W. Shang, X. Zhu and M. Liu, *Angew. Chem., Int. Ed.*, 2020, **59**, 4953–4958.
- 396 W. Zhou, Y. Chen, Q. Yu, P. Li, X. Chen and Y. Liu, *Chem. Sci.*, 2019, **10**, 3346–3352.
- 397 M. Inouye, K. Hayashi, Y. Yonenaga, T. Itou, K. Fujimoto, T. A. Uchida, M. Iwamura and K. Nozaki, *Angew. Chem., Int. Ed.*, 2014, **53**, 14392–14396.
- 398 K. Hayashi, Y. Miyaoka, Y. Ohishi, T. A. Uchida, M. Iwamura, K. Nozaki and M. Inouye, *Chem. – Eur. J.*, 2018, **24**, 14613–14616.
- 399 M. Yang, J. Huang, J. Fan, J. Du, K. Pu and X. Peng, *Chem. Soc. Rev.*, 2020, **49**, 6800–6815.
- 400 F. Gomollón-Bel, *Chem. Int.*, 2021, **43**, 13–20.
- 401 S. Gnaim, A. Scomparin, A. Eldar-Boock, C. R. Bauer, R. Satchi-Fainaro and D. Shabat, *Chem. Sci.*, 2019, **10**, 2945–2955.
- 402 Y. Kang, Z. Cai, X. Tang, K. Liu, G. Wang and X. Zhang, *ACS Appl. Mater. Interfaces*, 2016, **8**, 4927–4933.
- 403 Q. Hao, Y. Kang, J. F. Xu and X. Zhang, *Langmuir*, 2021, **37**, 6062–6068.
- 404 S. Munir and S. Y. Park, *Anal. Chim. Acta*, 2015, **893**, 101–107.
- 405 Y. Wu, R. Shi, Y. L. Wu, J. M. Holcroft, Z. Liu, M. Frascioni, M. R. Wasielewski, H. Li and J. F. Stoddart, *J. Am. Chem. Soc.*, 2015, **137**, 4111–4118.
- 406 Q. Li, D. Wang, X. Fang, X. Wang, S. Mao and K. Ostrikov, *Adv. Funct. Mater.*, 2021, **31**, 2104572.
- 407 H. L. Sun, Y. Chen, X. Han and Y. Liu, *Angew. Chem., Int. Ed.*, 2017, **56**, 7062–7065.
- 408 K. Harata and H. Uedaira, *Bull. Chem. Soc. Jpn.*, 1975, **48**, 375–378.
- 409 M. Kodaka, *J. Am. Chem. Soc.*, 2002, **115**, 3702–3705.
- 410 W. Zhi, Z. Pu, C. Ma, K. Liu, X. Wang, J. Huang, Y. Xiao and Y. Yan, *ACS Nano*, 2021, **15**, 19621–19628.
- 411 L. Ji, Q. He, D. Niu, J. Tan, G. Ouyang and M. Liu, *Chem. Commun.*, 2019, **55**, 11747–11750.